National Institute of Electricity and Electronics
INELEC - BOUMERDES
DEPARTMENT OF RESEARCH

THESIS

Presented in partial fulfilment of the requirements of the

DEGREE OF MAGISTER

in Applied Electronics

by

Hamid BENTARZI

Density Distribution of Mobile Ions in the Oxide of MOS Structures

Defended on November 15, 1992 before the jury:
President: Dr M. BENZOHRA, Professeur, USTO.
Members: Dr V. MITRA, Professeur, INELEC.
Dr M. BOUMAOURE, Charge de Recherche, UDTS.
Dr H. BOURDOUCEN, INELEC.
Dr L. REFOUFI, INELEC.

Registration Number: 04/92.

ABSTRACT

The present work aims to study the mobile ion distribution in the oxides of MOS structures. The subject is introduced with the necessary background concept of MOS structure dealing with various aspects of oxide and its charges. A review is then presented on the measuring techniques of mobile charge concentration in the oxides. This is followed by our new approaches to determine the density-distribution of the mobile ions along the oxide thickness of a MOS structure. In fact we have made two attempts each of which makes use of a different approach. In the first attempt, the equilibrium density-distribution of the mobile ions has been determined from the experimentally measured values of its flat-band voltage under three different conditions, namely, before contamination/activation, after contamination/activation and then after ion-drift due to thermal electric stressing. However in the other attempt a theoretical model for the density-distribution of the mobile ions has been developed which is based on the concept that at any point in the oxide the equilibrium

concentration of these mobile ions is attained when the combined mobilizing forces, arising from different origins, become just sufficient to provide necessary activation energy to the ions to surmount the effective potential well. In both investigations, the results are consistent and in good agreement with earlier results.

ACKNOWLEDGEMENTS

I would like to express my most sincere gratitude to my project adviser Dr V. Mitra for his continued and untiring interest and research guidance throughout this work. I would like also to acknowledge my colleagues Mr R. Bouderbala and A. Benfdila for their cooperation and many fruitful discussions.

I am especially grateful to Mr A. Moufek, director general of the institute, and Dr K. Hariche, head of research department, for providing all necessary research facilities and encouragements for developing this work. I am equally thankful to Dr. H. Bourdoucen for useful suggestions and discussions. In addition, I would like to thank all staff members for their support.

At last, I must acknowledge my family for continuous encouragement and support.

TABLE OF CONTENTS

CHAPTER 1

INTRODUCTION

In the past decades, the study of the thermally oxidized silicon system has been of great importance to the development of integrated circuit technologies. The motivation behind the use of the MOS capacitor has been the fabrication of stable and high performance devices and integrated circuits.

The metal-oxide-silicon (MOS) capacitor is used both in monitoring integrated circuit fabrication and studying the effects of oxide charges on the electrical parameters of MOS structures. The MOS capacitor has the advantages of simplicity of fabrication and of analysis [1-3].

Early attempts to fabricate MOS devices were unsuccessful because of the lack of controllable and stable surface. Until 1960, stable and reproducible solid-solid interface between silicon and a grown oxide film of known composition and structure, could not be produced. During this period, theoretical modeling of surface band bending and its consequences were formulated by Brown [4] in 1953, and Garret and Brattain [5] in 1955. This theoretical ground work was applied in the next decade to the silicon-oxide interface. The first good quality

oxide films of high dielectric breakdown strength and low loss were oxidized in high pressure steam by Ligenza [6] in 1960-1961.

A major breakthrough in semiconductor processing occurred in the early 1960, with the development of the silicon planar process which was described first by Hoerni [7]. However, attempts at MOSFET fabrication were blocked by charge migration problems, which led to deterioration of their electrical characteristics. In the period 1963-1964, various charges associated with the thermally oxidized silicon structure were observed to cause serious yield and reliability problems. Subsequently, a number of investigations concerning oxide charges were started in various laboratories and many have continued to the present time [8]. During the past 25 years or so, it has been generally established that four general types of charges are associated with the MOS system [9], [10]. The four general types of charges are : interface trapped charge, fixed oxide charge, oxide trapped charge and mobile ionic charge. Initially, most of the studies were devoted to the processing parameters so that their adverse effects on device properties could be minimized. More recently, efforts have been focussed on a quantitative understanding of the densities, cross sections, and the nature of

the oxide charges and traps so that ultimate device performance might be achieved. With further process refinements, the first reliable and reproducible discrete MOSFET's and simple integrated circuits (IC's) were produced on commercial basis in this period.

The serious problem of instability is caused in the devices by mobile oxide charge which is commonly quantified by using a MOS capacitor and by measuring ΔV_{fb}, the flat-band voltage shift, after a bias-temperature stress test (BTS) has been applied to it.

The mobile oxide charge is not related to the structure of the Si-SiO_2 system. It is just due to impurity ions introduced during or after processing . This means that in principle mobile oxide charge can be avoided if care is taken to prevent these impurities from reaching the device (during or after processing).

Back in 1965 the shift in the flat-band voltage was attributed by Snow et al [11] to the motion of alkali ions in SiO_2. At that time one knew from conductivity studies that the alkali atoms are so abundant every where that their ions could easily be introduced and incorporated in layers of oxide grown on silicon.

that a stable device could not be manufactured and thus the other types of charges could not be investigated. Nowadays these contamination problems have been greatly reduced by using gettering and very "clean" processing techniques. In laboratories it is somehow believed that mobile oxide charge no longer plays an important role in the observed instabilities of semiconductor devices and that mobile ions in SiO_2 are only of historical importance. This contention has been now disproved and the importance of the study of mobile ions in the oxides has again been revived. It is ,because, not only the initial mobile ion contamination but also the activation of the already existing neutral sodium of the device during the subsequent processing stages which can cause serious problems in device performance.

Since very clean processing conditions are not automatically present in all laboratories and are achieved only as a result of extra investment, experience and care during processing, ordinarily the level of ionic contamination may be too high and one has to know where to look for improvements [12].

The use of gettering techniques to render mobile ions to inactive form has several drawbacks which become more apparent with the reduction of the dimensions of modern devices. In such cases the quality of the SiO_2 layer and of the $Si-SiO_2$

interface becomes of greater importance.

Besides, the importance of the study of mobile ionic charge can be further established when intentionally contaminated MOS devices are used as tool in the device characterization. In this way more insight has been gained in fields such as :

-the structure of the Si-SiO_2 interface,

-the interaction between the electrodes material and SiO_2 during low temperature anneal processes,

-the wear-out and breakdown phenomena.

More recently studies of the electron-trapping on N^+-related traps and that of the relation between mobile ions and oxide defects have been carried out. Using samples with very low contamination levels, a kind of interface spectroscopy can be performed with extremely high sensitivity.

Even in samples containing initially very low concentrations of mobile ions, Na^+ contamination can be enhanced under the influence of exposure of ions, X-rays, and laser beams to the SiO_2 layer. As these types of beams play an increasingly important role in the present and future processes, some instabilities due to the resulting mobile Na^+ ions may be anticipated.

Finally, "dry" process steps, those using plasmas, are

more prone to pollution than first thought. They can contribute to the ionic contamination of all insulating layers that are etched. Although it does not usually affect the quality of the thermal oxide in contact with the silicon substrate, this contamination is of paramount importance when one considers the total charge distributed in the insulating layer.

The present thesis is devoted to the study of the density distribution of mobile ions along the oxide thickness of a MOS structure. The whole thesis is divided into 7 chapters. After introducing the subject in the present chapter, chapter 2 is devoted to the back ground study of the MOS structure dealing with various aspects of the oxide, oxide-charges and different effects of these charges on the device performance

The studies carried out on mobile ionic charge in thermally oxidized silicon system were primarily aimed at determining its total density. Accordingly several techniques have been developed for measuring the mobile ion concentration in oxides of MOS structures. These are described in chapter 3.

None of the techniques so developed has been used to obtain the density distribution of mobile ions in an explicit form. However, a few theoretical attempts have also been made in this direction which are reviewed in chapter 4.

In the present work certain new attempts have been made

towards the determination of the mobile ionic density-distribution. In the first attempt, a method is developed to determine the density-distribution of mobile ionic charge simply from the knowledge of the measured values of flat band voltage under three different conditions, namely, before contamination\activation, after contamination\activation, and finally after ion-drift [13]. In the other attempt the density-distribution of mobile ions in the oxide has been obtained analytically which is based on the argument that these ions must attain an equilibrium density-distribution under the influence of various internal and external forces which are acting upon them [14]. These two above mentioned new studies are presented in chapter 5 and 6 respectively. Finally the thesis is concluded in chapter 7 with a small discussion on the importance and future scope of the present work.

CHAPTER 2

MOS STRUCTURE

2.1 Introduction

The metal-oxide-semiconductor diode or MOS diode is an important structure which is incorporated in the surface of most semiconductor devices. For example it forms an essential part of a MOSFET which is an important device used in large scale integration. Therefore all the studies related to any kind of MOS device needs at first the basic understanding of the MOS structure. In order to achieve this objective, the present chapter is devoted to the study of MOS structure.

A simple physical approach to MOS structure and the behaviour of ideal MOS capacitor [2,15-18], which are necessary for understanding the analyses that will follow subsequently, are described in section 2 and 3 respectively. All the basic concepts and quantities are introduced in section 2. In section 3, the charge distribution that sets in a MOS structure when the latter is biased in either one of the three biasing modes (accumulation, depletion, and inversion) has been analysed and used to obtain the value of its capacitance and its dependence on the magnitude and the frequency of the

applied small signal using a phenomenological approach.

A real MOS structure always contains so-called "charges" located in the bulk of the oxide or at the oxide-silicon interface. These charges are traditionally classified in four groups. Their nomencluture, location, and electric properties have been discussed in section 4 along with the techniques which are used to detect them. Besides, the impact of these charges on the behaviour of real MOS structure and in particular on the flat-band voltage is also examined.

2.2 A Simple Physical Approach to MOS Structure

The MOS capacitor consists of an oxide film sandwished between a P- or N-type silicon substrate and a metal plate called gate as shown in Fig.2.1. The study of the behavior of this capacitor under a varying bias applied between substrate and gate, is a powerful way to investigate the quality of the oxide layer and the quality of the oxide-silicon interface.

2.2.1 Basic Concepts and Quantities

Figure 2.2 gives the energy band diagram of an unbiased MOS structure when the work function of the metal W_M and work function of silicon W_S are different. The diagram shows the position of the different energy levels such as Fermi level in the gate (E_{FM}) and in the silicon (E_{FS}). In this figure χ_s represents the electron affinity for the silicon and χ_{ox} for the oxide.

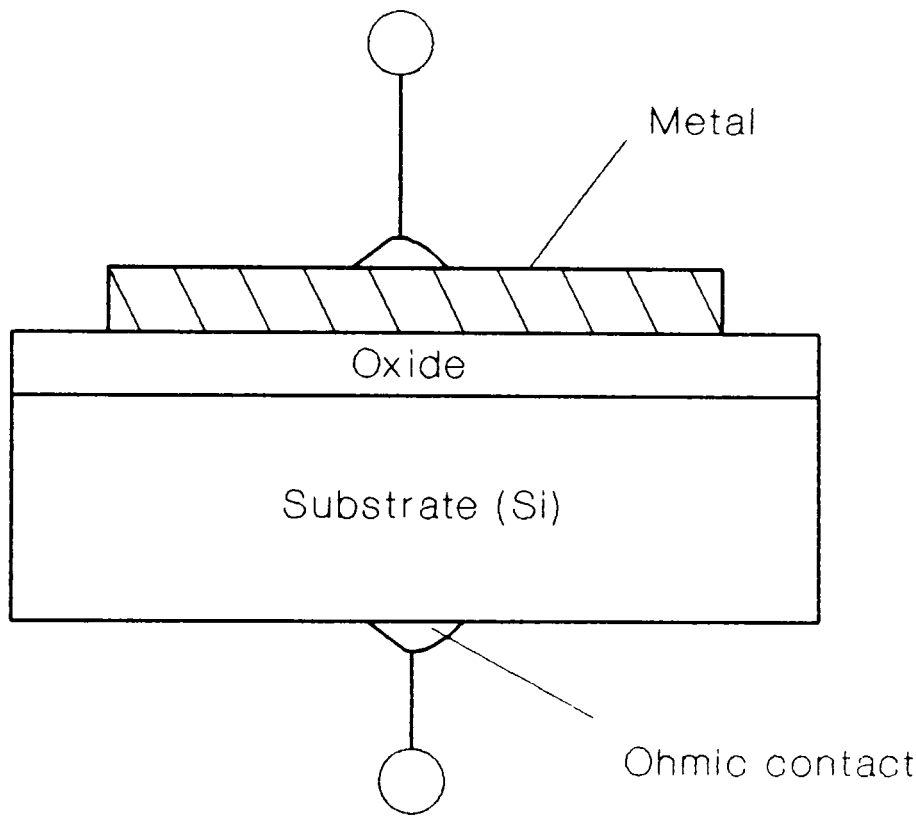

Fig.2.1 MOS structure.

Figure 2.2 shows that certain energy barriers exist between the metal and the oxide as well as between the silicon and the oxide. For example, an energy of $(W_M - q\chi_{ox})$ would be needed to move an electron from the Fermi level of the metal E_{FM} to the lowest unoccupied states in the oxide, and $A+(E_{cs}-E_{vs})$ would be needed to move an electron from the silicon valence band to the lowest unoccupied states in the oxide, where W_M is the work function of metal, Ecs and Evs the bottom of conduction band and top of valence band of silicon respectively, A the difference between the bottom level of the conduction bands of oxide and silicon at the Si-SiO2 interface and q the electron charge. The importance of these energy barriers is that they prevent the free flow of carriers from the metal to the silicon or vice versa. Some typical values for such a structure are shown in table 2.1 [19,20].

2.2.2 Definition of Potentials

Figure 2.2 shows the various potentials. The potential $\phi(x)$ may be defined by the equation

$$q\phi(x) = E_{FS} - E_{iS}(x) \qquad (2.1)$$

Where E_{FS} is the extrinsic Fermi level, and E_{iS} is the intrinsic energy level in the silicon. The potential $\phi(x)$ is called the *bulk potential* ϕ_B in the bulk $(x \to \infty)$ and the *surface potential* ϕ_s at the surface (x=0).

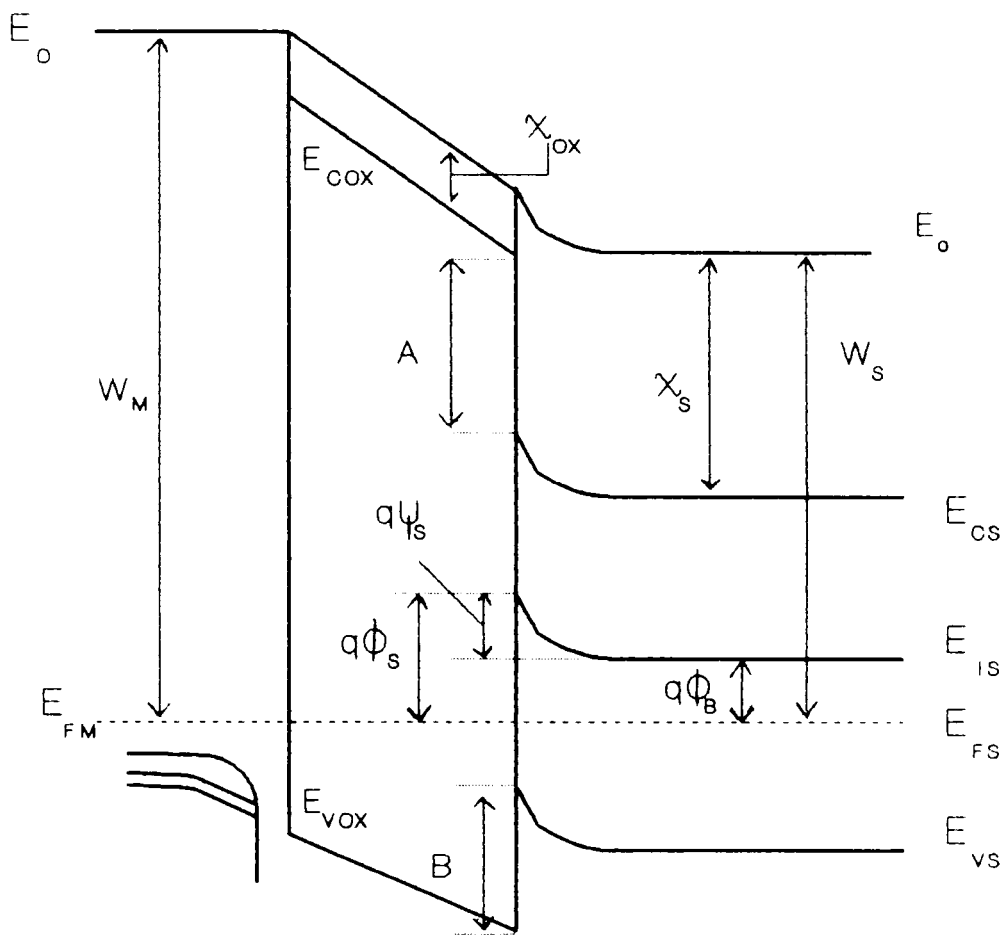

Fig. 2.2 Energy band diagram of unbiased real MOS structure ($W_M > W_S$).

Table 2.1 Some values in the energy bands of a MOS structure.

Metal	Oxide	Silicon
W_M = 4.8 eV (Au) W_M = 4.1 eV (Al)	$\chi_{ox} = 0.9eV$ $E_{C(ox)} - E_{V(ox)} = 8.1eV$ A=3.2 eV B=3.8 eV	$\chi_s = 4.1eV$ $E_{cs} - E_{vs} = 1.1eV$ $4.1eV < W_s^* < 5.2eV$

(*) Ws varies with doping and temperature.

Location of any other energy level e.g. an interface trap level within the silicon band gap may be specified by stating its distance in electron volt from the intrinsic level.
The *band bending* $\psi(x)$ is defined as

$$\psi(x) = \phi(x) - \phi_B \qquad (2.2)$$

Where $\psi(x)$ represents the potential at any point x in the depletion layer with respect to its value in the bulk. In particular, the barrier height $\psi_s = \phi_s - \phi_B$ is the *total band bending*.

2.3 Ideal MOS Capacitor

Before characterizing electrically the imperfections contained in the SiO_2 interface, at first, the ideal MOS structure will be studied. The structure is called ideal if the following two conditions are met:
1) The work function of metal W_M and work function of silicon W_S are equal, $W_M = W_S$, which implies that in the three materials, all energy levels are flat, when no voltage applied to the structure. This case is illustrated in Fig.2.3.
2) There exists no charge in the oxide and at the $Si\text{-}SiO_2$ interface which implies that the electric field is zero every where in the absence of any applied field.

MOS capacitance will vary with the applied gate to substrate voltage. The capacitance versus voltage characteristics of MOS capacitors that result from the modulation of the width

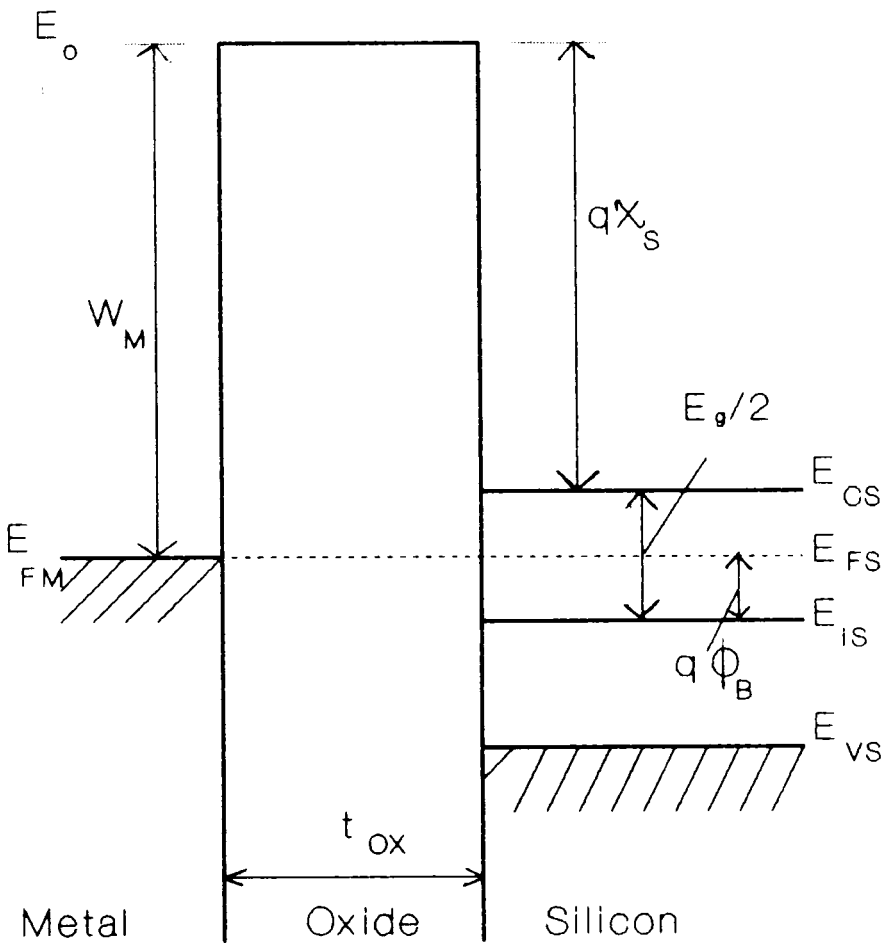

Fig. 2.3 Energy diagram of unbiased ideal MOS structure.

of the surface space charge layer (SCL) by the gate field have been found to be extremely useful in the evaluation of the electrical properties of oxide-silicon interfaces.

There are three regions of interest, namely, accumulation, depletion and inversion in the C-V characteristics of the MOS capacitor as shown in fig 2.4. The case of a MOS capacitor fabricated on a p-type substrate is treated here.

2.2.1 Accumulation

When an external voltage V_g is applied to the silicon surface in MOS capacitor, the carrier densities in its surface region change accordingly. With large negative bias on the gate, holes are attracted by the negative charge to form an accumulation layer (fig 2.5). The high concentration of these holes can be thought of as forming the second electrode of a parallel plate capacitor with first electrode at the gate. Since the accumulation layer is an indirect ohmic contact with the P-type substrate, the capacitance of the structure under accumulation conditions must be approximately equal to the capacitance of the oxide [21],

$$C_{ox} = \frac{\epsilon_o \epsilon_{ox}}{t_{ox}} \qquad (2.3)$$

Where ϵ_o is the permitivity of the free space, ϵ_{ox} the relative permitivity of oxide, and t_{ox} the oxide thickness. This capacitance is always expressed per unit gate area [$F.cm^{-2}$]. It does not vary with bias V_g as long as V_g maintains the structure in

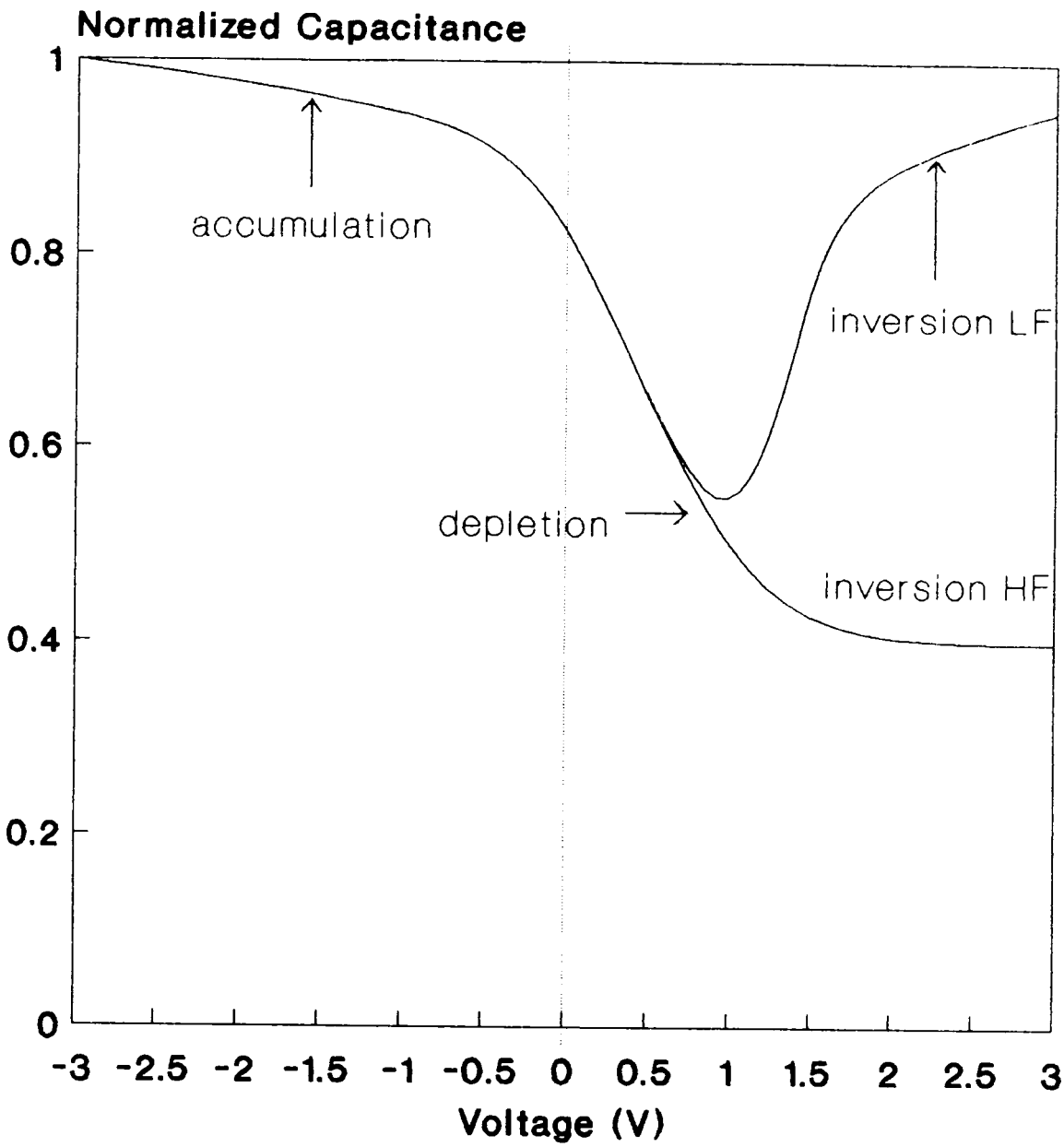

Fig.2.4 Representation of ideal C(V) curves showing the three modes : accumulation, depletion, inversion for both high and low frequency in a PMOS diode.

accumulation mode (Fig. 2.4). It is also independent of the frequency as long as the motion of the majority carriers, which contribute to substrate charge δQ_s, can keep pace with the incremental speed of gate charge δQ_M. This is true if the frequency of the applied small signal is smaller than the reciprocal of the dielectric time constant of silicon, i.e 10^{11} Hz.

Under this condition the Fermi level near the silicon surface will move to a position closer to the valance band edge as shown in Fig.2.5c.

2.3.2 Depletion

As negative charges are removed from the gate, holes leave the accumulation layer till the silicon will be neutral every where. This applied gate bias is called the *flat band voltage*. As the bias on the gate is made more positive with respect to flat band, holes are repelled and a region is formed at the surface which is depleted of carriers (see Fig. 2.6b). Under depletion conditions the Fermi level near the silicon surface will move to a position closer to the center of the forbidden region as illustrated in Fig.2.6c.

Increasing the positive voltage V_g will tend to increase the width of the surface depletion region X_D, the capacitance from the gate to the substrate associated with MOS structure will decrease, because the capacitance associated with the surface depletion region will add in series to the capacitance

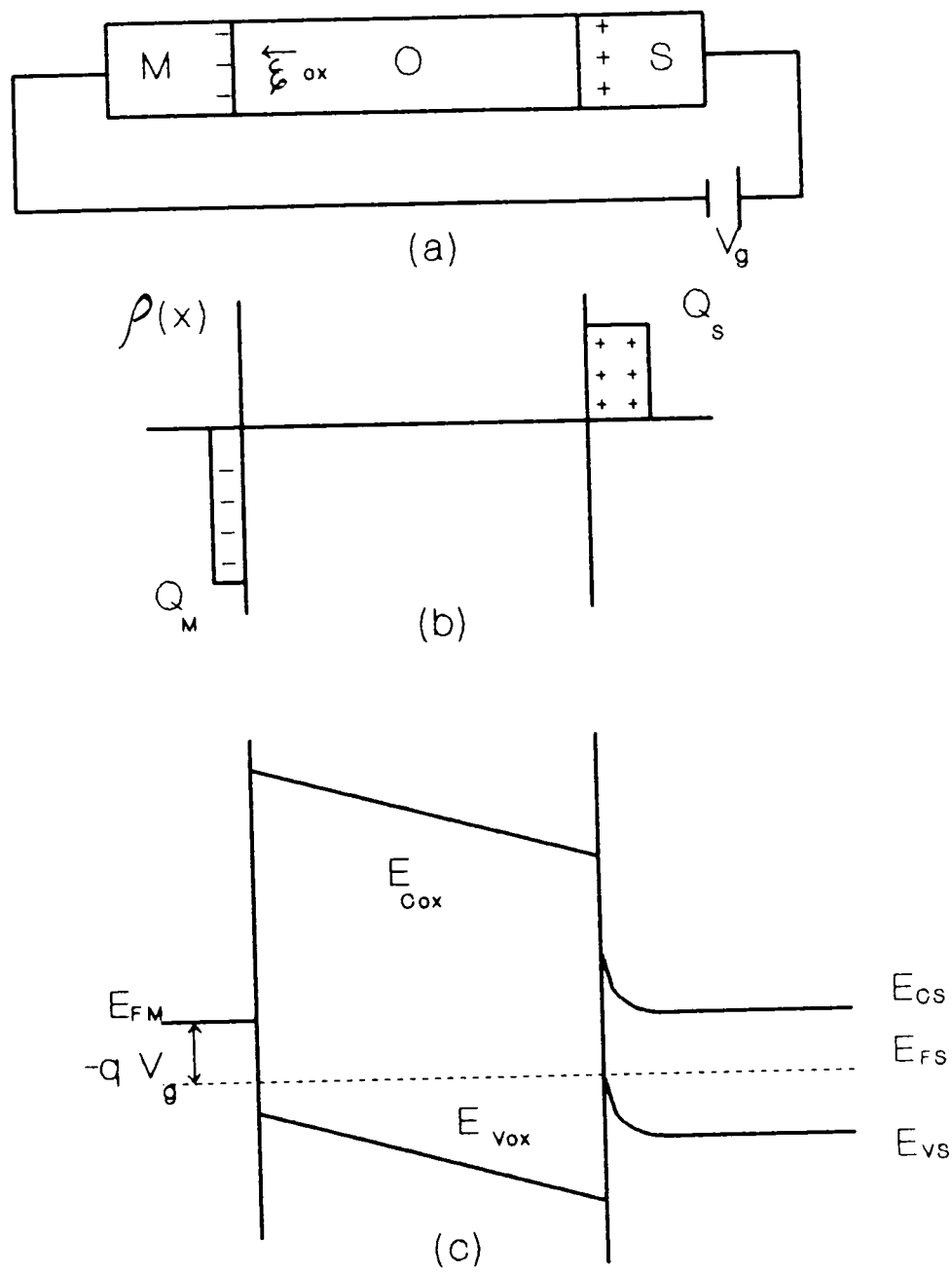

Fig.2.5 Schematic representation of a MOS structure under bias, accumulation mode, for P-type substrate. a) biasing condition ,b) charge distribution, c) energy band diagram.

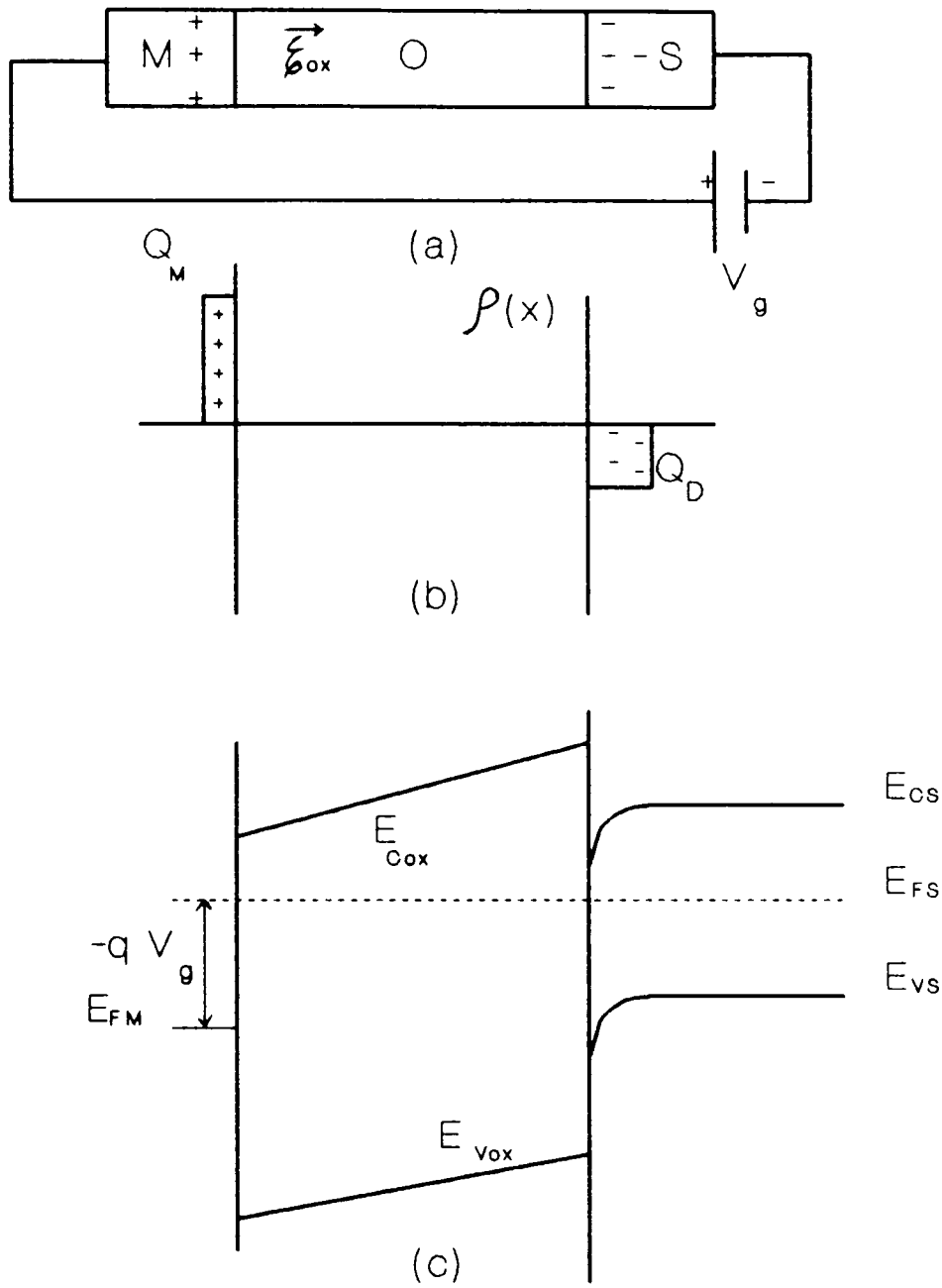

Fig.2.6 Schematic representation of a MOS structure under bias, in the depletion mode, for P-type substrate a) biasing condition ,b) charge distribution, c) energy band diagram.

across the oxide. Thus the total capacitance per unit area from the gate to substrate under depletion conditions is given by

$$C(V_g) = \left(\frac{1}{C_{ox}} + \frac{1}{C_s(V_g)} \right)^{-1}, \qquad (2.4)$$

where Cs is the silicon capacitance per unit area, is given by

$$C_S(V_g) = \frac{\epsilon_o \epsilon_s}{X_D} \qquad (2.5)$$

and,

$$X_D = \sqrt{\frac{2\epsilon_o \epsilon_S \psi_s}{qN_A}} \qquad (2.6)$$

where the relation between the applied gate voltage V_g and the total band banding ψ_S can be written as

$$V_g = \psi_S + \frac{\sqrt{2\epsilon_o \epsilon_S q N_A \psi_S}}{C_{ox}} \qquad (2.7)$$

Since only majority carriers contribute to the substrate charge δQ_D, the capacitance is independent of frequency.

2.3.3 Inversion

With increasingly positive applied voltage, the surface depletion region will continue to widen until the onset of surface inversion is observed (n-type inversion layer is

formed), the Fermi level near the silicon surface will now lie close to the bottom of conduction band (see Fig.2.7). This inversion layer is very thin (1 to 10 nm) and separated from the bulk of silicon by the depletion layer.

The build-up of inversion layer is a threshold phenomenon. The threshold condition marks the equality of the concentration of minority carriers to the doping concentration. At the onset of inversion, the depletion layer width reaches a limit, $X_{D\,lim}$ as shown in Fig.2.7b.

Since the charge density in the inversion layer may or may not be able to follow the ac variation of the applied gate voltage, it follows that the capacitance under inversion conditions will be a function of frequency.

2.3.3.1 Low frequency Capacitance

This case, illustrated in Fig. 2.1, corresponds to the thermal equilibrium in which the increase in the gate charge δQ_M is balanced by the substrate charge δQ_{inv}. It arises when the frequency of the small signal is sufficiently low (typically less than 10 Hz). The low frequency capacitance of the structure, C_{LF}, is equivalent to that of the oxide layer, just as in accumulation mode,

$$C_{LF} = C_{ox} \qquad (2.5)$$

2.3.3.2 High Frequency capacitance

This case, illustrated in Fig. 2.4, corresponds to the

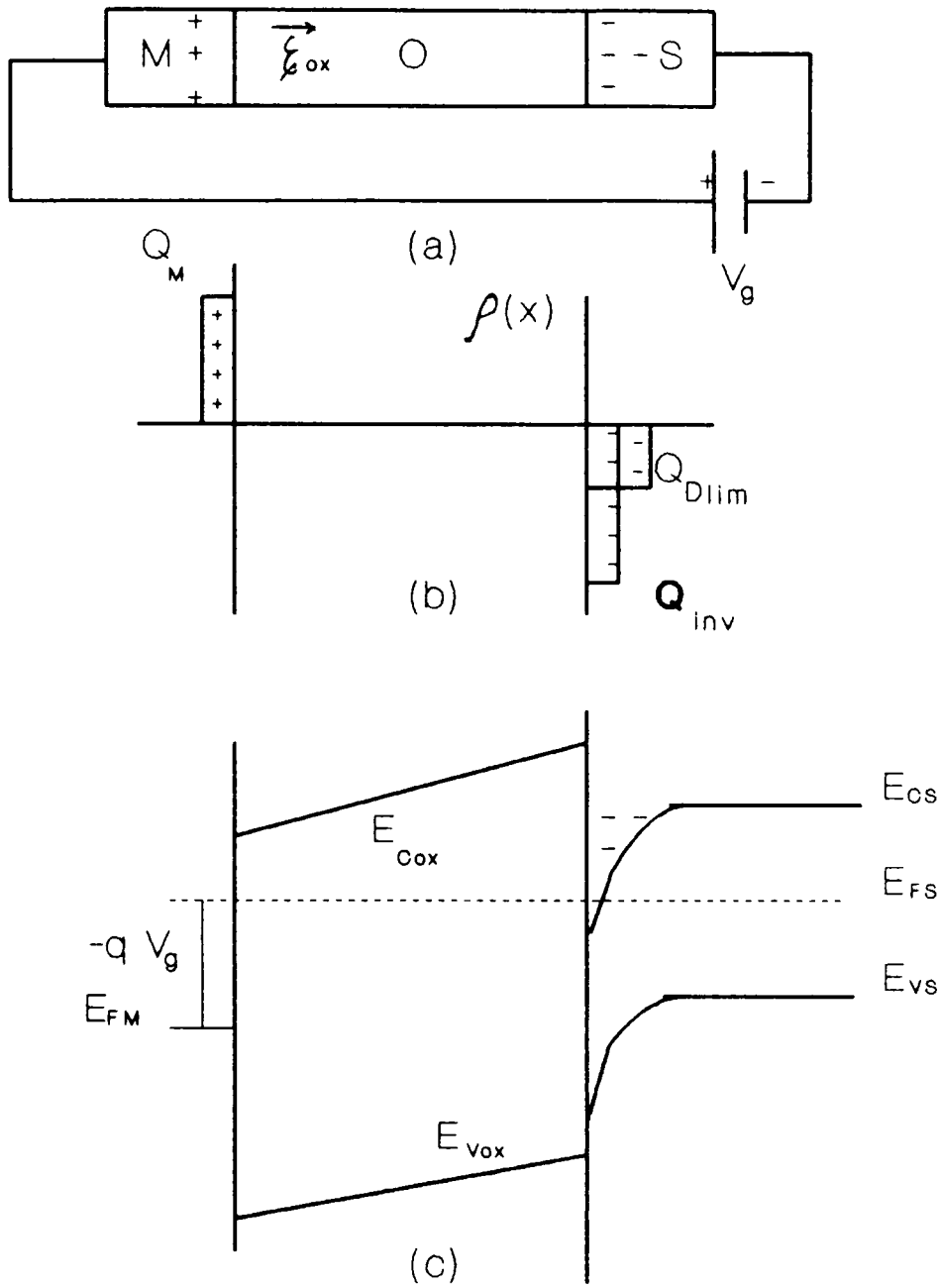

Fig.2.7 Schematic representation of a MOS structure under bias, in the inversion mode, for P-type substrate a) biasing condition ,b) charge distribution, c) energy band diagram.

higher frequencies of the applied small signal (typically above 10^5 Hz). The increase of charge in the metal side δQ_M is now balanced by the substrate charge, δQ_D, since the minority carriers can no longer adjust their concentrations. The charge modulation δQ_D occurs at distance X_{DLim} of the Si-SiO2 interface. It follows that the high frequency capacitance of the structure, C_{HF}, is given,

$$\frac{1}{C_{HF}} = \frac{1}{C_{ox}} + \frac{1}{C_{DLim}} \qquad (2.9)$$

Where,

$$C_{DLim} = \frac{\epsilon_o \epsilon_S}{X_{DLim}} \qquad (2.10)$$

and,

$$X_{DLim} = \sqrt{\frac{4\epsilon_o \epsilon_S kT \,\mathrm{Ln}\left(\frac{N_A}{n_i}\right)}{q^2 N_A}} \qquad (2.11)$$

As illustrated in Fig. 2.4, the capacitance is practically independent of bias both for high frequency inversion and low frequency inversion.

2.4 The Actual (Non-ideal) MOS Structure

An ideal MOS device does not agree with experimental results, and this difference is attributed to the presence of the oxide charges and the work function difference which exist in practice but were not taken into account in the theoretical treatment of an ideal MOS diode. Early studies of the MOS

devices showed that the threshold voltage V_t and the flat band voltage V_{fb} can strongly be affected by these charges. The understanding of the origin and nature of these charges is very important if they are to be controlled or minimized during device processing [2,10]. The net result of the presence of any charge in the oxide is to induce a charge of opposite polarity in the underlying silicon. The amount of charge induced will be inversely proportional to the distance of the charge from the silicon surface. Thus, an ion residing in the oxide very near the Si-SiO_2 interface will reflect all of its charge in the silicon, while an ion near the oxide outer surface will cause little or no effect in the silicon. The charge is measured in terms of the net charge per unit area at the silicon surface.

Most oxide charge evaluations can be made using the capacitance voltage (C-V) method. This method is simple and rapid [1,11] and in most cases provide a quantitative or at least a semiquantitative measure of the surface charge. The oxide charges can be classified into four types as proposed by a committee of scientists [22] in 1980, which are interface trapped charge, fixed oxide charge, oxide trapped charge, and mobile ionic charge. These four types of charges, which are found to be associated with thermally oxidized silicon structure, are shown in Fig.2.8. All these types of oxide charges

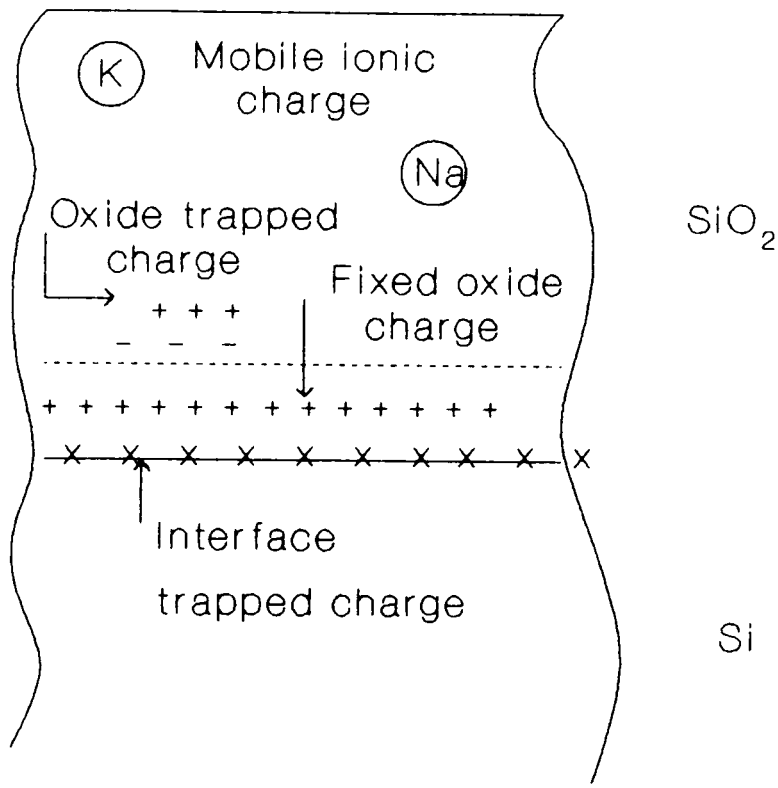

Fig.2.8 Names and location of charges in thermally oxidized silicon.

have been thoroughly studied along with the methods that allow to measure their distribution. They are summarized in table 2.2.

2.4.1 The Metal-Silicon Work Function Difference

In a real MOS structure, the work function of the metal and the work function of the silicon are different [19,20]. For this reason, there exists an electric field in the oxide and in the top layer of the silicon even in the absence of an applied field (see band diagrams of Fig. 2.2). To obtain the flat band conditions, $\psi_s = 0$, a bias on the gate must be applied relative to the substrate, which can be written

$$V_{fb} = \frac{W_{MS}}{q} \quad , \tag{2.12}$$

As an example, for Al-SiO_2-Si structure, a typical value of V_{fb} is 0.3 V for an n-type Si substrate and 0.8 V for a p-type [19].

The effect of a work function difference is to cause a shift of the actual C-V curve with respect to the ideal one. The flat-band-voltage shift V_{fb} occurs along the voltage axis as illustrated in Fig. 2.9.

2.4.2 The Interface Trapped Charge

It is found that certain energy states exist on the oxide-silicon interface (called interface trapped charge)

Table 2.2 Characteristics of Oxide-charges

Types / Properties	Interface trapped charge	Oxide trapped charge	Fixed trapped charge	Mobile ionic charge
Location	Si-SiO_2 interface	within the oxide	Near Si-SiO_2 interface	within the oxide
Charge	positive or negative	positive or negative	positve	positive
Causes	1) structural 2) metal impurities	1) ionizing radiations 2) avalanche injection	structural	ionic impurity (K^+,Na^+)
Dependence on V_g	it depends	it does not depend	it does not depend	it does not depend
Charging state	charged and discharged by V_g	charged and discharged under special condition	fixed	fixed below 390 C
Density determination method	1) LF C-V 2) CPC[1] 3) conductance	1) HF C-V 2)photocurrent	HF C-V	1) BTS[2] 2) TVS[3] 3) TSIC[4]
Degradation	hot-carriers	radiation and hot-carriers		thermal-electric stress

(1) CPC : Charge-Pumping Current
(2) BTS : Bias-Temperature Stress
(3) TVS : Triangular Voltage Sweep
(4) TSIC: Thermally Stimulated Ionic Current

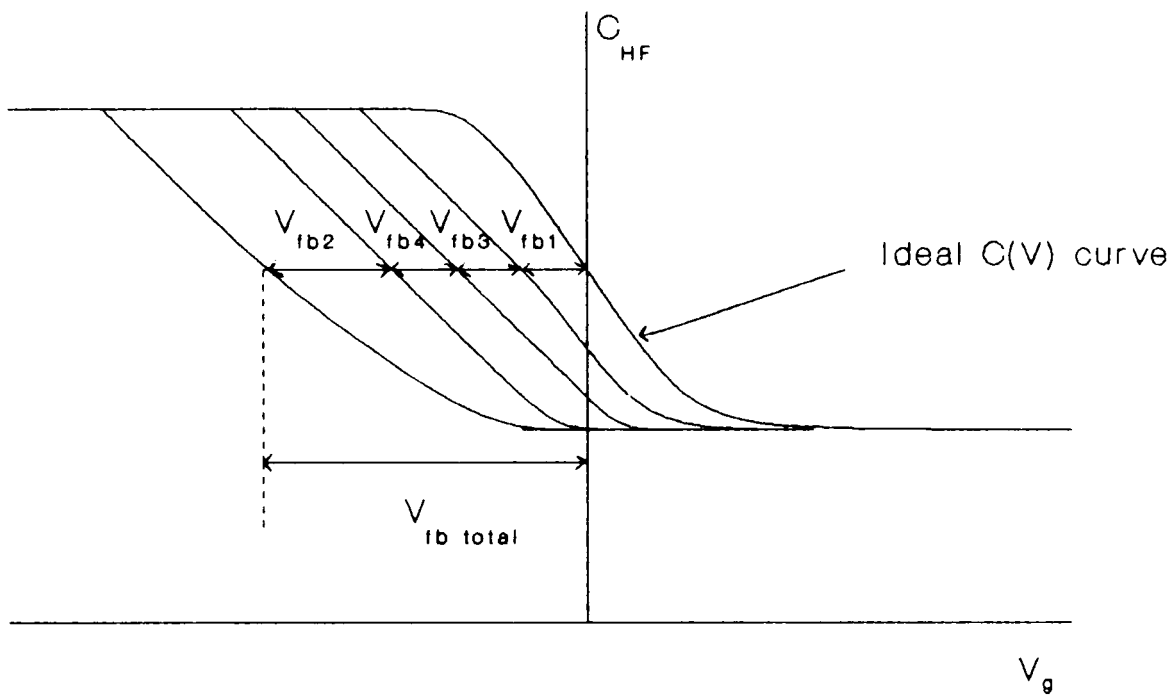

(a) $\Phi_M \neq \Phi_S \longrightarrow V_{fb1}$

(b) $Q_{it} \neq 0 \longrightarrow V_{fb2}$

(c) $Q_f \neq 0 \longrightarrow V_{fb3}$

(d) $Q_m + Q_{ot} \neq 0 \longrightarrow V_{fb4}$

Fig.2.9 Representation of the C(V) curve of an ideal P-type MOS structure. Additional curves show the shifts introduced by work function difference and various oxide charges.

which lie within the band gap and are originated due to structure [23,24], oxidation-induced defects [25,26], or other defects caused by radiation [27]. Interface trapped charges have been studied over a longer period of time than any of the other charges associated with passivated semiconductors. They were even studied in the early days of germanium; yet they are still the least understood. The interface trapped charges derive their name from the fact that the traps exist on the oxide-silicon interface. These charges in the past have been called surface states, fast states, interface states,..etc. When charge carriers electron\holes occupy these states, they attribute positive or negative charge to the interface depending upon the type of surface state whether donor or acceptor. The charging or discharging of these states depends upon the applied gate voltage. Nicollian and Goetzberger [28] and Brown and Gray [29] have reported data that indicate that the distribution of interface trapped charges across the silicon band-gap typically exhibits peaks near both band edges with a pronounced and uniform minimum occurring near the center of the forbidden region. Brown and Gray [29] have found that, the observed density of interface trapped charges as a function of silicon substrate orientation decreases in the order (111)>(110)>(100).

At high frequency, the presence of interface trapped charges does not modify the value of the overall high frequency capacitance but only the relationship between C and V_g.

This is because the interface traps cannot adjust their charge state fast enough to keep pace with the applied small alternative signal. The capacitance of the structure is equivalent to an ideal capacitance. This type of charge is responsible for a shift of the C_{HF}-V curve with respect to that of an ideal structure, in flat band condition (see Fig.2.9), by a quantity V_{fb2} given by,

$$V_{fb2} = -\frac{Q_{it} t_{ox}}{\epsilon_o \epsilon_{ox}} \qquad (2.13)$$

However, at low frequency, the presence of interface trapped charges modifies both the value of overall low frequency capacitance (whose minimum gets closer to C_{ox}) and relationship between C and V_g. This is because the interface trapped charges have time to adjust their charge states. The capacitance of the structure is now given by

$$\frac{1}{C} = \frac{1}{C_{ox}} + \frac{1}{(C_D + C_{it})} \qquad (2.14)$$

where C_{it} represents the capacitance associated with the interface trapped charges.

Several techniques have been used to measure the density and density-distribution of the interface trapped charges in MOS devices [30]. Most of these techniques are based on the measurement of MOS capacitance such as capacitance-voltage (C-V) method [31,32], deep-level-transient-spectropy (DLTS)

This is because the interface traps cannot adjust their charge state fast enough to keep pace with the applied small alternative signal. The capacitance of the structure is equivalent to an ideal capacitance. This type of charge is responsible for a shift of the C_{HF}-V curve with respect to that of an ideal structure, in flat band condition (see Fig.2.9), by a quantity V_{fb2} given by,

$$V_{fb2} = -\frac{Q_{it} t_{ox}}{\epsilon_0 \epsilon_{ox}} \qquad (2.13)$$

However, at low frequency, the presence of interface trapped charges modifies both the value of overall low frequency capacitance (whose minimum gets closer to C_{ox}) and relationship between C and V_g. This is because the interface trapped charges have time to adjust their charge states. The capacitance of the structure is now given by

$$\frac{1}{C} = \frac{1}{C_{ox}} + \frac{1}{(C_D + C_{it})} \qquad (2.14)$$

where C_{it} represents the capacitance associated with the interface trapped charges.

Several techniques have been used to measure the density and density-distribution of the interface trapped charges in MOS devices [30]. Most of these techniques are based on the measurement of MOS capacitance such as capacitance-voltage (C-V) method [31,32], deep-level-transient-spectropy (DLTS)

[33-35], photocapacitance-transient spectroscopy (PCTS) [36]. Some of them utilize low-frequency-capacitance e.g. C-V method, whereas others utilize high-frequency-capacitance e.g. DLTS and PCTS. The C-V method of analysis has helped to provide qualitative or even semiquantitative measurements in the range of trap-density 10^{10} or 10^{11} cm^{-2}. Comparatively, a fewer methods are developed which make use of the measurement of other electric quantities for studying the interface trapped charges. For example, in conductance method [28] the frequency dependent conductance of a MOS device is used to extract information about its surface states. In charge pumping-method [37-42], measurement of the dc substrate-current is utilized for studying the interface trapped charges. However, the use of the charge-pumping technique is limited only to certain specified MOSFETs.

It is well-known that the interface trapped charge can be neutralized by low-temperature (450 C) hydrogen annealing. Furthermore, its density can be reduced by annealing MOS structure in chlorine ambient [43].

2.4.3 The Fixed Oxide Charge

Fixed oxide charge is positive charge, primarily due to structural defects (oxidation process) in the oxide [44,45]. It is located in the oxide within 25 A of the silicon surface. This fixed oxide charge, which is denoted per unit area by Q_f, differs greatly from the interface trapped charge density in

that its magnitude, for all practical purposes, is not a function of the applied gate voltage or the surface potential in the silicon near the interface because the energy levels of the states associated with this type of charge lie outside the forbidden band gap. Its density is constant even under thermal or electrical stressing, which would normally cause movement of mobile ionic charges. Thus, it is not in any way related to sodium and other ions of mobile charge contamination that might be introduced during device fabrication. The density of fixed oxide charge is not significantly affected by the oxide thickness, or by the type or concentration of doping impurities in the silicon. But, since its origin is related to the oxidation process, then it depends on oxidation ambient and temperature, cooling conditions, and on silicon crystal orientation.

The observed density of the fixed charge N_f as a function of silicon substrate orientation under similar processing conditions decreases in the order (111)>(110)>(100) in approximately the ratio 3:2:1. Typical values of the density of fixed oxide charge, for an optimized fabrication process are below 10^{10} cm^{-2}.

These charges have an impact similar to other oxide charges on the C-V curve. They cause a shift V_{FB} of the C(V) curve with respect to that of an ideal structure as illustrated in Fig. 2.9 and given by

$$V_{fb3} = \frac{Q_f t_{ox}}{\epsilon_o \epsilon_{ox}} \qquad (2.15)$$

In the above formula the fixed oxide charge is considered as a charge sheet located at the oxide-silicon interface.

The fixed oxide charge density can be determined using the high-frequency capacitance-voltage (C-V) technique [46]. Since the density of this type of charges can not be determined unambiguously in the presence of moderate densities of interface trapped charge, it is only measured after a low temperature (450 C) hydrogen treatment which minimizes interface trapped charge density.

2.4.4 The Oxide Trapped Charge

Oxide trapped charges (symbol Q_{ot}) may be positive or negative due to holes or electrons trapped in the bulk of the oxide, similar to interface trapped charges with the only difference that they exist in the bulk [47]. Trapping may be resulted from any phenomenon which either create or inject carriers in the bulk of the oxide such as ionizing radiation (including X-ray, gamma ray, low and high-energy electron irradiation) or avalanche injection. The oxide trapped charges, like the interface trapped charges induced by radiation, could be eliminated by a low temperature (300 C) anneal in an inert ambient.

Either the oxide trapped charge distribution or the total trapped charge and its centroid can be quantitatively determined in the oxide by using the most common methods such as etch-off C-V method [48] or photo I-V method [49-51]. The former method can be investigated by etching off the oxide thickness and measuring either the number of traps in etched-off oxide or the number of traps remaining in the oxide by C-V technique. The latter method is used by DiMaria et al [47] to determine the total oxide trapped charge and the charge centroid. Przewlocki [51] also used this method to determine the trapped charge distribution.

2.4.5 The Mobile Ionic Charge

A mobile ionic charge in thermal oxides were the first charge to be extensively investigated since further studies in the SiO_2 system could not be carried out until the mobile ion level was minimized.

The mobile ionic charge is due to ionic impurities such as Li^+, Na^+, K^+, and possibly H^+. This charge can easily move from one edge to the other of the oxide layer under thermal-electrical stressing, and the resulting movement of charge can result an unwanted instabilities and a change in the electrical device parameters [2,10,12,16,52]

The techniques which can be used to study the effect of

mobile ionic charge and to determine its density, are discussed in chapter 3.

The effect of ionic drift which is caused by electric field, can be effectively minimized in a number of ways. The most commonly employed approach is to eliminate, through the use of ultra-clean processing techniques, as much ions to contamination in the oxide as possible. For example, great care must be taken to keep the quartz walls of the furnace in which the oxide is grown virtually sodium free. Krieglar et al [53] have reported that a mixture of hydrogen chloride gas and dry oxygen is extremely effective for the "cleaning" of quartz furnace tubes. They also found that the addition of a small percentage of hydrogen chloride or chlorine to the oxidizing atmosphere significantly improved the electrical stability of SiO_2 films grown in the presence of dry oxygen. They found that this technique not only decreases the mobile ion contamination originating from the furnace tube, but also tends to passivate the oxide films grown in this manner against ionic instabilities caused by the subsequent deposition of a contaminated metalization layer. By using radioactive tracers, Yon et al [54] showed that sodium ions tend to be much more soluble in the phosphosilicate glass than in the oxide below and consequently are gettered by the glass layer, thus preventing them from drifting across the oxide under the influence of the applied gate voltage.

2.4.6 Effect of the Charge Distributed in the Oxide

Whether they are due to mobile ions or to traps, oxide charges are distributed unevenly in the bulk, that is their density $\rho(x)$ varies with distance (and also with time in case of time-dependent stress).

To study the influence of a charge distribution on the properties of the MOS structure, at first, the effect of only those charges which are located in a layer between x and x+dx is calculated. The origin of the X-axis is taken at the metal-oxide interface as shown in Fig. 2.10.

In a second step, the effect of the various layers from zero to t_{ox} are added. Using Gauss`s law, the electric field in the oxide E_{ox} exhibits a discontinuity δE_{ox} when crossing this charge layer. This discontinuity is given by

$$\delta E_{ox} = \frac{\rho(x)dx}{\epsilon_0 \epsilon_{ox}} \qquad (2.16)$$

For ensuring flat band condition in the silicon, E_{ox} must be zero on the right hand side of the discontinuity. Thus the profile of the electric field should be such as shown in Fig.2.10b and the corresponding gate voltage which ensures flat band conditions is given by:

$$\delta V_{fb4} = -\frac{\rho(x)x dx}{\epsilon_0 \epsilon_{ox}} \qquad (2.17)$$

Using a classic result of electrostatics, namely the

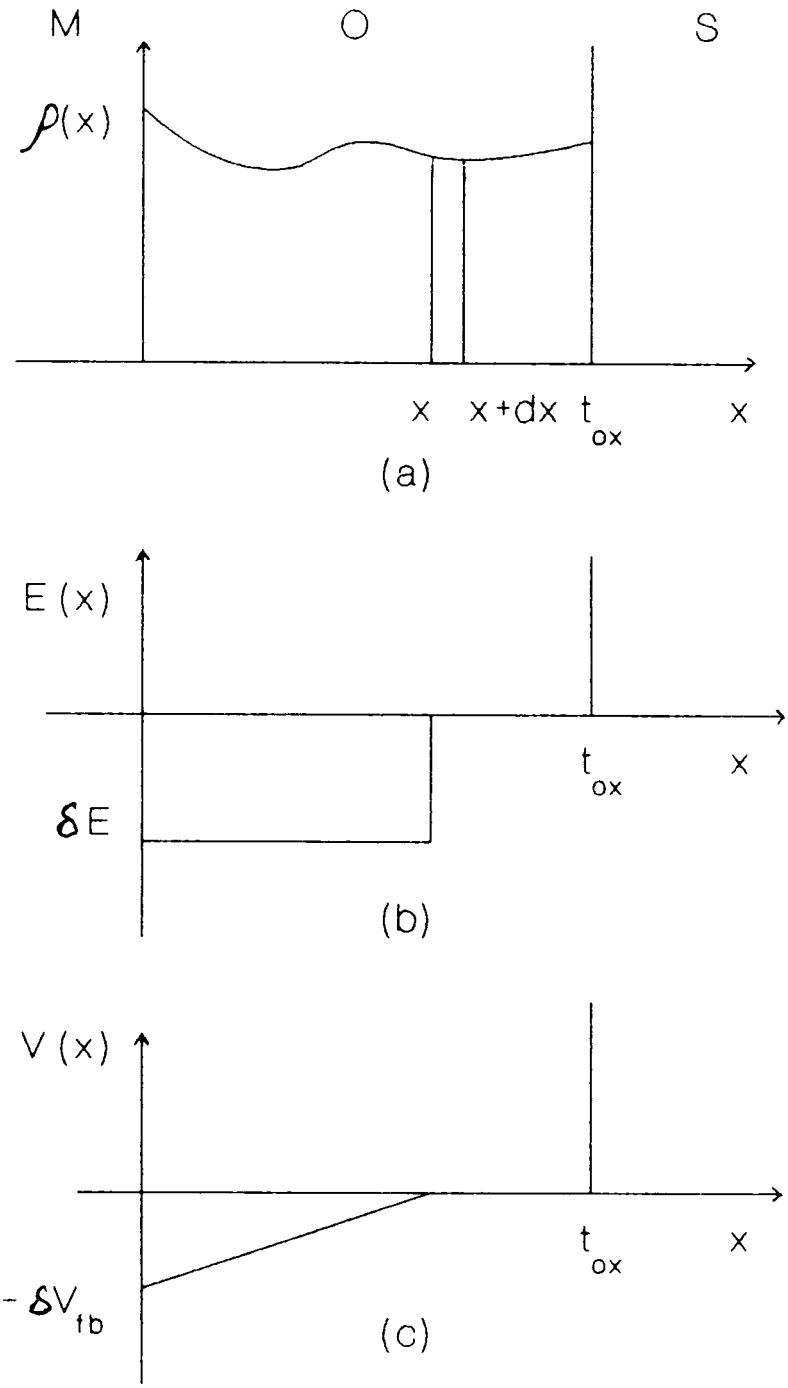

Fig. 2.10 Distribution of (a) charge, (b) field and (c) potential within the oxide of MOS structure.

superposition theorem, the effects of all layers comprised between zero and t_{ox} are added and the gate voltage V_{fb4}, which is necessary to ensure a flat-band condition at the Si-SiO_2 interface, is found to be

$$V_{fb4} = -\int_0^{t_{ox}} \frac{\rho(x)x\,dx}{\epsilon_0 \epsilon_{ox}} \qquad (2.18)$$

The effect of each charge layer depends on its distance from the oxide-silicon interface as can be seen in Eq.(2.17). A layer has no effect if it is located at the metal-oxide interface and has a maximum effect if it is located at the oxide-silicon interface.

If the charge contained in the oxide is only due to mobile ions Q_m a change in the distribution, caused by an applied stress (temperature + electric field), gives rise to a new value of V_{fb4}. This effect can be used to calculate the total amount of mobile ions or the density distribution of mobile ions.

If the charge contained in the oxide is only due to trapped charges a change in the distribution due to an excitation (temperature, photons) causes also a shift in the V_{fb4} value. This effect can be used to calculate the total trapped charge in the oxide.

THE MEASUREMENT TECHNIQUES OF THE MOBILE IONS

3.1 Introduction

The electrical methods, such as bias thermal stress (BTS) [11,15,54] and triangular voltage sweep (TVS) [55-61], which have been described in section 2 and 3 respectively, are the most sensitive methods to detect and measure sodium ions concentration. However, BTS technique is most commonly used because of its simplicity in use and analysis.

Recently another method called thermally stimulated ionic current (TSIC) method [62-66] is developed which is useful mainly for research studies of ion emission from the silicon and the gate electrodes. This is discussed further in section 4.

3.2 BTS Technique

In the BTS experiment, the usual high frequency C-V measurements under bias-temperature stress are used to determine the mobile ions concentration within the oxide layer in MOS capacitor. The high frequency (usually 1 MHz) C-V curve of

the given MOS capacitor is first measured before applying any stress. Then the MOS capacitor is heated to a certain temperature up to 300 C and held there for a period upto 30 min, which is long enough to ensure that all the available ions at the given temperature drift completely across the oxide. At the same time a positive gate bias is applied which is enough to produce an oxide field of a few MV/cm. After holding the MOS capacitor at elevated temperature and high field for the required period, it is cooled back to room temperature so that no further redistribution of charge takes place during the second C-V curve measurement. The flat band voltage shift between the C-V curve before and after bias-temperature drift is a measure of the mobile ion concentration drifted at the given temperature. Typical values in BTS experiments are a stress temperature of 200 to 250 C, a stress time of the order of 20-30 minutes, and a stress voltage which causes a field in the oxide of 1 to 2 MV cm^{-1}.

The experimental set up for measuring the high frequency C-V curves using BTS technique is shown schematically in Fig.3.1.

3.2.1 Determination of the Flat-Band Voltage

The BTS method is carried out by measuring the shifts in the flat-band voltage V_{FB}. A more reliable estimate of V_{FB} is obtained from the portion of high frequency C-V curve corresponding to depletion. The measurement of V_{FB} from the C-V curve, needs be carried out at the flat-band capacitance C_{FB}.

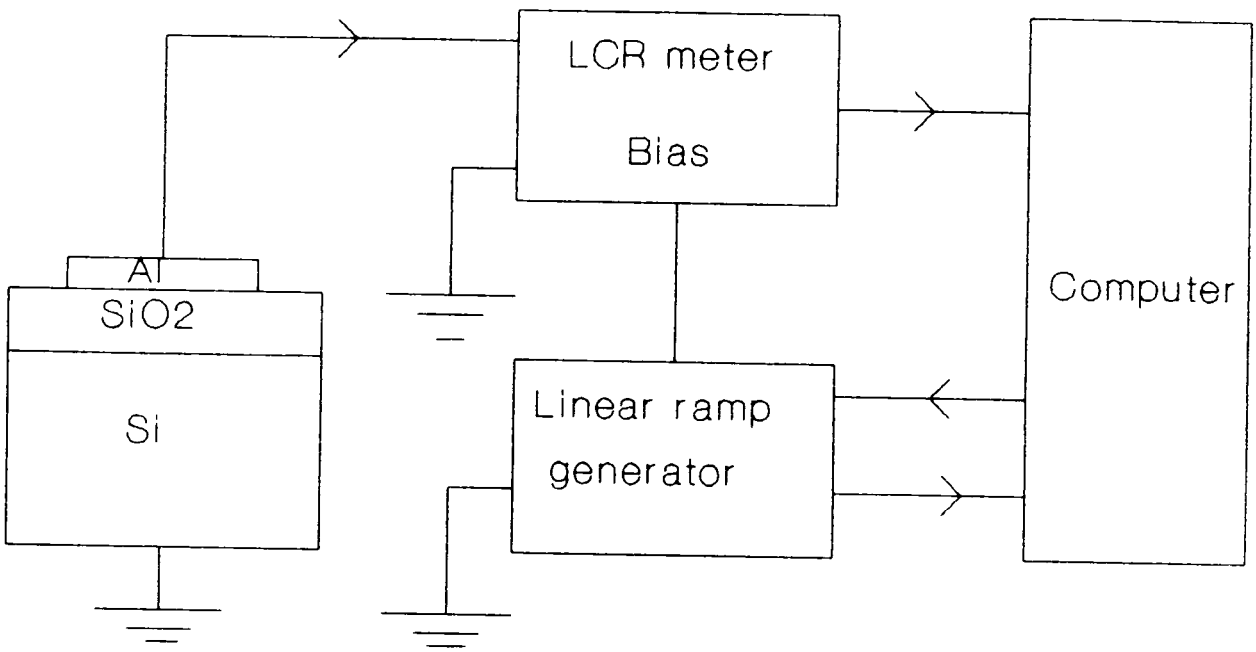

Fig.3.1 Experimental setup to measure C-V characteristics of MOS structure by using BTS technique.

As the name indicates, the flat-band capacitance C_{fb} is the capacitance of the MOS structure when the energy bands are flat near the Si-SiO_2 interface and has the following relation with the oxide capacitance:

$$C_{fb} = \frac{C_{ox} C_{fbs}}{C_{ox} + C_{fbs}} \quad . \tag{3.1}$$

The silicon flat-band capacitance C_{fbs} is given by

$$C_{fbs} = \frac{A \epsilon_0 \epsilon_s}{L_D} \quad , \tag{3.2}$$

Where A is the gate area, ϵ_s the relative permittivity and ϵ_0 the permittivity of the free space. The extrinsic Debye length L_D can be expressed in terms of the substrate doping concentration N_A as follows:

$$L_D = \sqrt{\frac{kT}{q^2 N_A}} \quad , \tag{3.3}$$

Where k is the Boltzmann constant, q the electron charge and T the temperature in Kelvin. The gate voltage corresponding to the flat-band capacitance on the high frequency C-V curve is the flat-band voltage as shown in Fig.3.2.

The results of mobile ion density as obtained by the measurement of the flat-band voltage shift δV_{fb} under bias-temperature ion drift are quite reliable and are not affected by any error in the measurement of V_{fb} which may be caused due to trap level density at Si-SiO_2 interface. It is so because in high frequency C-V curves the trap level density

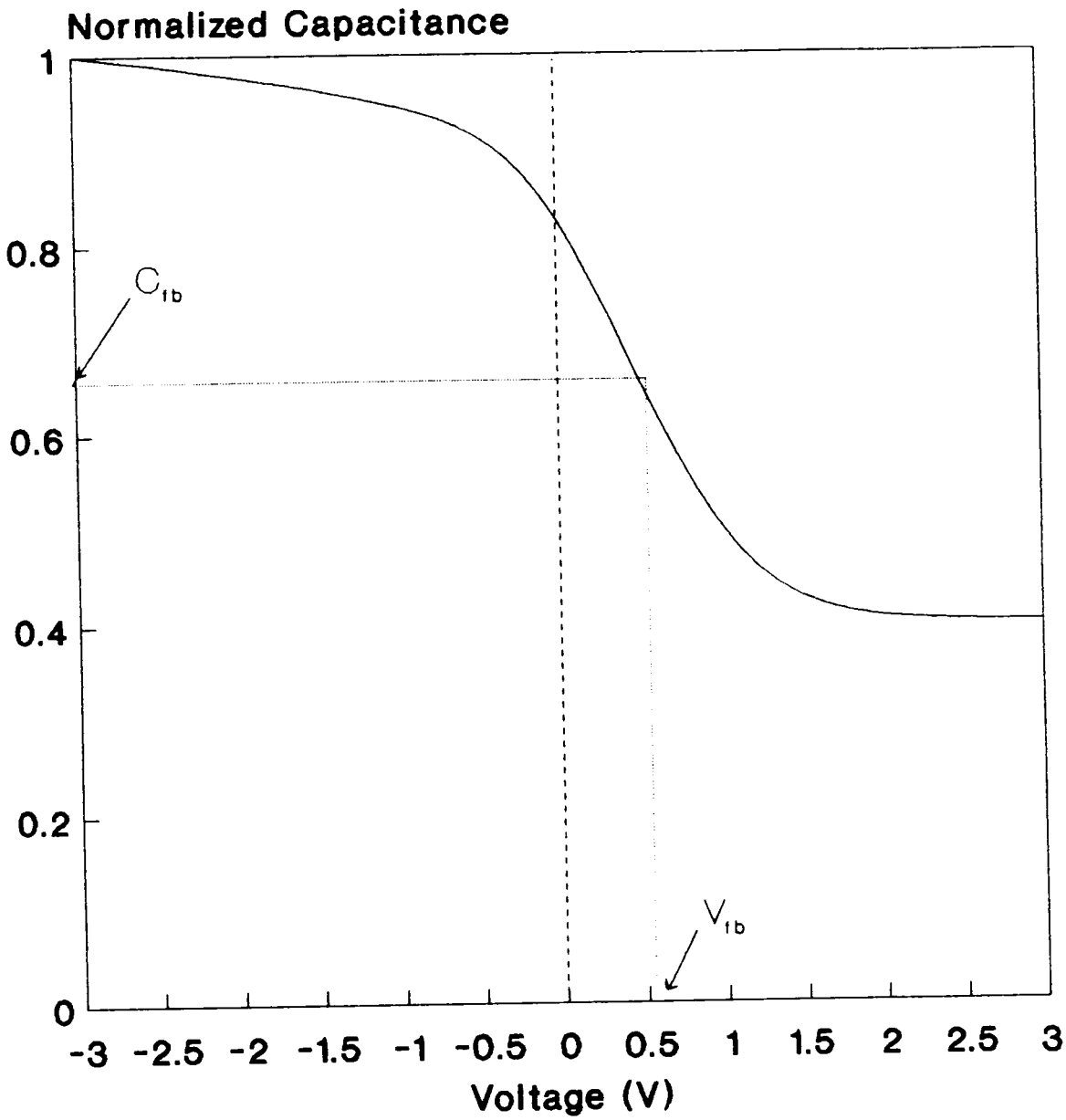

Fig.3.2 Flat band voltage determination by using high frequency C-V curves.

is not supposed to undergo any significant change and any error in the measurement of V_{FB} due to trap levels, remaining constant before and after the application of bias temperature, cancels out in the determination of δV_{fb}. As the bias-temperature treatment causes negligible changes in interface trap level density, the C-V curves before and after bias-temperature drift are parallel to each other. Then the flat band voltage shift is simply the parallel voltage shift. It may be noted that the shift in flat band voltage has a lower value when the same amount of ions is present in a thinner oxide.

For current IC fabrication processes, a flat-band shift of 50 mV is acceptable which in a technology using a 100 nm oxide thickness corresponds to an ionic density of about 10^{10} ions.cm^{-2}. In several contaminated wafers, flat band shifts of several volts may be encountered.

3.2.2 How the Mobile Charge Effect can be Separated

In the case of a real structures the shift in the flat-band voltage is due to the sum of the effects of oxide charges and the work function difference (see chapter 2). This section presents how to distinguish between flat-band voltage shift due to mobile ionic charge and those due to the other types of oxide charge.

Considering an experiment where the only oxide charge is oxide fixed charge, the initial high frequency C-V curve is labelled (o) in Fig.3.3a. After heating at 180 C for half an

hour with a positive gate bias (with respect to substrate) producing a field of a few million volts per centimeter across the oxide, and cooling back to room temperature, the curve labelled (+) in Fig.3.3a is obtained. Repeating the bias-temperature stress with negative gate bias yields curve (-) in Fig.3.3a. Figure 3.3a shows that no shift in the C-V curve is produced. Therefore the oxide fixed charge distribution does not change under this treatment.

Repeating this bias temperature stress experiment with oxide trapped charge of the type that anneals out at low temperature, curves (o), (+), and (-) in Fig.3.3b show that the oxide trapped charge density is reduced. Gate bias polarity has no effect. Therefore, it is most likely that the oxide trapped charge centers are immobile.

Finally, Fig.3.3c shows the results of repeating this experiment on an oxide contaminated by mobile ions. Initially V_{FB} is low, and after positive bias stress it increases. With negative bias stress, V_{FB} returns to its original value. These results are attributed to mobile ion movement that alters the flat-band voltage.

3.2.3 Theory

By assuming all the contaminated mobile ions to be concentrated in a thin charge sheet at either the metal-oxide or the silicon-oxide interface, Eq.(2.18) can be used to

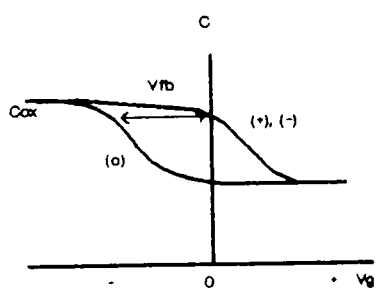

Vfb = Qot/Cox

(b)

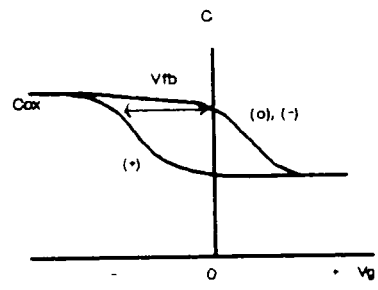

Vfb = Qm/Cox

(c)

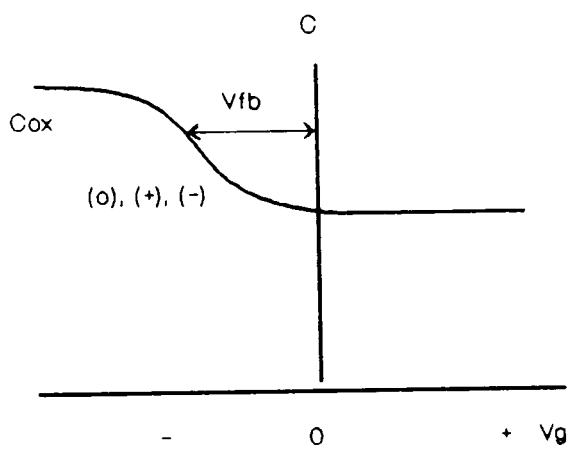

Vfb = Qf/Cox

(a)

Fig. 3.3 Diagram illustrating how mobile ionic charge can be distinguished from the other oxide charges by using a BTS experiment. (o) denotes the initial C-V curve, (+) after positive bias stress, (-) after negative bias stress.

calculate charge density from the flat band voltage shift after introducing an average distance $\overline{X}$ called the centroid of the charge distribution. The charge centroid is defined by

$$\overline{X} = \frac{\int_0^{t_{ox}} x\rho(x)dx}{\int_0^{t_{ox}} \rho(x)dx} \qquad (3.4)$$

In addition the total quantity of ions Q_{tot} is supposed to remain constant within the oxide before and after the drift and is given by

$$Q_{tot} = \int_0^{t_{ox}} \rho(x)dx \qquad (3.5)$$

With the help of Eq.(3.5), Eq.(3.4) becomes

$$\overline{X}Q_{tot} = \int_0^{t_{ox}} x\rho(x)dx \quad . \qquad (3.6)$$

From equations (2.18) and (3.6), the flat band-voltage shift V_{fb4} can be written as

$$V_{fb4} = \frac{\overline{X}Q_{tot}}{\epsilon_o \epsilon_{ox}} \quad . \qquad (3.7)$$

Since mobile ions can be considered as sheet of charge located at the Si-SiO_2 interface, Q_{tot} is obtained directly from a measurement of V_{fb} because the centroid is taken to be the

oxide thickness (within about 3 nm or less). For this case, Eq.(3.7) becomes

$$V_{fb4} = -\frac{t_{ox} Q_{tot}}{\epsilon_o \epsilon_{ox}} = -\frac{Q_{tot}}{C_{ox}} \qquad (3.8)$$

3.3 TVS Technique

A fast, simple and very sensitive technique is TVS method which is capable of detecting better than 10^8 mobile ions/cm^2 and is based on the measurement of the displacement current response to a slow linear ramp voltage at elevated temperatures. This yields an ionic displacement current peak whose area is proportional to the total mobile ionic charge. This method has been independently developed by Yamin [55] and Chou [56] who have tested and confirmed its validity using the simpler and electrochemically symmetrical Si(poly)-SiO_2-Si(100) MOS structure. This technique is expected to be very useful for routine process and quality control applications. Further more it has been used to study positive mobile charge behavior in oxide [55,57-59].

The experimental setup for performing mobile ion drift measurements using TVS technique is shown schematically in Fig.3.4. Figure 3.5 shows the variation of applied voltages (gate voltage varies linearly with time).

In the TVS technique the starting conditions are as follows: all mobile ions are initially at one of the interfaces, they are not trapped, but virtually free to move because the

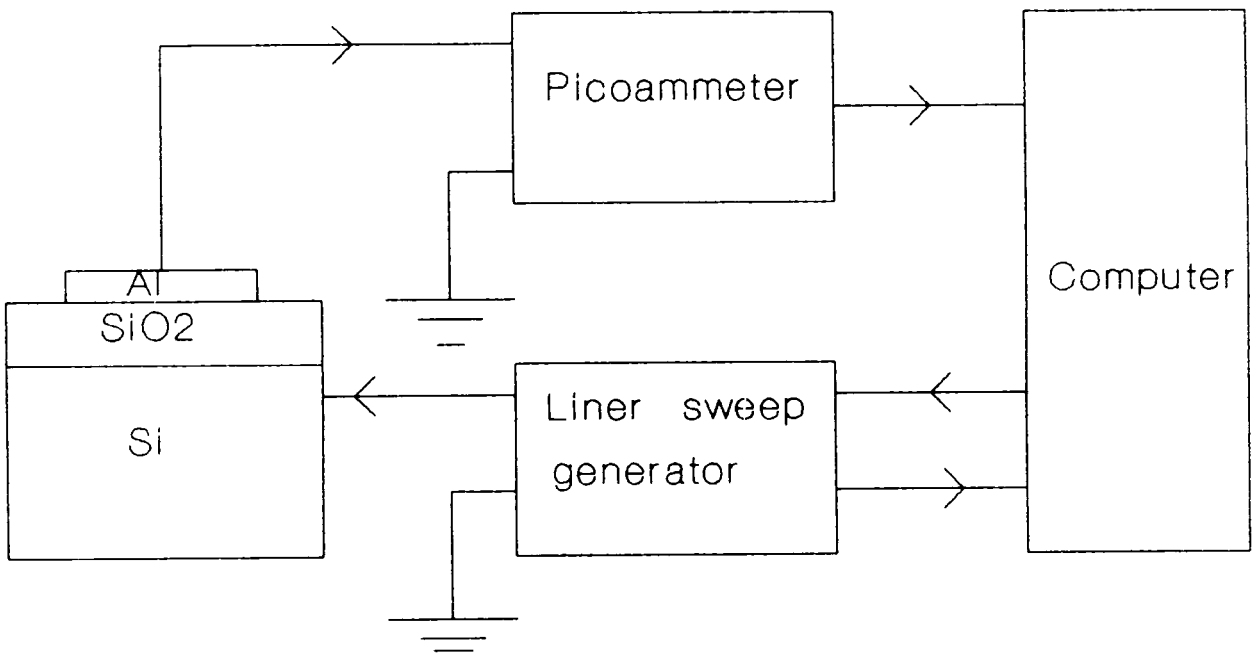

Fig.3.4 Experimental set up to record ionic current through oxide by using TVS technique.

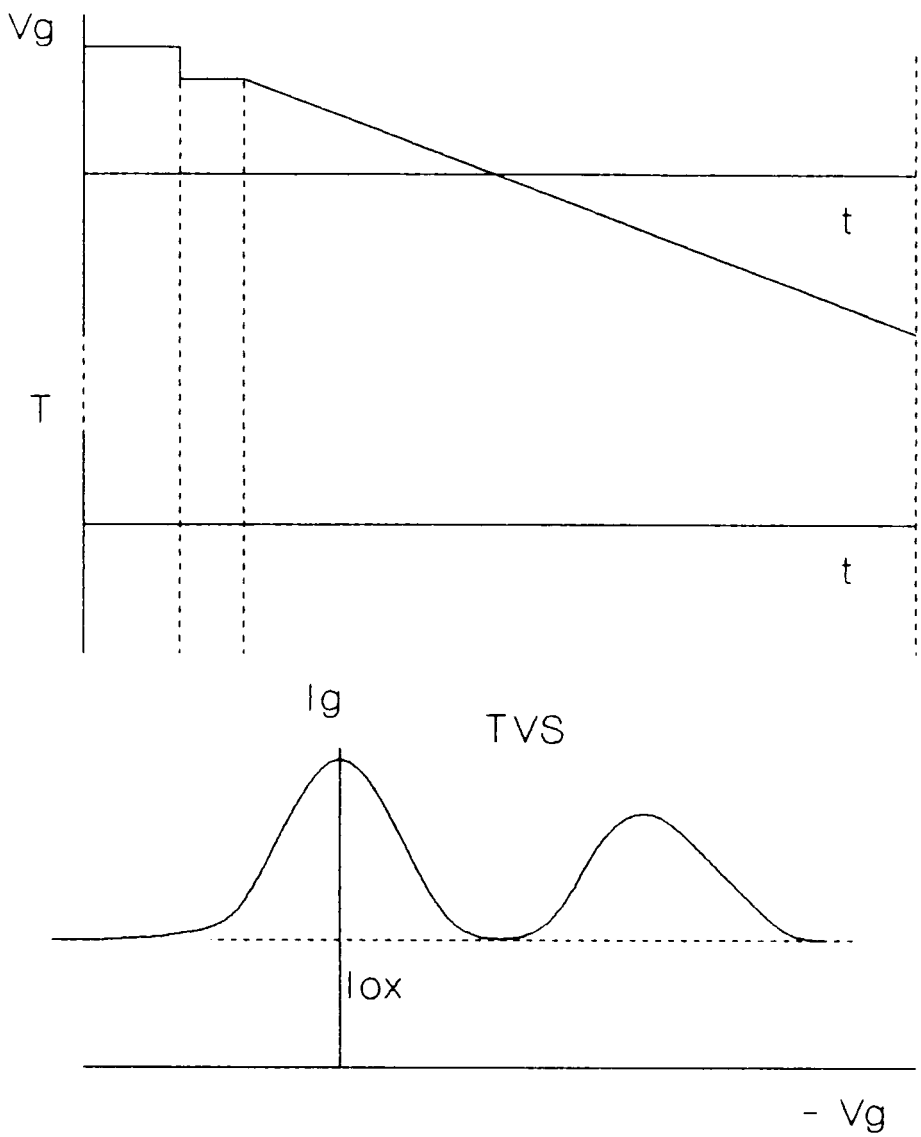

Fig. 3.5 Variations of applied gate voltage during TVS technique.

MOS capacitor is brought to elevated temperature. The triangular ramp voltage which should be applied to the gate, is defined by

$$V_g = V_o + \alpha t \qquad (3.9)$$

Where t is time and $\alpha = \frac{dV}{dt}$ is sweep rate. A resulting gate current is measured against gate bias as the mobile ions drift from one interface to the other. Two modes can be distinguished: the quasistatic and non-quasistatic mode. In the *quasistatic* mode, the sweep rate α is chosen low enough during the entire measurement. The recording gate current is then similar to the quasistatic C(V) curve since

$$I_g = \frac{dQ_g}{dt} = \left(\frac{dQ_g}{dV_g}\right)\left(\frac{dV_g}{dt}\right) = \alpha C(V_g) \qquad (3.10)$$

Where $C(V_g)$ is the differential capacitance. But in the *non-quasistatic* mode, the sweep rate is high, and the ions can not follow the change in the applied field. In this situation the TVS technique can be used either to determine accurately the number of ions which cross the oxide or to determine the mobility of the ions [67,68].

The idealized gate current response as function of applied bias with and without mobile ionic charge is shown in Fig.3.6. At room temperature the mobile ions are firmly trapped near the interfaces. In this situation, the observed I(V) curve is strictly similar to a quasistatic C(V) curve as shown in curve (a). At higher temperatures (typically about 300 C) and if no

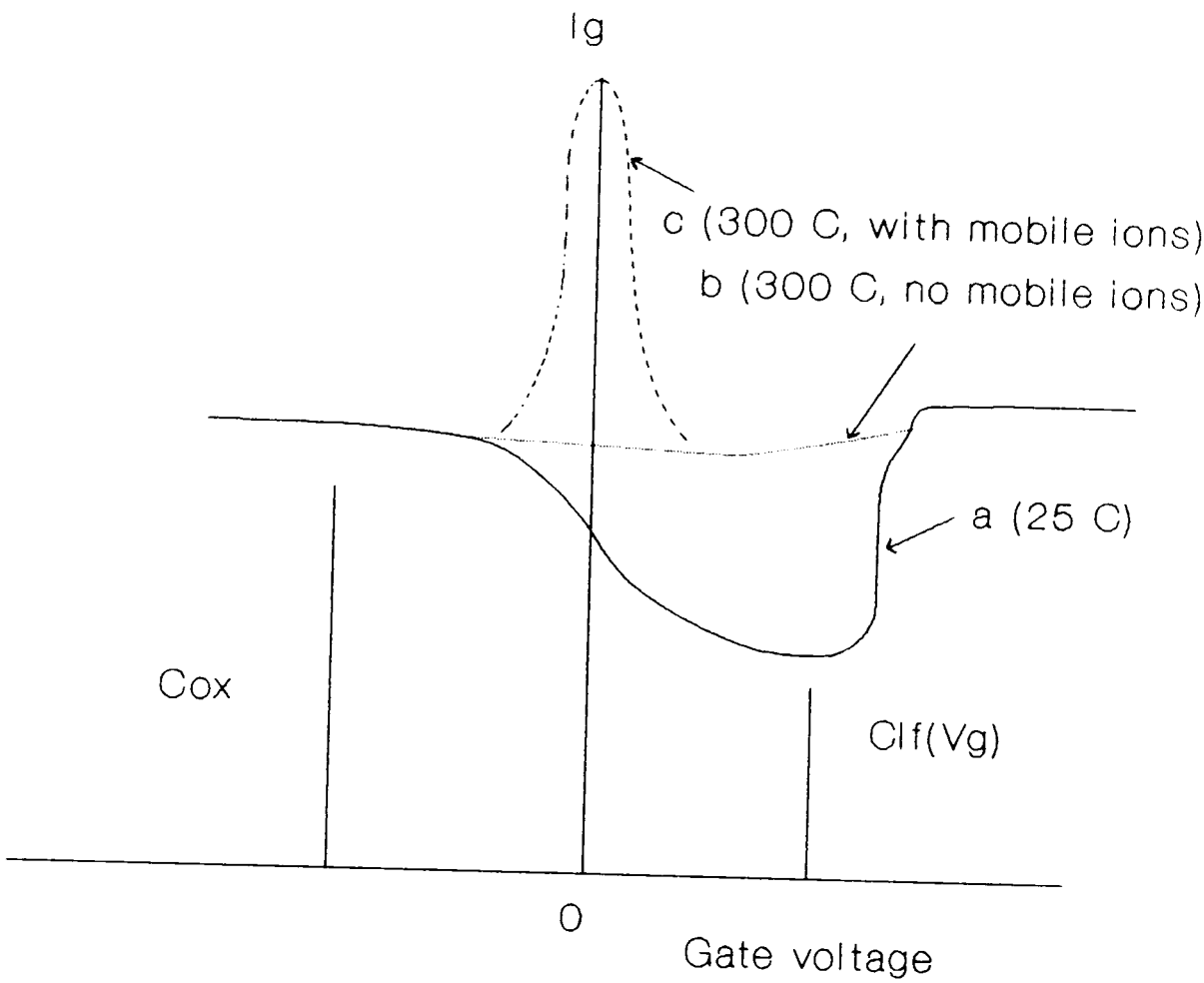

Fig.3.6 Idealized gate current as function of gate bias in a MOS capacitor having a P-type substrate.

mobile ions are present, a quasistatic I(V) curve is obtained again, due to nearly constant value of capacitance equal to C_{ox} as shown in curve (b). If mobile ions are present, they contribute an additional component to the charging current of the MOS capacitor as shown in curve (c).

The peak in the current of curve (c) arises as follows. At large negative gate bias all the mobile ions are at the metal-oxide interface, and the gate current that flows is proportional to C_{ox}. As gate voltage increases, mobile ions begin drifting toward the Si-SiO_2 interface, attracting an increasing number of electrons to the silicon surface. That is, the ionic movement causes extra electrons to flow from the gate to the silicon through the external circuit, increasing thereby the gate current. This excess current peaks when the largest number of mobile ions is crossing the oxide layer. As gate voltage is increased further, mobile ions pile up at the Si-SiO_2 interface. Consequently fewer ions flow, and the excess gate current falls. Ultimately, all the mobile ions that will drift at the given temperature have piled up at the Si-SiO_2 interface. At this stage the gate current again becomes proportional to C_{ox}.

3.3.1 Theory

The mobile ion density drifted at a given temperature is proportional to the area under the peak in the gate current

caused by the ionic motion. To show this, the current per unit area I_g may be defined as

$$I_g = \frac{dQ_g}{dt} \tag{3.11}$$

Where Q_g is the gate charge which is given by

$$Q_g = C_{LF}(V_g - V_{fb}) \tag{3.12}$$

where $C_{LF}(V_g)$ is the low frequency MOS capacitance per unit area which is approximately equal to C_{ox} at elevated temperatures as shown in Fig.3.6.

Substitution of Eq.(3.12) in Eq.(3.11) gives

$$I_g = C_{LF}(V_g)\frac{d(V_g - V_{fb})}{dt} \tag{3.13}$$

Equation (3.13) can be rewritten as

$$I_g = C_{ox}\left(\alpha - \frac{dV_{fb}}{dt}\right) \quad . \tag{3.14}$$

where α is the constant voltage sweep rate. Integrating from a gate bias $(-V_g)$ to a gate bias V_g, Eq.(3.14) gives

$$\int_{-V_g}^{V_g}(I_g - \alpha C_{ox})dV_g = -C_{ox}\int_{-V_g}^{V_g}\left(\frac{dV_{fb}}{dt}\right)dV_g,$$

$$= -\alpha C_{ox}\int_{t(-V_g)}^{t(V_g)}\left(\frac{dV_{fb}}{dt}\right)dt$$

$$= -\alpha C_{ox}\{V_{fb}[t(V_g)] - V_{fb}[t(-V_g)]\} \quad . \tag{3.15}$$

The integration over gate bias on the right of Eq.(3.15) is carried out with respect to time. The integral on the left of

Eq.(3.15) is the area between the $I_g(V_g)$ curve and the straight line $I_g = \alpha C_{ox}$, representing the gate current of the MOS capacitor when no ions move. The right side of Eq.(3.15) can be evaluated by using Eq.(3.7). Considering the mobile charge centroid to be located at $\bar{X}(-V_g)$ at time $t(-V_g)$ and $\bar{X}(V_g)$ at time $t(V_g)$, it can be shown that

$$V_{fb}[t(V_g)] - V_{fb}[t(-V_g)] = \frac{qN_m}{\epsilon_o \epsilon_{ox}}[\bar{X}(V_g) - \bar{X}(-V_g)] \quad (3.16)$$

where N_m is the mobile ionic charge density per unit area. Therefore, Eq.(3.15) becomes

$$\int_{-V_g}^{V_g} [I_g - \alpha C_{ox}] dV_g = \alpha q N_m \left[\frac{\bar{X}(V_g)}{t_{ox}} - \frac{\bar{X}(-V_g)}{t_{ox}} \right] \quad (3.17)$$

For most values of bias and time, the centroids in Eq.(3.17) are bias and time independent. Consequently, Eq.(3.17) shows that for linear voltage ramp, at which temperature is enough to make $C_{LF}=C_{ox}$, the area under an $I_g(V_g)$ curve in excess of $I_g = \alpha C_{ox}$ is proportional to mobile ion density per unit area.

To use Eq.(3.17) to estimate N_m, one ordinarily assumes $\bar{X}(V_g) = t_{ox}$ (all positive ions drifted to the silicon surface) and $\bar{X}(-V_g) = 0$ (all ions drifted to the gate). These assumptions probably are valid to within 10 nm.

3.3.2 Earlier Investigation

Experimental determination of $I_g(V_g)$ curves have been carried out [57] which employ TVS technique. In such experiments a heavy contaminated oxide with mobile ions is used. A

typical $I_g(V_g)$ curves at 202 C is given in Fig.3.7. The sweep from positive to negative gate bias, when ions drift from the $Si-SiO_2$ interface to the metal-oxide interface, is shown in the upper curve. The voltage sweep from negative to positive, when ions drift from the metal-oxide interface, is shown in the lower curve. The area of the peak above the C_{ox} baseline corresponds to 2.5×10^{12} ions/cm^2.

The most striking feature of these curves is the strong asymmetry of the $I_g(V_g)$ curves in the two directions of the voltage sweep. The ionic current response, when sweeping from the negative to positive gate bias, is distorted and broadened over the entire positive voltage range, and results in a very broad peak as shown in the lower curve of Fig.3.7. This clearly indicates that ion transport is independent of a transport mechanism limited by the emission from ionic traps located at the metal-oxide interface. The area under both peaks in Fig.3.7 are identical so that all ions transported to metal-oxide interface can be brought to the silicon-oxide interface by changing the polarity of the voltage ramp. As expected from quasi-equilibrium arguments, the area under the peaks are independent of voltage sweep rate, as long as the rate is sufficiently slow to establish the boundary conditions (the mobile ions are concentrated as a thin sheet of charge at either interfaces).

The temperature dependence of the ionic current response is given in Fig.3.8. The ionic current peak does not saturate

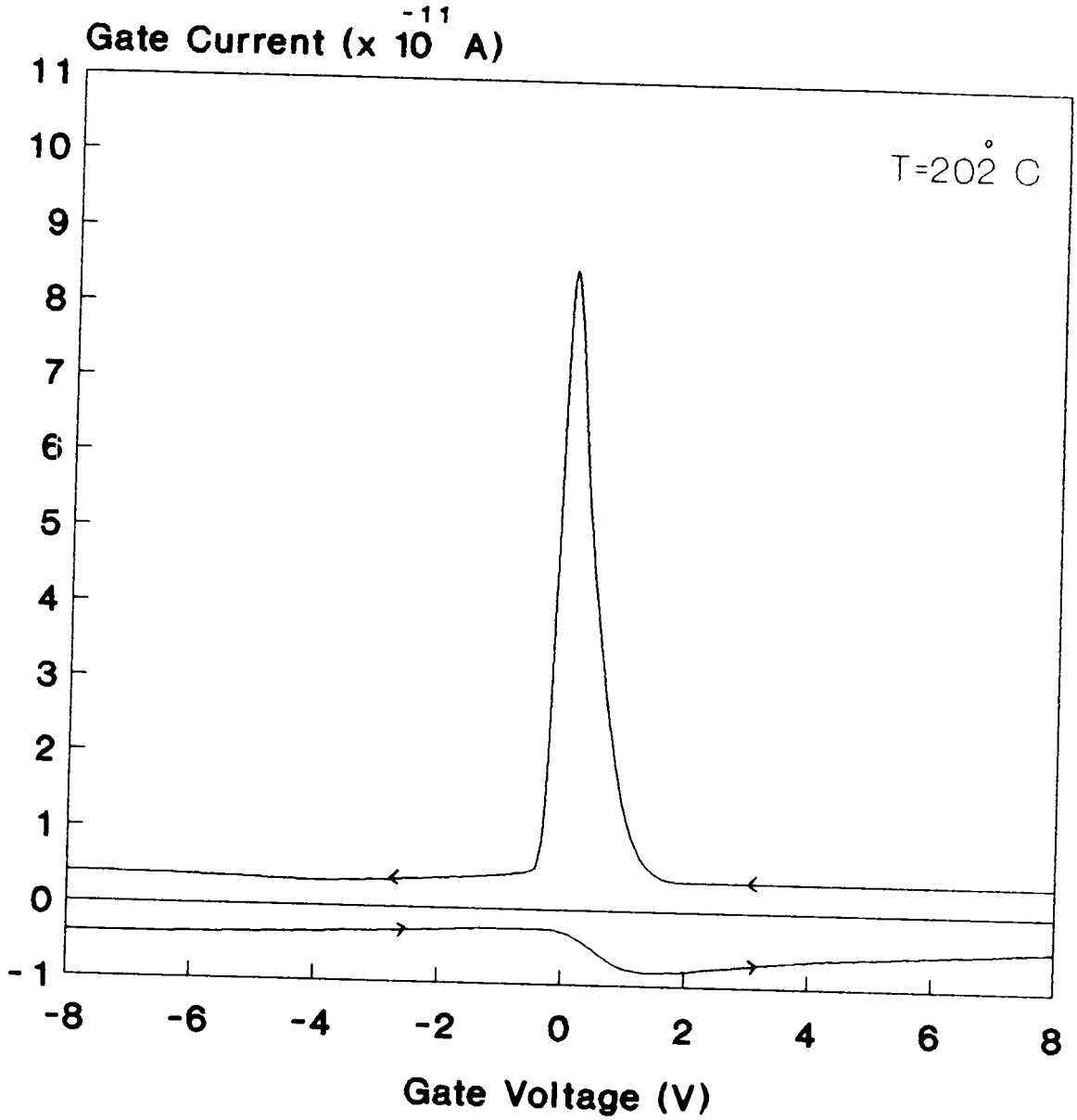

Fig.3.7 Gate current as function of gate voltage for a heavily contaminated oxide. at 202 C. [57]

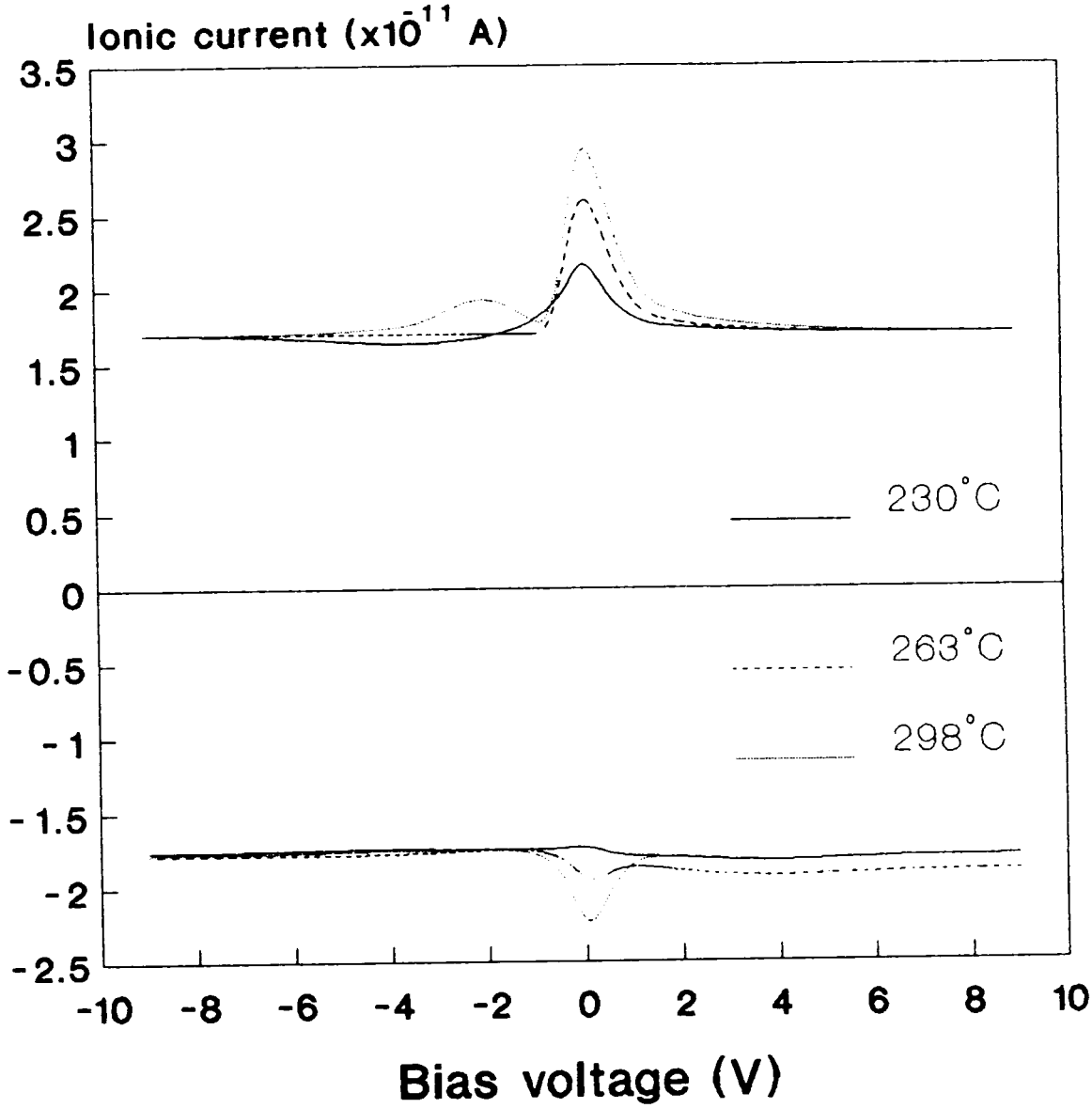

Fig.3.8 Ionic current as function of gate voltage for a heavily contaminated oxide.

but continues to increase with temperature. At low temperature the sweep from negative to positive gate bias yields a broadened structure, resulting from the trapping emission mechanism at the metal-oxide interface. At higher temperatures this peak sharpens and approaches were closely the ideal shape (or the shape of the peak for the opposite sweep) as expected if emission of ions from traps is more rapid at higher temperatures. Furthermore, an additional structure is observed above the C_{ox} baseline at elevated temperature (T=298 C), as shown in the upper trace of Fig.3.8. This structure typically takes the form of a second broadened peak displaced by approximately -2 V from the first peak. This second peak is due to the K^+ ions drift. It can be noted that the peaks due to potassium may not be visible at low temperature. Thus, the TVS technique might provide a simple means for identifying the density of sodium and potasium separately because the peak in the ionic displacement current occurs at a different gate bias [69].

3.4 TSIC Technique

The TSIC technique is usually applied to MOS capacitors which can be brought to an elevated temperature. As the temperature varies as a function of time, the current in the external circuit of the MOS capacitor is measured. In principle, the measured current is a superposition of the charging current of the MOS capacitor, caused by changes in temperature, and the ionic current (the displacement current) caused by moving ions. This ionic current has been studied in the

past by a variety of methods [62]. Boudry and Stagg [65], and Hillen [64] have used TSIC measurements to study the kinetic behavior of mobile ions in MOS structure.

The thermally stimulated currents were always measured after an appropriate BTS treatment (15 min at 350 C and a gate voltage + 5 V). Before measurements at a positive gate voltage the stress voltage is initially kept negative (all ions are then driven to the oxide-metal interface), and for measurements at a negative gate voltage the stress voltage is initially kept positive. The starting temperature of the measurement must be low enough to ensure that reversing the electric field in the oxide will not cause any ionic current, meaning thereby that the ions are deeply trapped near the Si-SiO_2 interface (one usually uses a temperature of -20 C). The experimental setup for measuring TSIC curves is shown in Fig.3.9.

Figure 3.10 shows the variations of the applied temperatures during TSIC experiment, in which ion motion from the Si-SiO_2 interface to the metal-SiO_2 interface is studied. During the current measurement, the temperature varies linearly with time. Typical results obtained on an MOS capacitor having Na^+ and K^+ ions in its oxide layer are also shown in this figure; two current peaks are shown in the temperature range 0-400 C, at a maximum applied field 1 $MV.cm^{-1}$. These peaks are attributed to the motion of Na^+ and K^+ ions respectively.

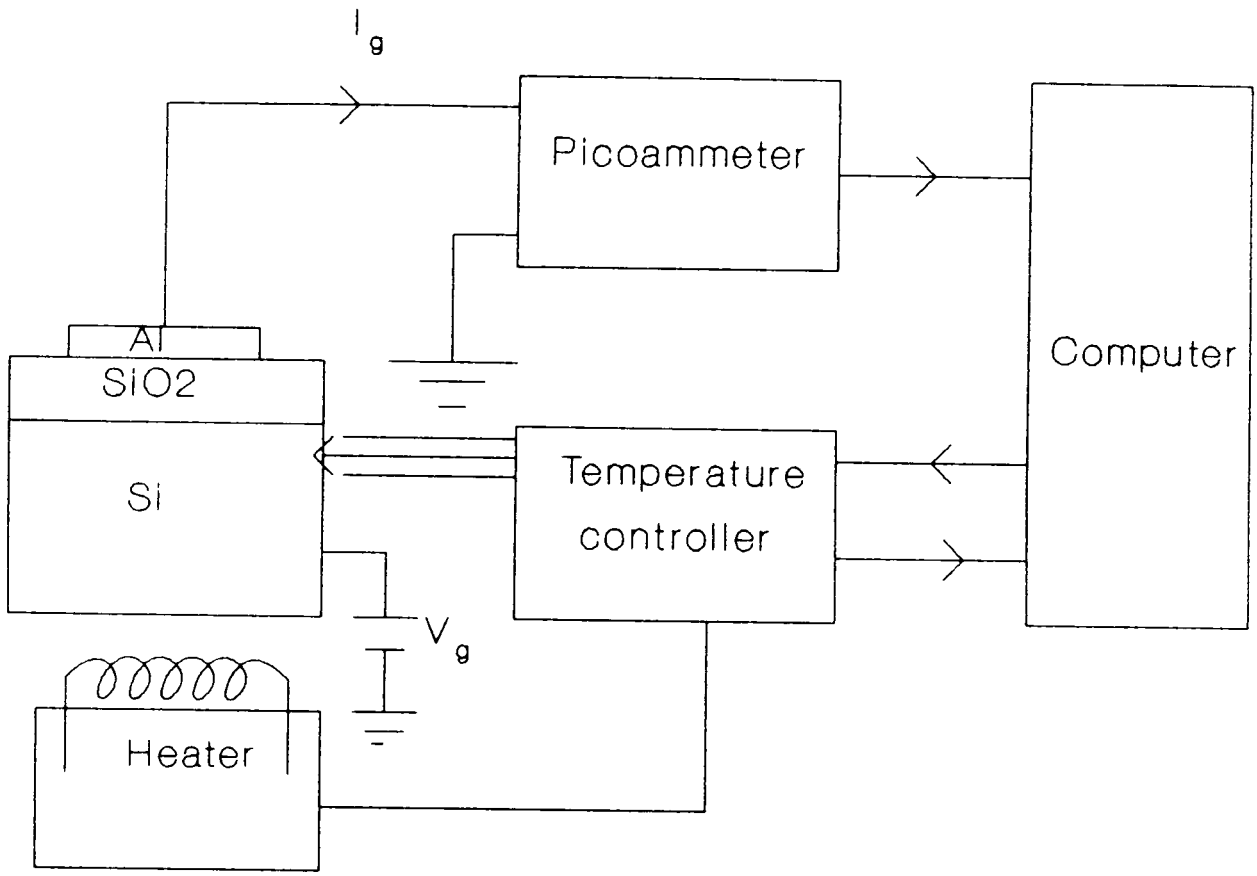

Fig. 3.9 Experimental set up to record ionic current through oxide by using TVS technique.

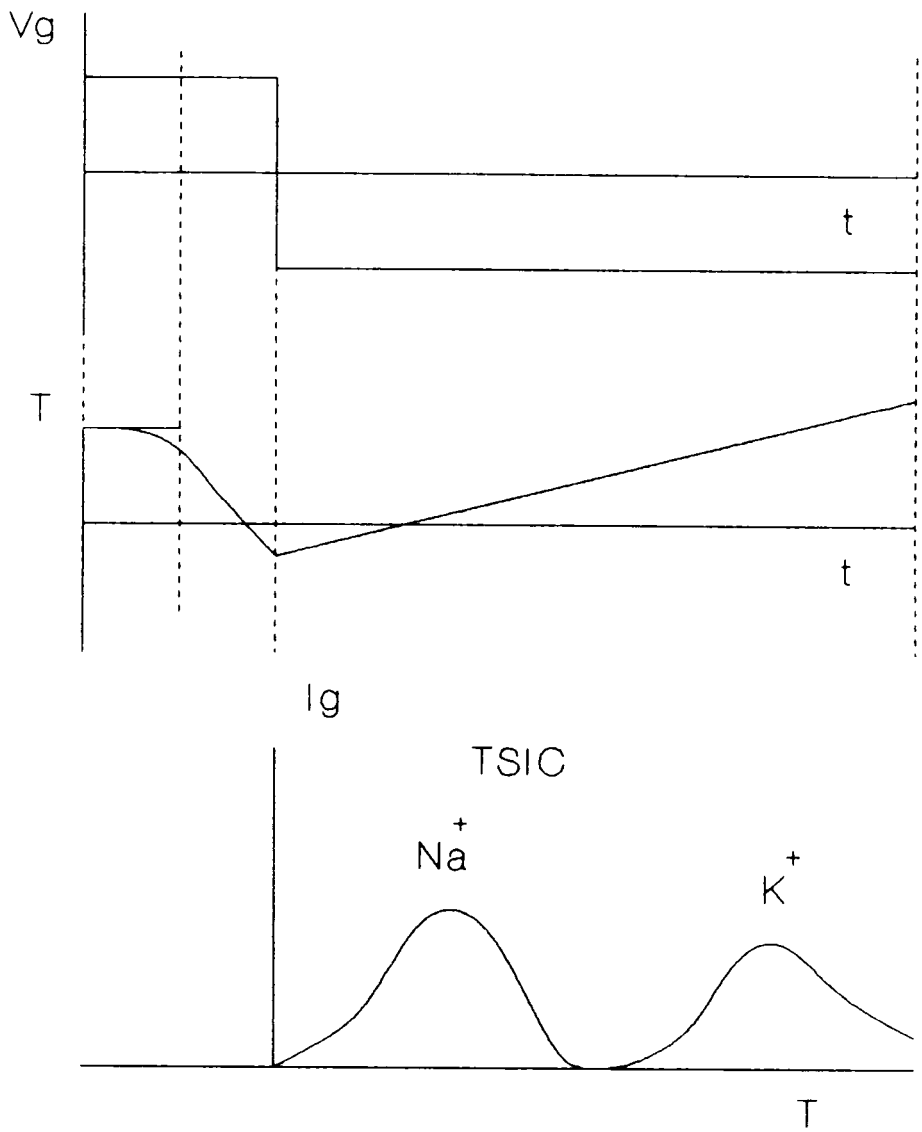

Fig.3.10 Variations of applied gate voltage and temperature during TSIC technique.

3.4.1 Theory

The simplest model which explains the TSIC current states that, once the mobile ions are detrapped after acquiring a sufficient energy they are immediately driven to the other side of the oxide where they are trapped again. Thus the thermally stimulated current is controlled (or *limited*) by the emission mechanisms of the ion traps located at either edge of the oxide layer.

Hickmott [62] explained several TSIC curves using a single level theory. The ionic current is expressed as :

$$I(t) = -qA\frac{dn(t)}{dt} \quad . \tag{3.18}$$

where,

$$\frac{dn(t)}{dt} = -n(t) \;\; S \;\; \mathrm{EXP}\left[-\frac{E_o}{kT(t)}\right] \tag{3.19}$$

and,

$$n = n_o \qquad at \;\; t = 0 \tag{3.20}$$

where n is the number of ions (per unit area) still trapped at time t, E_o the activation energy required to excite an ion from a trap at the emitting interface to a point just outside the trap from which it is free to move through the oxide, A the area of the device, k the Boltzmann's constant, and S a factor which may be roughly interpreted as the number of times per second an ion attempts to leave the trap. Since an ion is

carried away from the interface by the applied field immediately after it has left the trap, it seems reasonable to ignore the possibility of its retrapping in this situation. After taking n_o, E_o, and s as adjustable parameters, Hickmott [62] was able to obtain an adequate fit only to the leading slope and maximum of the negative peak and found E_o to be ranging from 0.7 to 1.2 eV and S from 10^7 to 10^{12}.

The model describes the experimental curves well when a Gaussian spread in the activation value for the emission time constant is assumed (10^{-12} s). Further an activation energy is found that is consistent with an emission-limited process [63,64].

TSIC method in MOS structure complements BTS method for studying the metal-SiO_2 interface [66]. This method is also used by Stagg [70] to identify the drift mobilities of Na^+ and K^+ ions in SiO_2 films.

CHAPTER 4

EARLIER THEORETICAL INVESTIGATIONS ON MOBILE IONS DISTRIBUTION IN INSULATING LAYERS

4.1 INTRODUCTION

The very fact that the mobile ions in the oxide of MOS structures can undergo a drift under the influence of thermal electric stress, led the scientists to form a general belief that these mobile ions can attain an equilibrium density distribution under a given temperature-bias condition. Accordingly a number of attempts [56,59,60,71] have been made to obtain this equilibrium density distribution of mobile ions from theoretical considerations. All these attempts have been made under certain simplifying assumptions and limitations. The simplifying assumptions, which are common to all the theoretical investigations, are:

1) The oxide layer of MOS structure is uniform, and its thickness is small in comparison to the electrode diameter, so that the problem may be considered one dimensional.

2) There is no charge exchange between the oxide layer and

electrodes (ideal blocking electrodes).

3) An uncompensated charge of positive mobile ions exists in the oxide layer. There is no charge generation and recombination in the oxide layer.

4) The changes in the applied electric field are such that the mobile ions are always able to attain their equilibrium distribution.

There are three prominent approaches [56,69,71] which may be considered as the main landmarks in the theoretical development of the subject of mobile ions distribution in the insulating layers. These are reviewed in the following sections.

4.2 Theoretical Approach of Chou

The first theoretical attempt to tackle the problem of the mobile ions distribution in insulating layers was made by Chou [56]. In fact he extended the flux equation which was used earlier by Snow et al [11] for studying the ion transport in insulating films. In the presence of concentration gradient $\partial N/\delta x$ and electric field E in the insulating film, the equation of ions-flux F can be written as

$$F = -D\left(\frac{\partial N(x,t)}{\partial x}\right) + \mu E N(x,t) \qquad (4.1)$$

where D and μ are the diffusion coefficient and drift mobility of the mobile ions at a depth x as measured from the metal-oxide interface. A combination of Eq.(4.1) with equation of

continuity, $\partial N/\partial t = -\partial F/\partial x$, gives the equation governing the time-dependent concentration of ions in the oxide,

$$\frac{\partial N(x,t)}{\partial t} = D\left(\frac{\partial^2 N(x,t)}{\partial x^2}\right) - \mu\left(\frac{\partial E N(x,t)}{\partial x}\right) \qquad (4.2)$$

Under a given applied voltage V_A a static equilibrium of mobile ions is established when $\frac{\partial N}{\partial t} = 0$. Thus

$$D\left(\frac{\partial^2 N(x,t)}{\partial x^2}\right) - \mu\left(\frac{\partial E N(x,t)}{\partial x}\right) = 0 \qquad (4.3)$$

Since the electrodes are blocking, there is no mobile ion now across the boundary and therefore

$$D\left(\frac{\partial N(x)}{\partial x} - \mu E N(x) = 0 \quad for \quad x = 0, t_{ox}\right) \qquad (4.4)$$

Integration of Eq.(4.3) between o and x and application of the boundary condition (Eq.(4.4)) gives the following important differential equation

$$D\left(\frac{dN(x)}{dx}\right) - \mu(E N(x)) = 0 \qquad (4.5)$$

By virtue of the Einstein relationship, $\mu/D = q/kT$, Eq.(4.5) becomes

$$\frac{kT}{q}\frac{dN(x)}{dx} - E N(x) = 0 \qquad (4.6)$$

Standard substitution of y=ln(N(x)) in eq.(4.6) gives

$$\frac{kT}{q}\frac{dy}{dx} - E(x) = 0 \qquad (4.7)$$

and

$$\frac{kT}{q}\frac{d^2y}{dx^2}=\frac{dE(x)}{dx} \tag{4.8}$$

Combination of Eq.(4.8) with Poisson's equation

$$\frac{dE(x)}{dx}=\frac{q}{\epsilon_o\epsilon_{ox}}N(x), \tag{4.9}$$

gives a new differential equation in the ion distribution N(x) as

$$2\frac{d^2y}{dx^2}=\frac{1}{k_1}(N(x)-N_o) \tag{4.10}$$

where

$$k_1=\frac{kT\epsilon_o\epsilon_{ox}}{2q^2} \tag{4.11}$$

Setting $\frac{dy}{dx}$=v, Eq.(4.11) may be reduced to

$$k_1 d(v^2)=(e^y-1)dy \tag{4.12}$$

Using the frequently used relation

$$2\frac{d^2y}{dx^2}=\frac{d}{dy}\left[\left(\frac{dy}{dx}\right)^2\right] \tag{4.13}$$

Eq.(4.12) yields

$$\int_{v_o}^{v}k_1 d(v^2)=\int_{y_o}^{y}(e^y-1)dy \tag{4.14}$$

or

$$k_1 v^2=k_1 v_o^2+e^y-e^{y_o}-(y-y_o) \tag{4.15}$$

or

$$\sqrt{k_1}\frac{dy}{dx}=\left[k_1 v_o^2+e^{y}-e^{y_o}-(y-y_o)\right]^{\frac{1}{2}} \qquad (4.16)$$

Integration of Eq.(4.16) results in

$$\int_{y_o}^{y}\left[k_1 v_o^2+e^{y}-e^{y_o}-(y-y_o)\right]^{-\frac{1}{2}}dy=\frac{x}{\sqrt{k_1}} \qquad (4.17)$$

Equation (4.17) can not be integrated in a closed form. It must be numerically integrated by a trial-and-error scheme. However, even numerically Chou could not solve the differential equation to get any concrete mobile ions distribution curve. Therefore, his investigation can not give any idea about the final solution. Therefore, his analysis remains only suggestive rather than conclusive of giving concrete mobile ion density profiles. Moreover Chou assumed the presence of immobile negative ions in his treatment. Marciniak and Przewlocki [59] elaborate Chou's method by considering only the presence of positive mobile ions but did not add anything more concrete to the solution except for a little different mathematical procedure and analysis to solve the differential equation of Chou.

4.3 Theoretical Approach of Tengena et al

The next theoretical attempt in this direction which needs mentioning is due to Tengena et al [60]. Although they used a different physical idea to obtain the basic equation but the resulting equation is again the same as flux equation used by Chou. Tangena et al argued that under equilibrium

condition of density distribution, the electrochemical potential $\bar{\mu}_{ion}$ of an ion everywhere in the oxide should have the same value so that

$$\bar{\mu}_{ion} = E_o + q(V(x)) + kT \ln\left[\frac{N(x)}{N_o}\right] = const \qquad (4.18)$$

where E_o denotes the energy level of the positive ions in the oxide, q the electron charge, V(x) the electrical potential at x, k the Boltzmann constant, T the absolute temperature and N_o the total density of the energy states which is available for the ions in the oxide. In fact the distribution of energy E corresponding to third term on the right hand side of Eq.(4.18) is supposed to be governed by Boltzmann law so that

$$N(x) = N_o \mathrm{EXP}\left[\frac{-E(x)}{kT}\right] \qquad (4.19)$$

Equation (4.19) provides the value of the third term on the right hand side of Eq.(4.18). Differentiation of Eq.(4.18) gives

$$q\frac{dV(x)}{dx} + \frac{kT}{N(x)}\frac{dN(x)}{dx} = 0 \qquad (4.20)$$

Substituting the electric field E(x) for the negative gradient of the potential, Eq.(4.20) becomes

$$\frac{kT}{q}\frac{dN(x)}{dx} - E(x)N(x) = 0 \qquad (4.21)$$

Equation (4.21) is combined with the Poisson's equation as given in Eq.(4.9). However Unlike Chou [56], Marciniak and

Przewlocki [59], Tangena et al eliminated N(x) in the oxide and got

$$\frac{kT}{q}\frac{d^2E(x)}{dx^2} - E(x)\frac{dE(x)}{dx} = 0 \qquad (4.22)$$

Integration of Eq.(4.22) gives

$$\frac{2kT}{q}\frac{dE(x)}{dx} - E^2(x) = C_1 \quad , \qquad (4.23)$$

where C_1 is an integration constant. Equation (4.23) can be transformed into the following form:

$$\frac{2kT}{q}\int_E \frac{dE(x)}{E(x)^2 + C_1} = \int_o^x dx = x \quad . \qquad (4.24)$$

Left hand side of Eq.(4.24) is a standard integral with three different solutions depending upon the value of the integration constant C_1. It is argued out that only the case $C_1>0$ is important whereas the other cases when $C_1 \leq 0$ correspond to the situation when the ions are located at either of the interfaces. Tangena et al [60] solved therefore Eq.(4.24) only under the case $C_1>0$ and obtained a solution

$$\frac{2kT}{q}\left[\frac{1}{(C_1)^{\frac{1}{2}}}\arctan\left(\frac{E(x)}{(C_1)^{\frac{1}{2}}}\right)\right] + C_2 = x \quad . \qquad (4.25)$$

where C_2 is another integration constant. Equation (4.25) can be rewritten as

$$E(x) = \frac{2akT}{q}\tan(ax+b) \qquad (4.26)$$

where

$$a = \frac{q(C_1)^{\frac{1}{2}}}{2kT} \tag{4.27}$$

and

$$b = \frac{q(C_1)^{\frac{1}{2}}}{2kT} C_2 \quad . \tag{4.28}$$

Combining Eq.(4.26) with Poisson's equation, the density distribution of mobile ions can be expressed by

$$N(x) = \frac{2kT\epsilon_o\epsilon_{ox}}{q^2} \frac{a^2}{\cos^2(ax+b)} \quad . \tag{4.29}$$

The value of the two constants a and b has been obtained under the boundary conditions :

$$\int_0^{t_{ox}} E(x)dx = -V_A \tag{4.30}$$

and

$$\epsilon_o\epsilon_{ox} \int_{E(0)}^{E(t_{ox})} dE = Q_{tot} \tag{4.31}$$

Graghic solution of Eq.(4.29) is obtained for certain assumed value of device parameters which is shown in Fig.4.1.

However the results as depicted by Fig.4.1 suffer with an ambiguity that by increasing the gate voltage to more positive value, the curve is shifted towards the metal-oxide interface instead of towards the Si-SiO2 interface. This may be attributed partly to the boundary conditions using assumed

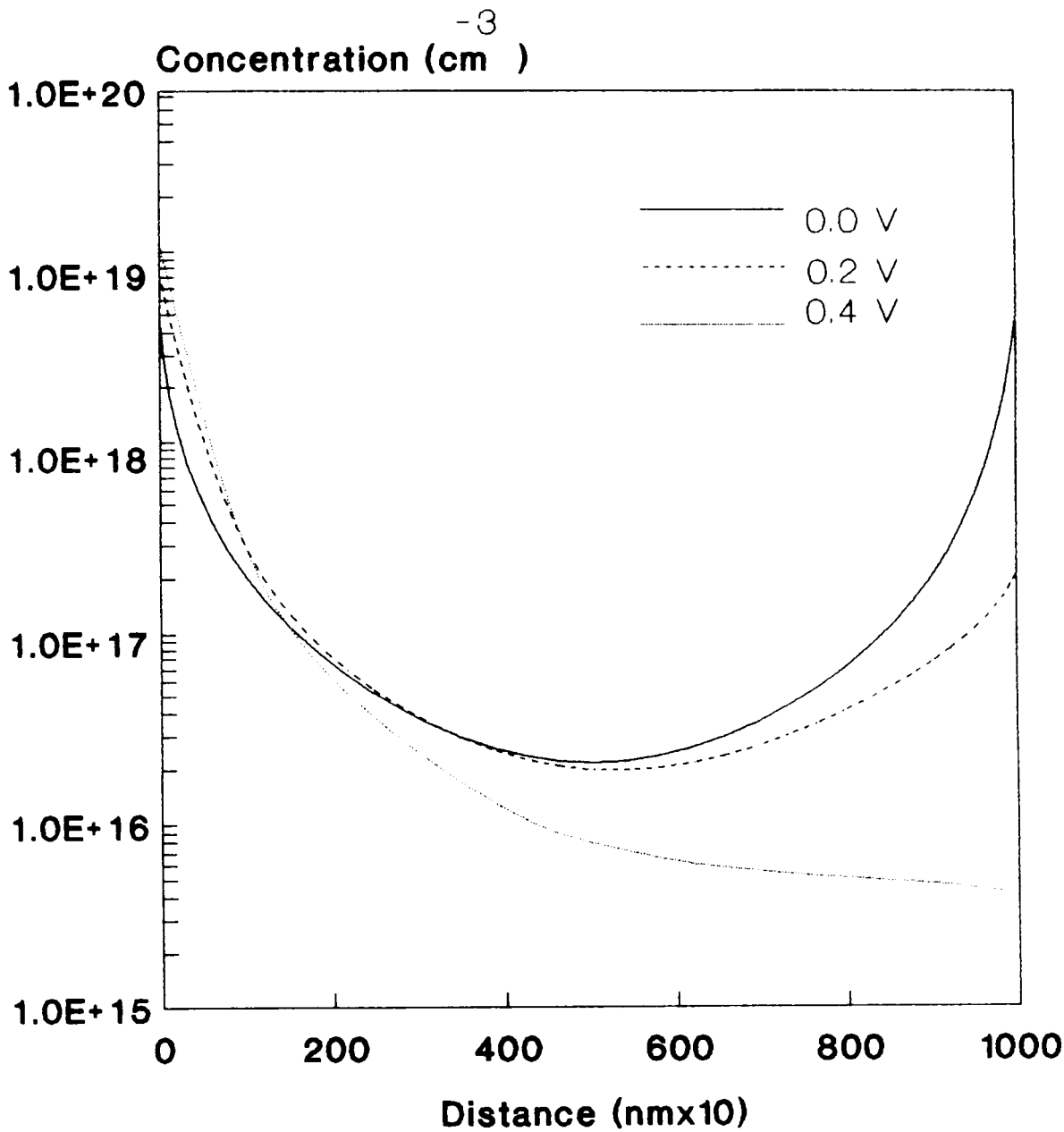

Fig.4.1 The ion distribution N(x) in the oxide at different applied voltages across the oxide (T=250 C) [60].

value of oxide voltage and oxide charge. In fact the effective voltage in the oxide may be quite different from that of the applied voltage. Moreover, the method does not provide any explanation why only a certain part of the energy of the mobile ion is governed by Boltzmann law. Further the method does not throw any light on the separate effect of different forces operative on the ions.

4.4 Theoretical Approach of Romanov et al

Another noteworthy theoretical model is due to Romanov et al [71]. They derived the equilibrium distribution of mobile ions in the oxide of MOS structures by commencing their theoretical treatment with the following current density equation

$$j = -qD\frac{dN(x)}{dx} + q\mu E(x)N(x) \qquad (4.32)$$

They considered in an oxide layer with boundaries impermeable to ions, the equilibrium state may take place only for j=0. They combined Eq.(4.32) with Poisson's equation (4.9) and obtained the following relation

$$\frac{d^2E(x)}{dx^2} - \frac{q}{kT}\frac{E(x)dE(x)}{dx} \qquad (4.33)$$

In fact they solved Eq.(4.33) itself to get, at first, the following equation for the electric field distribution :

$$E(x)=\sqrt{\frac{2kT}{q}C_1}\tan\left[\sqrt{\frac{C_1 q}{2kT}}(x+C_2)\right] \qquad (4.34)$$

where C_1 and C_2 are the integration constants. Equation (4.34) when combined back with Poisson's equation (4.9), gives

$$N(x)=\frac{\epsilon_o\epsilon_{ox}C_1}{q}\cos^{-2}\left[\sqrt{\frac{C_1 q}{2kT}}(x+C_2)\right] \quad , \qquad (4.35)$$

The following boundary conditions are used in terms of the potential V(x) and the total oxide charge Q_{tot}

$$q\int_o^{t_{ox}} N(x)dx = Q_{tot} \qquad (4.36)$$

$$V(0)=V_A \qquad (4.37)$$

$$V(t_{ox})=0 \qquad (4.38)$$

For the case $C_1>0$ the integration constants C_1 and C_2 are shown to be given by the following equations

$$\frac{Q_{tot}}{\epsilon_o\epsilon_{ox}}=\sqrt{\frac{2kTC_1}{q}}\left[\tan\left\{\sqrt{\frac{C_1 q}{2kT}}(t_{ox}+C_2)\right\}-\tan\left\{C_2\sqrt{\frac{qC_1}{2kT}}\right\}\right]$$

(4.38)

$$V_A=\frac{2kT}{q}\ln\frac{\cos\left[C_2\sqrt{\frac{C_1 q}{2kT}}\right]}{\cos\left[\sqrt{\frac{C_1 q}{2kT}}(t_{ox}+C_2)\right]} \qquad (4.39)$$

Similar sets of equations giving the value of C_1 and C_2 have been obtained for the other cases corresponding to the condi-

tions $C_1 \leq 0$. The value of the integration constants obtained in this way are used in Eq.(4.35) to obtain the density distribution profiles of the mobile ions for certain assumed value of V_A which are shown in Fig.4.2. Although the results obtained by their method show more consistency with respect to the variation of the gate voltage as compared to model of Romanov et al but still it lacks in providing precise quantitative results. For example the density profiles as shown in Fig.4.2 correspond to certain assumed value of the oxide potential V_A. Therefore this method also like others is not capable of giving precise value of the density of the mobile ions for a given device. Further it also does not throw light on the effect of different internal and external forces on the mobile ions separately.

4.5 Discussion

All the above theoretical approaches are based on the direct or indirect use of the ion transport equation which has been obtained in different investigations using different physical ideas. The ion transport equation so obtained is then coupled with the Poisson's equation in all the methods to get a differential equation either in terms of electric field or ion density. These methods however differ in their subsequent analysis of solving the differential equation to obtain the mobile ion density profiles.

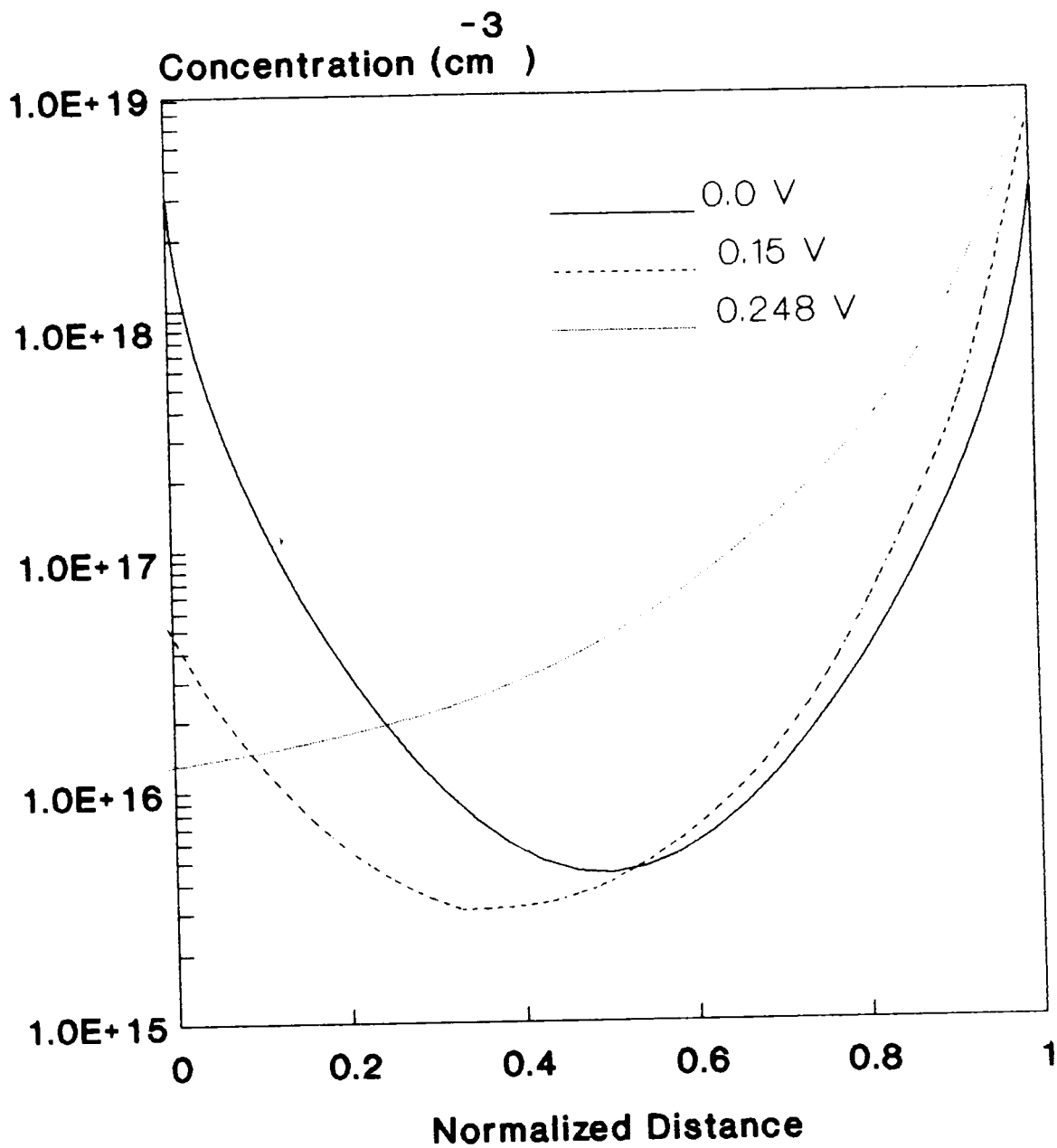

Fig.4.2 The ion distribution N(x) in the oxide at different applied gate voltage [71].

The differential equation so obtained is either not solved completely as in section 4.2 or it is solved under certain assumed boundary conditions using assumed value of parameters such as electric potential, field or charge in the oxide. Thus none of the studies is capable of giving precise distribution for a given device under given temperature-bias condition. Besides, all the methods are incapable of giving the effect of individual factors on the mobile ion distribution.

The subject of mobile ion distribution in oxides of MOS structures, therefore, still remains open for further exploration. It would be worthwhile if a more detailed and deeper analytical approach be undertaken by considering the influence of all the internal and external forces on the ions separately and then combining them suitably to obtain a final equation which is capable of giving the mobile ion distribution in terms of the known device parameters and physical constants. Such an attempt is done in the present work and it is described in chapter 6.

DETERMINATION OF THE DENSITY-DISTRIBUTION OF THE MOBILE IONS IN MOS STRUCTURE

5.1. Introduction

The flat-band voltage and hence the electrical characteristics of a MOS device can undergo significant change by the presence of the mobile ions in its oxide. This change depends not only upon the total amount of these ions but also upon their actual distribution within the oxide. Sodium ions are the most abundant among these mobile ions. Certain investigations [72] show that sodium is present in the oxides of MOS structures quite abundantly even in the neutral form. Although these sodium atoms are harmless in the neutral form but they can adversely affect the device-characteristics after becoming activated eventually into an ionic form during any subsequent processing stage which involves their exposure either to plasma or radiations. Therefore even the clean fabrication-process and gettering do not ensure full safeguard against the problem of the mobile ions. This suggests that the knowledge of the

mobile ions. This suggests that the knowledge of the equilibrium density-distribution of the mobile ions is necessary so that the presence of the mobile ions can be precisely accounted for in a given MOS device under the given circumstances. The importance of this subject is further enlarged by the use of the intentionally contaminated samples for the determination of the electrical characteristics of MOS oxides by preparing them under the concerned vapour-ambient.

Certain profiling experiments which employ the step-etching technique, have been carried out [54]. In such experiments an intentionally contaminated MOS device is used to overshadow the effect of all the other types of oxide-charge. However these experiments do not yield the true concentration-profile. It is because, firstly these experiments give the total ion-concentration (the average concentration in the residual oxide left after etching the top oxide-layer) as a function of the etched oxide-thickness. Secondly this total ion-concentration in the residual oxide is manipulated in these experiments from the measured flat-band-voltage shift under an assumption that the mobile ions occupy a very thin layer at the oxide-edges.

A few theoretical attempts have also been made [6,60,72] to obtain the equilibrium density-distribution of the mobile ions in the oxides of MOS structures. However, in the absence of any precise experimental results, the validity of such theoretical studies is not ascertained.

So far no method is known to determine the mobile-ion-concentration from the experimental measurements in an explicit form. The present investigation, the first attempt in this direction, describes a method for the determination of the equilibrium density-distribution of the mobile ions along the oxide-thickness of a MOS device from the experimentally measured value of its flat-band voltage under three conditions, namely, before contamination, after contamination and then after ion-drift due to thermal-electric stressing. It is based on the concept that the mobile ions attain in general an equilibrium density-distribution after their entry in the oxide-layer and that the flat-band voltage of the contaminated device has a strong dependence upon this equilibrium-distribution. The results of the present study are found to be in accordance with the theoretical predictions of the analytical model recently developed by us which is presented in chapter 6.

5.2.General Formulation

It is well known that the flat-band voltage of a MOS device undergoes a shift whenever there is any change in the concentration or distribution of the mobile ions within its oxide-layer. A device which is fabricated under controlled conditions is supposed to have insignificant mobile ion-concentration and such a device will be referred as controlled device. If such a controlled device is intentionally contaminated further by introducing additional mobile ions, the

flat-band voltage V_{fb} of the controlled device changes by an amount δV_{fb} given by [16]

$$\delta V_{fb} = \frac{1}{\epsilon_o \epsilon_{ox}} \int_0^{t_{ox}} x \rho(x) dx \quad , \qquad (5.1)$$

Where $\rho(x)$ is the volume-density of the mobile ionic charge within the oxide, t_{ox} the oxide thickness, ϵ_o the permitivity of the free space, ϵ_{ox} the relative permitivity of oxide and the distance x is measured from the metal-oxide interface. The quantity δV_{fb} depends upon the distribution of the mobile ions and hence on the volume ion-density $\rho(x)$ within the oxide. The flat-band-voltage shift δV_{fb} can itself undergo a significant change if the ion-distribution is changed somehow within the oxide. The value of δV_{fb} as determined soon after the intentional contamination but before the drift of the mobile ions is due to the initial distribution of the ions and may be referred as δV_{fb1}. By applying an external electric field at a certain elevated temperature, the mobile ions undergo a drift towards the $Si-SiO_2$ interface and attain another equilibrium-distribution soon after the removal of the applied stress. The resulting flat-band-voltage shift under this second equilibirium-distribution may be referred as δV_{fb2}. In all previous studies, the quantity δV_{fb1} has been ignored by assuming all the contaminated mobile ions to be concentrated in a thin sheet at the metal-oxide interface. These ions have been considered to be concentrated again in a thin sheet of

charge but at the other interface after they have undergone drift under the thermal-electric stress. However, the present study is based on the contention that the mobile ions attain in general an equilibrium-distribution before as well as after the drift rather than being concentrated in a thin sheet near either of the interfaces. Such an equilibrium-distribution is supposed to occur under the action of several types of internal forces which are considered to be essentially operative within the oxide and which form the basis of all the theoretical models worked out for the equilibrium density-distribution of the mobile ions. This equilibrium-distribution is expected to differ only in sign when measured before and after the ion-drift as nothing changes between the two cases except the direction of the concentration-gradient. In fact the ion-redistribution resulting from the thermal-electric stress may be considered equivalent to the case as if the mobile ions have been introduced from the second interface instead of the first. In any case, the total quantity of the ions Q_t is supposed to remain constant within the oxide before and after the drift and is given by

$$Q_t = \int_0^{t_{ox}} \rho(x)dx \quad . \qquad (5.2)$$

An idea of the general form of the anticipated mobile ion-distribution can be had from the parallel examples of the impurity-distribution in certain known processes such as thermal diffusion and ion-implantation. These examples reveal that the impurity-distribution involves either gaussian or error function both of which employ an exponential term. In the light of these examples, the following general forms of the anticipated mobile ion-distribution may be considered :

$$\rho_1(x) = \rho(o)\ \ \mathrm{EXP}\left[-\frac{x^n}{C}\right] \qquad for\ \ 0 < x < t_{ox} \quad (5.3)$$

and,

$$\rho_2(x) = \rho(o)\mathrm{EXP}[Ax^n + Bx^{n-1}] \qquad for\ \ 0 < x < t_{ox} \quad (5.4)$$

where $\rho(o)$, A, B, C and n are constants and x is measured from the metal-oxide interface. Out of the above two general forms of the distribution the purpose of the first distribution, as given by Eq.(5.3), is to fix at first an approximate value of the index n. After the value of the index n is already fixed approximately the other distribution, as given by Eq.(5.4), may then be used to obtain a more precise distribution by introducing one more term in the exponent with an index value equal to (n-1).

In the light of the arguments given above, the mobile ion-distributions of Eqs.(5.3) and (5.4) take the following

forms after undergoing drift under the thermal-electric stress:

$$\rho'_1(x) = \rho(0)\mathrm{EXP}\left[(-1)^{n+1}\frac{(x-t_{ox})^n}{C}\right] \quad , \qquad (5.5)$$

and

$$\rho'_2(x) = \rho(o)\mathrm{EXP}[A(x-t_{ox})^n + B(x-t_{ox})^{n-1}] \quad . \qquad (5.6)$$

Substitution of the expression of $\rho_1(x)$ from Eq.(5.3) in Eqs.(5.1) and (5.2) gives

$$\delta V_{fb1} = \frac{\rho(0)}{\epsilon_o \epsilon_{ox}} \int_0^{t_{ox}} x \ \ \mathrm{EXP}\left(-\frac{x^n}{C}\right) dx \quad , \qquad (5.7)$$

and ,

$$Q_i = \rho(0) \int_0^{t_{ox}} \mathrm{EXP}\left(-\frac{x^n}{C}\right) dx \quad . \qquad (5.8)$$

Equations (5.7) and (5.8) yield

$$\delta V_{fb1} = \frac{Q_i}{\epsilon_o \epsilon_{ox}} \frac{\int_o^{t_{ox}} x \ \ \mathrm{EXP}\left(-\frac{x^n}{C}\right) dx}{\int_o^{t_{ox}} \mathrm{EXP}\left(-\frac{x^n}{C}\right) dx} \quad . \qquad (5.9)$$

By using the mobile ion-distribution after the drift as given by Eq.(5.5), the expression of δV_{fb2} can be obtained which comes out to be

$$\delta V_{fb2} = \frac{Q_i}{\epsilon_o \epsilon_{ox}} \frac{\int_0^{t_{ox}} x \ \ \mathrm{EXP}\left[(-1)^{n+1}\frac{(x-t_{ox})^n}{C}\right] dx}{\int_0^{t_{ox}} \mathrm{EXP}\left[(-1)^{n+1}\frac{(x-t_{ox})^n}{C}\right] dx} \quad . (5.10)$$

Proceeding exactly in the same way with the mobile ion-distributions as given by Eqs.(5.4) and (5.6), another set of equations for $\delta' V_{fb1}$ and δ'_{fb2} can be obtained which are reproduced below:

$$\delta V'_{fb1} = \frac{Q_t}{\epsilon_o \epsilon_{ox}} \frac{\int_o^{t_{ox}} x \ \mathrm{EXP}[Ax^n + Bx^{n-1}]dx}{\int_o^{t_{ox}} \mathrm{EXP}[Ax^n + Bx^{n-1}]dx} \quad , \quad (5.11)$$

and

$$\delta V'_{fb2} = \frac{Q_t}{\epsilon_o \epsilon_{ox}} \frac{\int_0^{t_{ox}} x \ \mathrm{EXP}[A(x-t_{ox})^n + B(x-t_{ox})^{n-1}]dx}{\int_0^{x_{ox}} \mathrm{EXP}[A(x-t_{ox})^n + (x-t_{ox})^{n-1}]dx} \quad . \quad (5.12)$$

From the measured values δV_{fb1} and δV_{fb2} before and after the ion-drift and that of the total mobile charge Q_t, at first the distribution-parameters n and C can be obtained with the help of Eqs.(5.9) and (5.10) by using numerical method. After fixing the value of the index n in this way, the distribution-parameters of Eq.(5.4) can be obtained numerically by using again the measured value of $\delta' V_{fb1}$, $\delta' V_{fb2}$ and Q_t in Eqs.(5.11) and (5.12).

5.3.Results and Discussion

The experimental measurements, needed for the computation in the present study, consist of high frequency C-V

characteristics of the MOS structure under three cases as mentioned earlier besides the determination of the total mobile charge Q_t. However, in the present study the experimental data of certain earlier works [11,73] is being used for better reliability and comparison of the results. For example, Snow et Al [11] have obtained the high frequency C-V characteristics of a MOS diode before contamination and then after its contamination using rinse of dilute NaCl solution. The final characteristics were obtained by them after the ions-drift in the contaminated device. The total ionic charge Q_t was determined by them from the direct charge-measurement as well as the saturation value of the flat-band-voltage shift under thermal-electric stressing. However, Raychaudhuri et al [73] have used neutron-activation to increase the mobile ion-concentration in the controlled device. The high frequency C-V curves of both the above mentioned measurements are shown in Figs.5.1 and 5.2 respectively in which the curve before contamination/activation is marked as (a), after contamination/activation as (b) and the final curve after ion-drift as (c). It may be mentioned that δV_{fb1} and δV_{fb2} have been obtained from these curves in this present study by measuring the relative shifts between the curves (b) and (a) and between (c) and (a) at the flat-band capacitance in both the cases.

The computation has been carried out in two steps. In the first step the values of δV_{fb1} and δV_{fb2}, as measured from

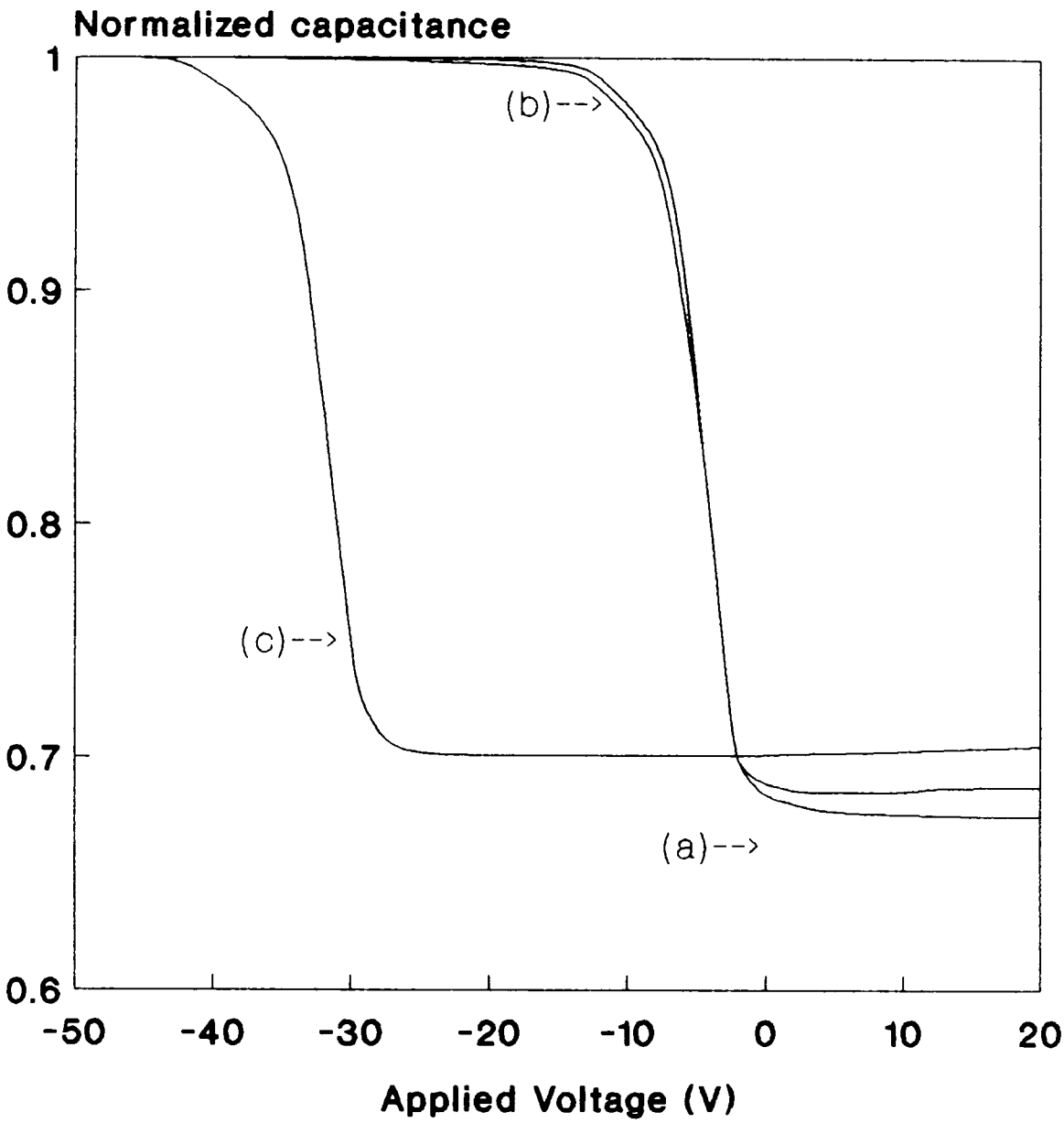

Fig. 5.1 Capacitance-voltage (C-V) curves of MOS structure [11]. (a) before and, (b) after contamination (c) after 5 min of biasing.

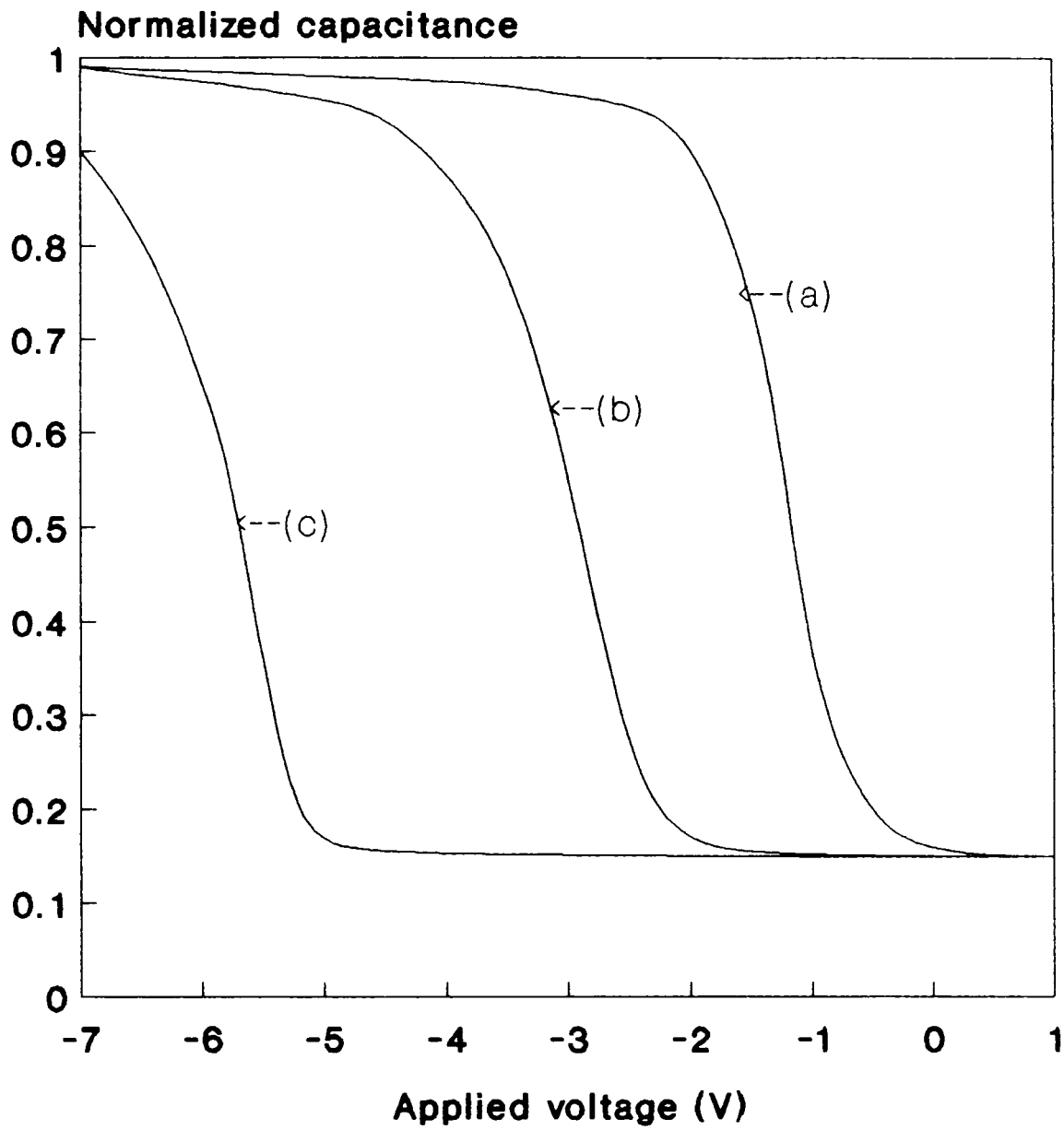

Fig. 5.2 Capacitance-voltage (C-V) curves of MOS capacitor (a) before activation, (b) after activation, (c) after 2700 sec of biasing [73].

the experimental C-V curves, are used in Eqs.(5.9) and (5.10) and the values of the distribution-parameters C and n of Eq.(5.3) are obtained. Values of the different quantities e.g. δV_{fb1}, δV_{fb2} and Q_t as used in this first step are shown in Table 4.1 along with the computed values of the parameters C and n for both the sets of the experimental C-V curves. It may be noted that the value of the index n comes out to be the same and equal to 2 for both the measurements inspite of quite diversified values of the device-parameters such as the oxide-thickness t_{ox} and the total ion-concentration Q_t used by them. A constant value of the index n=2 as obtained in different cases indicates that the anticipated mobile ion-distribution is close to gaussian. It further suggests that the index n is more fundamentally related to the physical processes leading to the equilibrium-distribution of the mobile-ions rather than depending upon the device-parameters. After finding the proximity of the index n, the second step of the computation is carried out using Eqs.(5.11) and (5.12) to ascertain if the addition of another term in the exponent with an index value equal to (n-1) also contributes anything to the distribution. Obviously this part of the computation is expected to provide a more precise distribution in terms of the distribution-parameters A and B. The values of the parameters A and B are also included in Table 1 for both the experimental measurements. The computed parameter values

Table.1 The calculated distribution parameters.

Ref.	Q_t (cm^{-2})	V_{fb1} (V)	V_{fb2} (V)	t_{ox} (nm)	n	C	A	B
[11]	$2.9x10^{12}$	1.4	28	200	2	57	$2.5x10^{14}$	$1.0x10^{8}$
[73]	$4.0x10^{12}$	1.6	4.5	35	2	62	$7.5x10^{15}$	$3.0x10^{8}$

have been carried out by using a program in HP basic which has been developed. The flow chart of this program is shown in Figs.5.3a,b The distribution curves obtained after using the computed value of the parameters A and B in Eq.(5.4) are shown in Figs.5.4 and 5.5 for both the experimental measurements. Results of the present study will be compared with that of our analytical model in chapter 6.

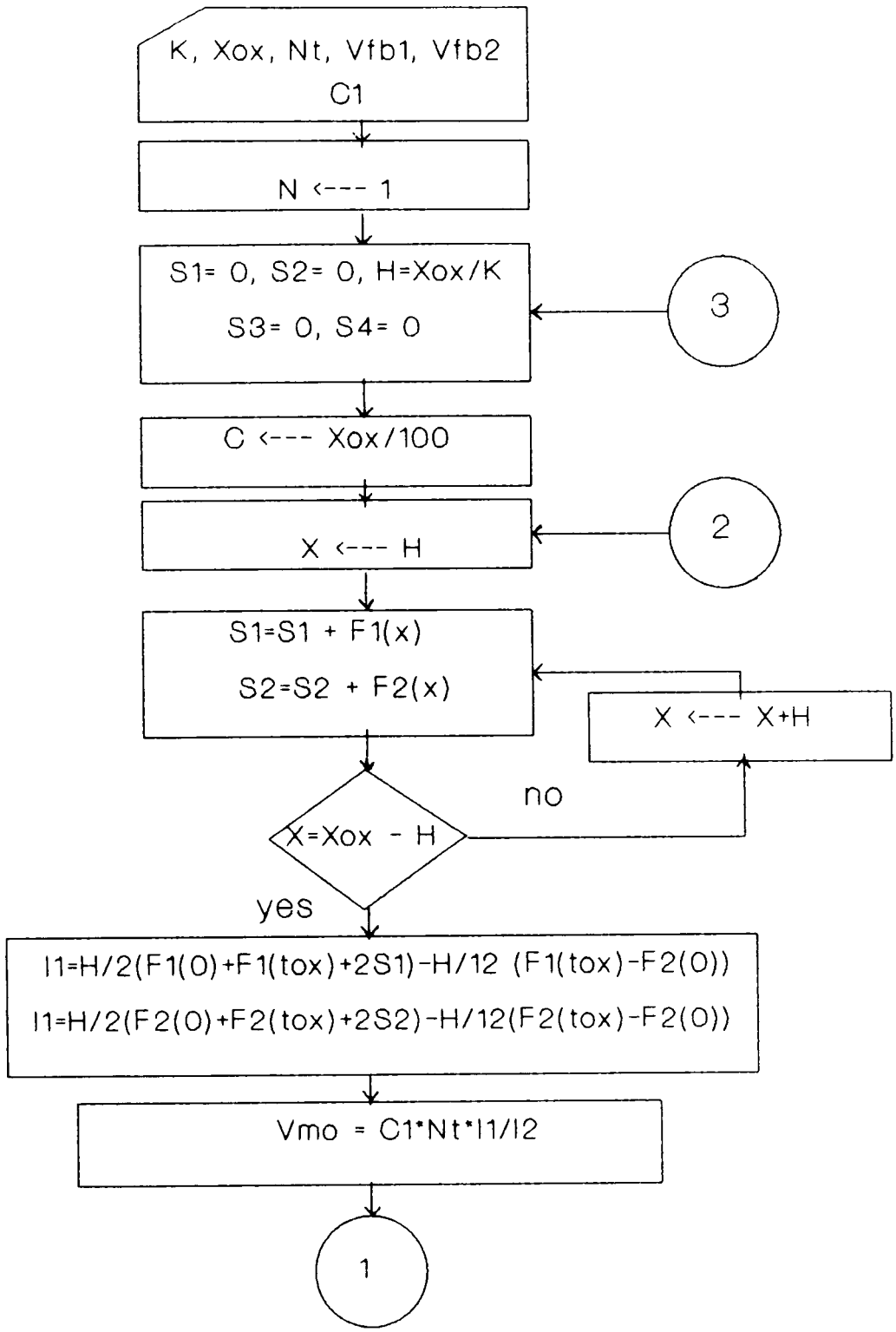

Fig. 5.3a flow chart for computing flat band voltage shift.

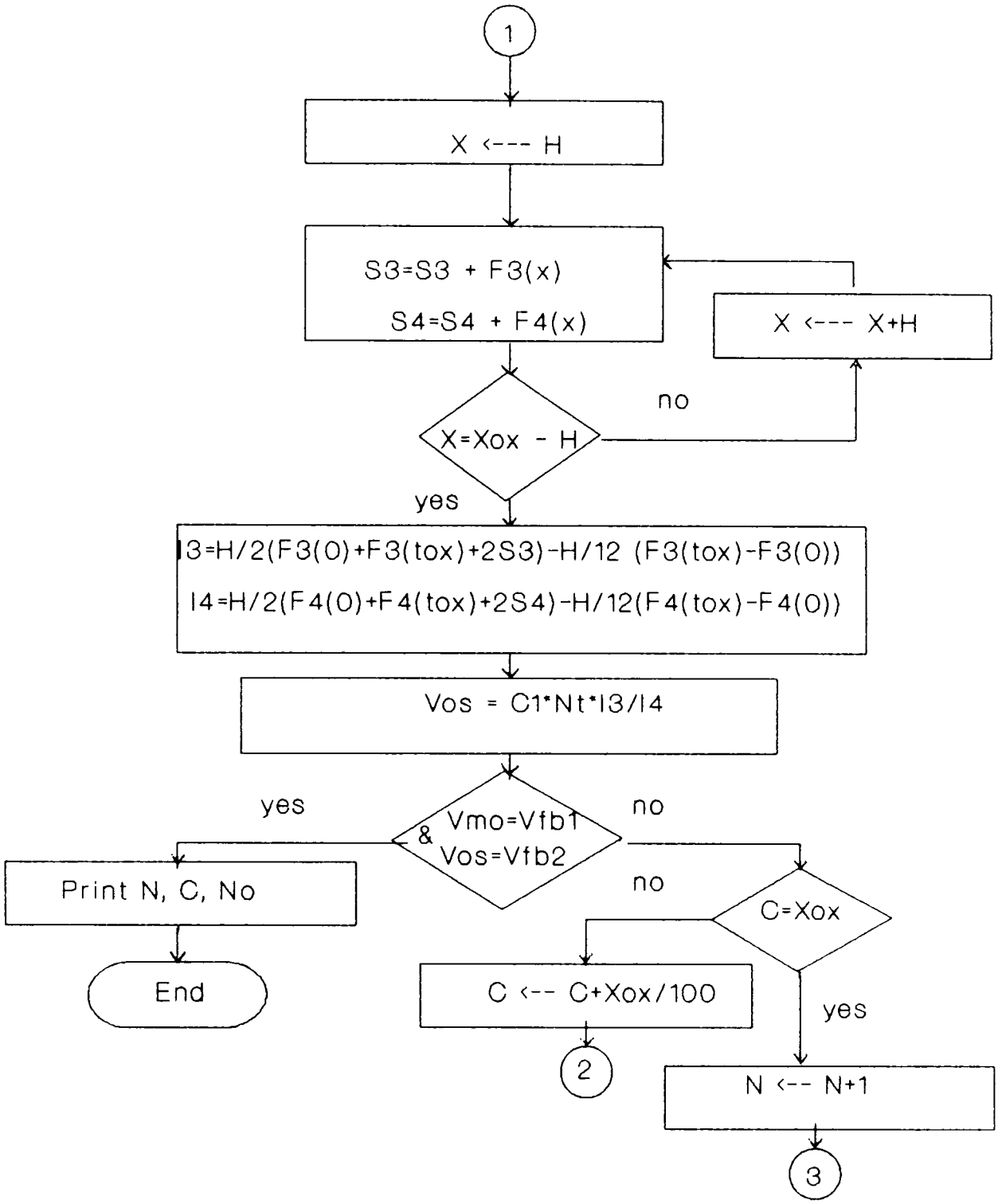

Fig. 5.3b flow chart for computing flat band voltage shift.

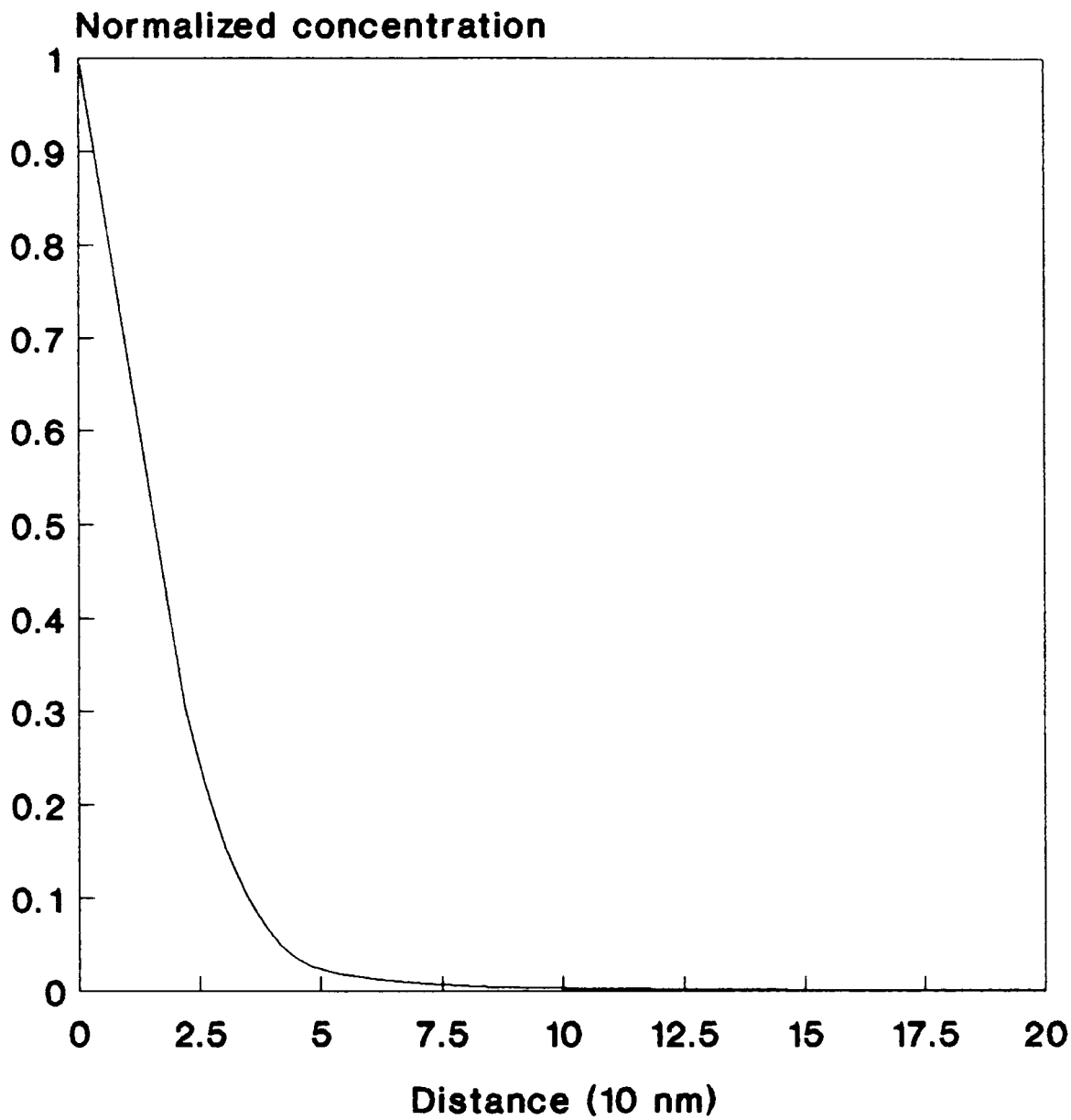

Fig. 5.4 Mobile ions concentration profile in MOS structure of oxide thickness 200 nm.

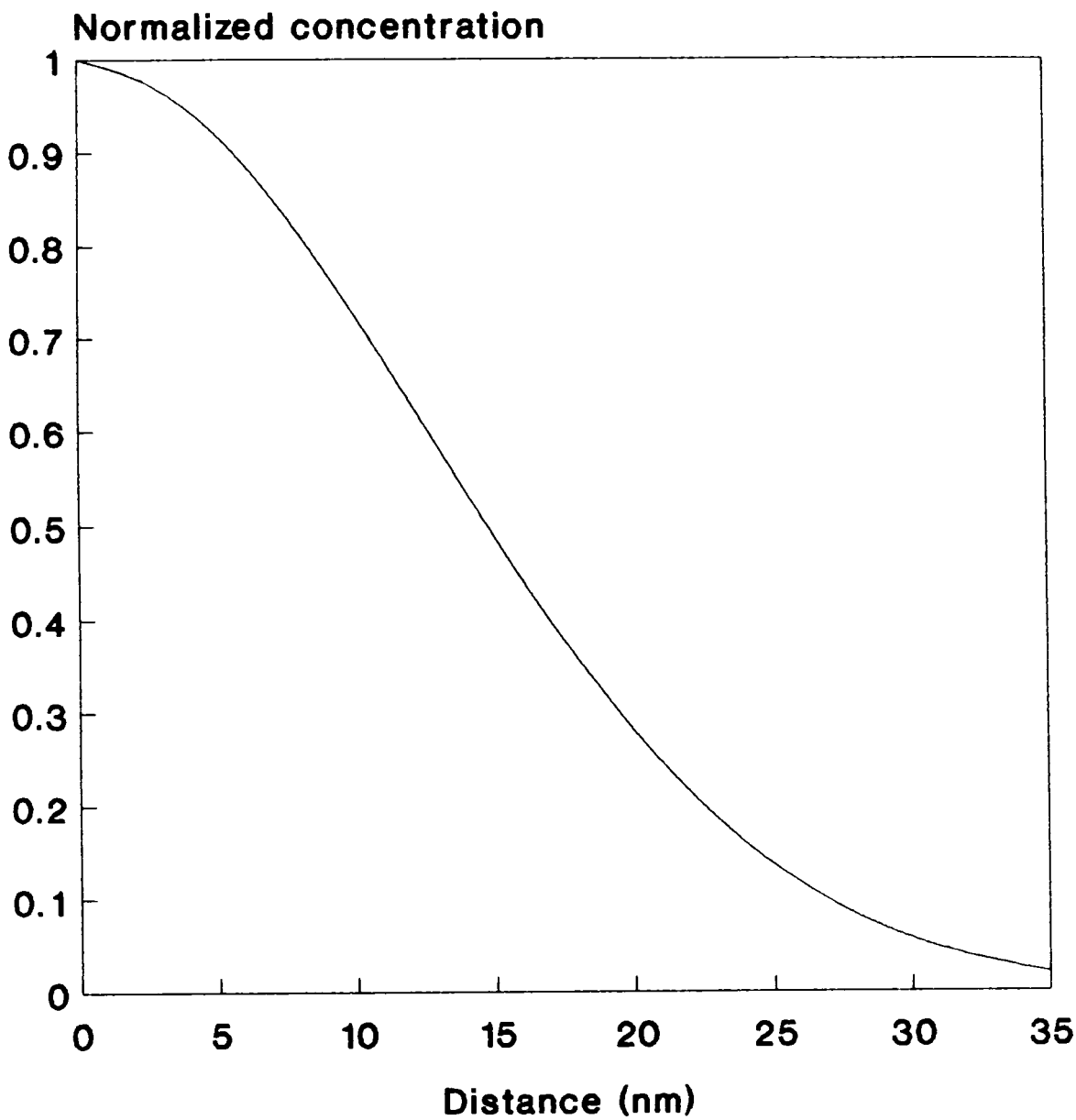

Fig. 5.5 Mobile ions concentration profile in MOS structure with oxide thickness 35 nm.

CHAPTER 6

A THEORETICAL MODEL FOR THE DENSITY-DISTRIBUTION OF MOBILE IONS IN THE OXIDE OF MOS STRUCTURE

6.1. Introduction

It is well known that the presence of the mobile ions in the oxide of a MOS device can greatly influence its electrical characteristics. Although a general feeling prevailed for some time that this problem can be avoided if the concentration of the mobile ions is reduced in the basic Si-SiO_2 structure by gettering or clean processing but soon it had to be revived in view of the fact that certain processes such as heat, X-rays, laser or plasma-treatment of the MOS structures in any subsequent stage can either introduce fresh ions or reactivate those existing already in an inactive form in the oxide. Therefore the study of the different aspects of the mobile ions in the oxide is still of considerable importance in MOS devices. The importance of the subject is further enlarged on account of the use of the

intentionally contaminated samples for studying the electrical characteristics of MOS oxides by preparing them under the desired vapour or gas ambient.

One important aspect of the study of these mobile ions is their density-distribution along the oxide-thickness. A number of attempts [2,11,55,56,62] have been made for the experimental determination of the density-distribution of the mobile ions in the oxide. Generally an intentionally contaminated sample is used for this purpose to overshadow the effect of other types of charge in the oxide. The determination of the density-distribution of mobile ions in such a sample is then carried out by etching its top-layer in steps and each time measuring the total mobile charge in the remaining oxide by using either of the commonly used techniques [54]. Apart from such experimental studies, a few theoretical attempts have also been made [59,60,72] to obtain the density-distribution of the mobile ions in the oxide of MOS structures based on the argument that these ions must attain an equilibrium density-distribution under the influence of various internal forces which are operative during the normal course of fabrication of the MOS devices. This present work, is another attempt in the same direction, presents a one-dimensional analytical model of the distribution of the mobile ions along the oxide-thickness of a MOS

structure. It is based on the concept that the equilibrium concentration of the mobile ions is attained in the oxide when all the mobilizing forces together, arising from different origins, namely, thermal diffusion, internal and external electric fields, become just sufficient to impart the necessary activation energy to the ions to surmount the effective potential well. Unlike the previous studies [59,72], all these forces acting on a single ion have been obtained here independent of each other from fundamental considerations and finally combined to get the density-distribution of the ions under the equilibrium condition. The results of the present analytical model are consistent and in good agreement with the earlier results.

6.2. Preliminary Considerations

Earlier investigations [74] on the transport of the mobile charge in the oxide have led to the conclusion that, in order to produce ionic current, these ions have to overcome potential wells at the interfaces as well as in the bulk of the oxide. The potential wells or ion-traps at the interfaces have been found to be somewhat deeper than those existing in the bulk of the oxide. Different estimates about the depth of the potential wells yield values ranging from 0.8 to 0.9 eV near the interfaces [62,65,12] and from 0.62

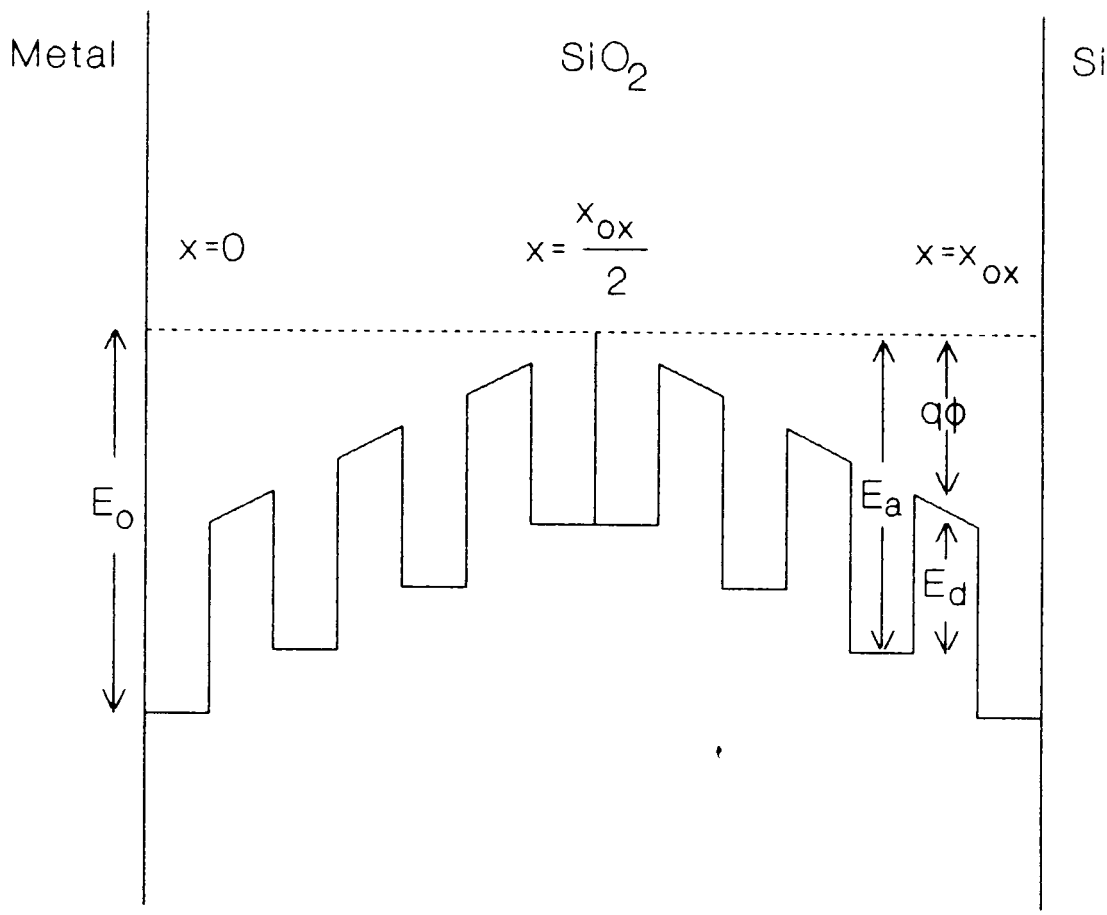

Fig. 6.1 Built of the effective activation energy E(x) at any point in the oxide as a sum of trap-energy Ed and barrier-energy qϕ.

to 0.7 eV in the bulk of the oxide [12,70]. Whereas a little is known [12] about the origin of the ion-traps at the interfaces, the ion-traps in the bulk of the oxide are supposed to be associated with the periodic inter-atomic potential fluctuations. It will be assumed here that the ion-traps at the oxide-interfaces are basically of the same nature as that of the oxide-bulk and all of them have an energy E_d. However, at any point near the interfaces, the energy of these ion-traps is effectively increased by an amount $q\phi$ (Fig.6.1) on account of the creation of a potential barrier ϕ by the positive trap-charges of the oxide. In fact oxide-traps are known to be associated with the defects in SiO_2. These oxide-traps may have any kind of charge, positive or negative, depending upon the predominant process which is responsible for the flow of the carriers [16] during the oxide-formation or subsequent processing. Reference to a number of phenomena is made [75-78] in connection with the conduction-processes in the oxide which may be held responsible for the electron-flow through the oxide. The one which may be cited here is the Schottky emission which consists of thermionic emission across the metal-oxide or oxide-semiconductor interface. In view of the proposed formation of a potential barrier and hence an effective increase of the trap-energy at the interface, the activation

energy E_a of the mobile ions may be supposed to vary from a certain maximum energy E_o at the interfaces (metal-oxide-interface located at x=0 and oxide-semiconductor interface located at $x=x_{ox}$) to a minimum energy E_d at a certain point x=W close to the middle of the oxide-thickness. In fact the exact location of the point of minimum activation energy E_d, which is the same as point of zero potential barrier, would depend upon the activation energies E_{o1} and E_{o2} at the two interfaces respectively. In the absence of any precise estimate of these trap-energies E_{o1} and E_{o2}, it is assumed here that $E_{o1}= E_{o2}= E_o$. Under this condition, the point of minimum energy lies at $x=W=\frac{t_{ox}}{2}$.

In case the mobile ions are introduced from the metal-oxide interface, all these ions may be assumed to be concentrated in the beginning at x=0. This excessive concentration of positive ions at x=0 gives rise to two forces, one F_1 due to the internal electric field and the other F_2 due to thermal diffusion. These two forces F_1 and F_2 together are much greater in the beginning to overcome the potential barrier existing at the metal-oxide interface and so they mobilize such ions which possess enough energy to surmount the trap-energy E_d. Due to Boltzmann distribution of thermal energy, a certain fraction of the ions is always supposed to have enough thermal energy to overcome E_d and must respond to the

influence of the force $F_1 + F_2$. This should lead, although slowly, to the attainment of equilibrium density-distribution of the mobile ions even at room temperature. However, at an elevated temperature, certain more fraction of the ions would possess the required thermal energy and the attainment of the equilibrium is much faster. During the above process of the attainment of equilibrium, some positive ions drift deeper into the oxide under the action of forces F_1 and F_2 and this process continues till the sum of the forces F_1 and F_2 goes down to a value which is just enough to overcome the local barrier ϕ. This marks the condition of equilibrium density-distribution of the positive ions. The present model, therefore, necessitates the evaluation of the forces F_1, F_2 and the potential barrier ϕ which is done in the following section.

6.3. Theoretical Model

As proposed earlier, in the present study, only one-dimensional distribution of the mobile ions is considered. In order to visualize such a model, reference may be made to Fig.(6.2) in which the ion-concentration N_x varies along the oxide-thickness in the direction x so that the whole oxide-volume may be considered to be composed of thin successive parallel layers of positive ions like A,B and C.

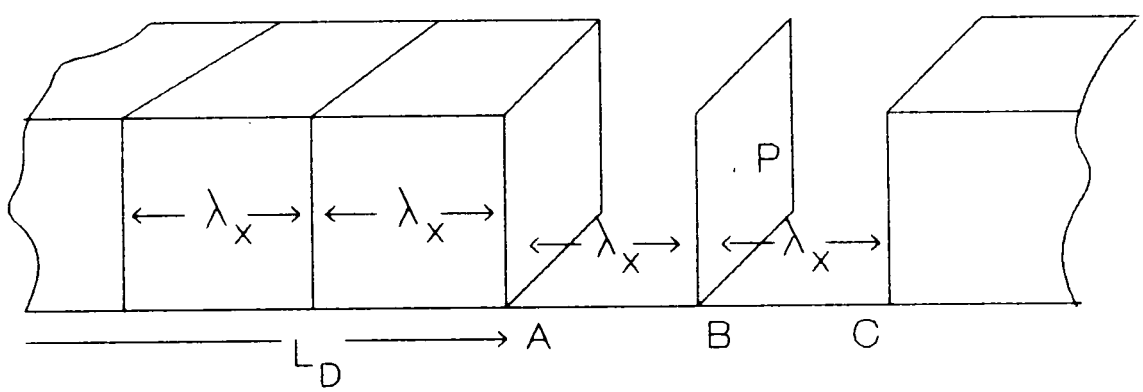

Fig. 6.2 Sectional view of the oxide-thickness showing it to be composed of parallel mono-molecular layers like A, B, and C with inter-distance λ_x.

Let the layers A, B and C be located at $x-\lambda_x$, x, and $x+\lambda_x$ and have ion-concentration $N_{x-\lambda_x}$, N_x, and $N_{x+\lambda_x}$ respectively such that the mutual distance λ_x between the adjacent layers does not vary significantly within a small thickness-element at x.

At any point P of the layer B, the electric field $E_{x-\lambda x}$ due to all the positive ions situated in the layer A should be pointing towards right and can be written as

$$E_{x-\lambda_x} = \frac{\sigma_{x-\lambda_x}}{2\epsilon_o\epsilon_{ox}} \quad , \tag{6.1}$$

where $\sigma_{x-\lambda_x}$ is the charge-density in the layer A, ϵ_{ox} the relative permittivity of the oxide and ϵ_o that of the free space. Similarly the electric field $E_{x+\lambda_x}$ on the same point P due to all the positive ions of layer C should be pointing towards left and can be written as

$$E_{x+\lambda_x} = \frac{\sigma_{x+\lambda_x}}{2\epsilon_o\epsilon_{ox}} \quad . \tag{6.2}$$

The forces $F_{x-\lambda_x}$ and $F_{x+\lambda_x}$ on a single positive ion of charge q located at P due to the electric field $E_{x-\lambda_x}$ and $E_{x+\lambda_x}$ respectively can be written as

$$F_{x-\lambda_x} = \frac{q\sum\sigma_{x-\lambda_x}}{2\epsilon_o\epsilon_{ox}} \quad , \tag{6.3}$$

and

$$F_{x+\lambda_x} = \frac{q\sum \sigma_{x+\lambda_x}}{2\epsilon_0\epsilon_{ox}} \quad , \tag{6.4}$$

where the summation is to be carried out on all such layers on the right side of A in Eq.(6.3) and on the left side of C in Eq.(6.4) which can have influence on the layer B. The net force F_1 experienced by a single ion at P comes out to be

$$F_1 = q\frac{\left(\sum \sigma_{x-\lambda_x} - \sum \sigma_{x+\lambda_x}\right)}{2\epsilon_0\epsilon_{ox}} \quad . \tag{6.5}$$

Let $(L_D)_x$ be the Debye length at the layer B, that is, the distance upto which the positive ions on the left or the right of layer B can exert influence on the considered single ion at P. Considering the whole region upto a distance $(L_D)_x$ on the right side of the layer B to be divided into similar parallel layers of positive ions with an inter-distance λ_x, the right-hand term of Eq.(6.3) can be easily evaluated since it simply equals to the sum of the following arithmetic series containing $\frac{(L_D)_x}{\lambda_x}$ terms:

$$\sum \frac{q}{2\epsilon_0\epsilon_{ox}}\sigma_{x-\lambda_x} = \frac{q^2}{2\epsilon_0\epsilon_{ox}}\left[\lambda_x N_x + \lambda_x\left(N_x - \frac{\partial N_x}{\partial x}\lambda_x\right) + \lambda_x\left(N_x - \frac{\partial N_x}{\partial x}2\lambda_x\right) + \ldots\ldots\right] ,$$

or

$$\sum \frac{q}{2\epsilon_o \epsilon_{ox}} \sigma_{x-\lambda_x} = \frac{q^2}{2\epsilon_o \epsilon_{ox}} \left[\lambda_x N_x \frac{(L_D)_x}{\lambda_x} - \lambda_x \frac{\partial N_x}{\partial x} \frac{(L_D)_x^2}{2\lambda_x} \right] \quad (6.6)$$

Similarly right-hand side of Eq.(6.4) can be written as

$$\sum \frac{q}{2\epsilon_o \epsilon_{ox}} \sigma_{x+\lambda_x} = \frac{q^2}{2\epsilon_o \epsilon_{ox}} \left[\lambda_x N_x \frac{(L_D)_x}{\lambda_x} + \lambda_x \frac{\partial N_x}{\partial x} \frac{(L_D)_x^2}{2\lambda_x} \right] \quad (6.7)$$

Substitution of the expressions of $\sum \sigma_{x-\lambda_x}$ and $\sum \sigma_{x+\lambda_x}$ in Eq.(6.5) gives

$$F_1 = -\frac{q^2}{2\epsilon_o \epsilon_{ox}} \frac{\partial N_x}{\partial x} (L_D)_x^2 \quad . \quad (6.8)$$

It may be pointed out that the force F_1 is directing down the concentration-gradient in the case of positive ions. Yet another force F_2 is supposed to come into play on the considered single ion at P in the same direction which is due to thermal diffusion on account of the concentration-gradient $\frac{\partial N_x}{\partial x}$. This force can be obtained from kinetic considerations. In case all these positive ions are free to move and have only thermal energy, they can be treated like free molecules of a gas with concentration gradient $\frac{\partial N_x}{\partial x}$. The difference of the partial pressure of this so-called gas on the two faces of a volume-element between the layers A and C is a measure of the collective force $\sum F_2$ which is acting on all the positive ions contained in the considered volume-element

with unit area of cross-section. In this way the average force F_2 can be written as

$$F_2 = \frac{\frac{1}{3}mc^2 N_{x-\lambda x} - \frac{1}{3}mc^2 N_{x+\lambda_x}}{N_x(2\lambda_x)} \quad , \qquad (6.9)$$

or

$$F_2 = -m\frac{c^2}{3N_x}\frac{\partial N_x}{\partial x} \quad . \qquad (6.10)$$

Where m is the mass of ion and c the R.M.S velocity. Considering the positive ions to be in thermal equilibrium with the bulk of the oxide-layer at T° k

$$\frac{1}{2}mc^2 = \frac{3}{2}kT \quad , \qquad (6.11)$$

where k is the Boltzman constant. Equation (6.10) combined with Eq.(6.11) gives

$$F_2 = -\frac{kT}{N_x}\frac{dN_x}{dx} \quad . \qquad (6.12)$$

The forces F_1 and F_2 play quite an important role in establishing the equilibrium-distribution of the mobile ions soon after these ions are introduced in the oxide. Since these ions require enough activation energy to move from one

place to another, the process of attaining this equilibrium-distribution may not be as fast as it would be if the ions are completely free. As already discussed, the total activation energy E_a is made up of two parts. The first is needed to overcome the trap-energy E_d which is constant throughout the width of the oxide-layer and the other part is required to overcome the barrier energy $q\phi$ which varies with the position of the ion. Of these two parts, whereas the first part E_d is provided by the thermal energy of the ion, the other part $q\phi$ is built-up by the mobilizing forces F_1 and F_2. Thus the speed, how quickly the equilibrium density-distribution can be obtained, depends upon the thermal energy and hence the temperature of the oxide. Obviously at higher temperature the attainment of equilibrium density-distribution is faster. In any case, the equilibrium distribution of ions occurs when the sum of the forces F_1 and F_2 comes down to such a limiting value F_3 which is required to overcome the barrier energy $q\phi$ so that

$$F_1 + F_2 = F_3 \quad . \tag{6.13}$$

In order to evaluate the force F_3 which is required to overcome the potential barrier ϕ, it is essential to know how the barrier ϕ varies with the depth of the oxide as measured from the metal-oxide interface at x=0. This can be

known under a simple assumption that the positively charged traps, which are responsible for the creation of the potential barrier ϕ, have uniform density N_t along the thickness of the oxide. The potential ϕ at any point distant x from the metal-oxide interface can, therefore, be easily obtained by solving the Poisson's equation under proper boundary-conditions. In the light of the earlier discussions, these boundary-conditions may be fixed such that the electric potential ϕ as well as the electric field $F = -\frac{d\phi}{dx}$ both are zero at $x = \frac{t_{ox}}{2}$. Although such a boundary condition does not reconcile with the idea of a uniform distribution of oxide-traps continuously from one end of oxide to another, but it can do so under a limiting case when the point of zero potential and field does not exactly lie at $x = \frac{t_{ox}}{2}$ but little away from it separately for the two halves of the oxide. Under this physical picture, the boundary condition can be fixed separately for the two halves such that $\phi = 0$ and $-\frac{d\phi}{dx} = 0$ at x_1 for the first half and at x_2 for the second where x_1 is a little smaller than $\frac{t_{ox}}{2}$ and x_2 a little greater than $\frac{t_{ox}}{2}$. The expressions for the electric potential (which is related to activation of the ion) and that of the electric field (which is related to the activation force) can be obtained separately for the two halves under the above the boundary conditions. Any set of two such expressions,

obtained in this way for the two halves, can be then combined into common expression which may be applicable for the whole oxide-thickness under the limit when $x_1 = x_2 \cong \frac{t_{ox}}{2}$. Proceeding at first for the first half under the boundary conditions $\phi = 0$, $-\frac{d\phi}{dx} = 0$ at x=x1, the potential ϕ_1 and the field E1 can be written respectively as

$$\phi_1 \cong \frac{-qN_T}{2\epsilon_o\epsilon_{ox}}\left(\frac{t_{ox}}{2} - x\right)^2 \qquad (6.14)$$

and

$$E_1 \cong \frac{-qN_T}{\epsilon_o\epsilon_{ox}}\left(\frac{t_{ox}}{2} - x\right) \quad . \qquad (6.15)$$

Similarly proceeding for the second half under the boundary conditions $\phi = 0, -\frac{d\phi}{dx} = 0$ at x=x2 with respect to the origin at x=x2, the potential ϕ'_2 and the field E'2 can be written respectively as

$$\phi'_2 \cong \frac{-qN_T x^2}{2\epsilon_o\epsilon_{ox}} \quad , \qquad (6.16)$$

and

$$E'_2 \cong \frac{qN_T x}{\epsilon_o\epsilon_{ox}}, \qquad (6.17)$$

After transforming the coordinates with respect to the origin from x=x2 to x=0, the new expressions for the potential

ϕ_2 and the field E2 are

$$\phi_2 \cong \frac{-qN_T}{2\epsilon_o\epsilon_{ox}}\left(\frac{t_{ox}}{2}-x\right)^2 \quad . \qquad (6.18)$$

and

$$E_2 \cong \frac{qN_T x}{\epsilon_o\epsilon_{ox}}\left(\frac{t_{ox}}{2}-x\right) \quad . \qquad (6.19)$$

Since Eqs. (6.18) and (6.19) merge into Eqs. (6.14) and (6.15) respectively in the limiting case when $x_1 = x_2 = \frac{t_{ox}}{2}$, the following common equations for the potential ϕ and the field E can be written which are applicable for the whole oxide-thickness :

$$\phi = \frac{-qN_T}{2\epsilon_o\epsilon_{ox}}\left(\frac{t_{ox}}{2}-x\right)^2 \quad , \qquad (6.20)$$

and

$$E = \frac{-qN_T}{\epsilon_o\epsilon_{ox}}\left(\frac{t_{ox}}{2}-x\right) \quad . \qquad (6.21)$$

The difference between the activation energy Ea and the trap-energy Ed gives at any point x the value of $q\phi$ so that

$$(E_a - E_d) = \frac{-q^2N_T}{2\epsilon_o\epsilon_{ox}}\left(\frac{t_{ox}}{2}-x\right)^2 \quad . \qquad (6.22)$$

From Eq.(6.22), the difference $(E_a - E_d)$ between the maximum and minimum activation energy can be written as

$$E_o - E_d = \frac{-q^2 N_T t_{ox}^2}{8\epsilon_o \epsilon_{ox}} \quad . \qquad (6.23)$$

Equation (6.22), combined with Eq.(6.23), yields the following expression for the activation energy $E_a(x)$:

$$E_a(x) = (E_o - E_d)\left(1 - 2\frac{x}{t_{ox}}\right)^2 + E_d \quad . \qquad (6.24)$$

The activation force F_3, which is required to provide this much activation energy E_a, can be written as

$$F_3 = -\frac{dE_a(x)}{dx} = \frac{4(E_o - E_d)}{t_{ox}^2}(t_{ox} - 2x) \quad . \qquad (6.25)$$

Equation (6.13) combined with Eqs.(6.8), (6.12) and (6.25), finally yields the following condition for the equilibrium distribution of the mobile ions in the oxide:

$$-\frac{q^2 L_D^2}{2\epsilon_o \epsilon_{ox}}\frac{dN_x}{dx} - \frac{kT}{N_x}\frac{dN_x}{dx} = \frac{4(E_o - E_d)}{t_{ox}^2}(t_{ox} - 2x) \quad . (6.26)$$

It may be pointed out here that Eq.(6.26) does not include the effect of the applied voltage V_A and that of any charge which may exist in the oxide other than the mobile positive ions and positively charged oxide-traps. However, in practice two more kinds of charge are supposed to exist in the oxide, namely, the fixed oxide-charge and interface trapped charges both of which are located at the $Si-SiO_2$ interface.

In most cases these two kinds of charge amount to an effective negative gate-voltage $-V_F$. The mobilizing force F_1' due to the combined effect of the voltages V_A and V_F on an ion can be written as

$$F_1' = \frac{q(V_A - V_F)}{t_{ox}} \quad . \tag{6.27}$$

After taking into account this force F_1', Eq.(5.26) becomes

$$\frac{q(V_A - V_F)}{t_{ox}} - \frac{q^2 L_D^2}{2\epsilon_o \epsilon_{ox}} \frac{dN_x}{dx} - \frac{kT}{N_x} \frac{dN_x}{dx} = \frac{4(E_o - E_d)}{t_{ox}^2}(t_{ox} - 2x) \quad . \tag{6.28}$$

In an assembly of distributed point-charges under equilibrium, the Debye length L_D is the distance over which the effect of any single point-charge dies out and is expressed [16] in terms of the equilibrium-density N_x of such point-charges. This expression of L_D, as applied to the case of mobile oxide-charges, can be written as

$$(L_D)_x = \sqrt{\frac{\epsilon_o \epsilon_{ox} kT}{q^2 N_x}} \quad . \tag{6.29}$$

Using the expression of Debye length in Eq.(6.28) and then integrating the resulting equation under the boundary-condition $N_x = N_o$ at x=0, the following relation for the equilibrium density-distribution of mobile ions can be obtained:

$$\mathrm{Ln}\frac{N_x}{N_o}=\frac{8(E_o-E_d)}{3kTt_{ox}^2}(x^2-xt_{ox})+\frac{2}{3}\frac{q(V_A-V_F)}{kT}\frac{x}{t_{ox}} \quad (6.30)$$

or

$$N_x=N_o\exp\left[\frac{8(E_o-E_d)}{3kTt_{ox}^2}(x^2-xt_{ox})+\frac{2}{3}\frac{q(V_A-V_F)x}{kTt_{ox}}\right] . \quad (6.31)$$

Equation (6.31) can be used to obtain the concentration-profile (N_x-x curve) of the mobile ions along the oxide-thickness. However, profiling experiments are so carried out that they yield the total mobile-charge-density $(N_x)_T$, which is the average ion-density in the oxide from x to x_{ox}, as a function of x. In order to compare the results of the present theoretical model with the experiments, it would be therefore worthwhile to obtain an expression for $(N_x)_T$ which can be easily done with the help of Eq.(6.31). The following expression for $(N_x)_T$ can be written :

$$(N_x)_T=\frac{1}{(t_{ox}-x)}\int_x^{t_{ox}}N_x\,dx \quad . \quad (6.32)$$

Further, the flat-band-voltage shift δV_{fb} due to the introduction of mobile charges, distributed according to the N_x-x profile given by Eq.(6.31), in the oxide can be written as [16]

$$\delta V_{fb} = \frac{q}{\epsilon_o \epsilon_{ox}} \int_0^{t_{ox}} x N_x dx \quad . \qquad (6.33)$$

6.4. Results and Discussion

Values of the minimum and maximum activation energy as required in the computation are taken to be E_o=0.8 to 0.9 eV [12,62,65] and E_d=0.62 to 0.70 eV [12,70]. Based upon the above experimental values of E_o and E_d, the maximum and minimum limits of the quantity $(E_o - E_d)$ may be fixed to be nearly 0.3 and 0.1 eV respectively. Therefore in the present computation, three different values of $(E_o - E_d)$ equal to 0.1,0.2 and 0.3 eV are used. Theoretical plots for the mobile ion density-distribution, as obtained with the help of Eq.(6.31), are given in Fig.6.3 for $(E_o - E_d)$=0.1, 0.2 and 0.3 eV respectively at T=300 K and using $(N_o)_T = 2 \times 10^{18}$ cm^{-3}, oxide-thickness 540 nm, and $(V_A - V_F)$=-0.35. The same curves have been repeated for a number of values of applied effective voltage $(V_A - V_F)$ ranging from -0.5 V to +0.5 V. These results are reproduced in Figs. 6.4 and 6.5 for $(E_o - E_d)$=0.1 and 0.3 respectively. Finally the effect of the temperature is studied by repeating a few typical curves at different values of the temperature which are reproduced in Figs. 6.6 and 6.7.

It may be seen that before the effective gate-voltage

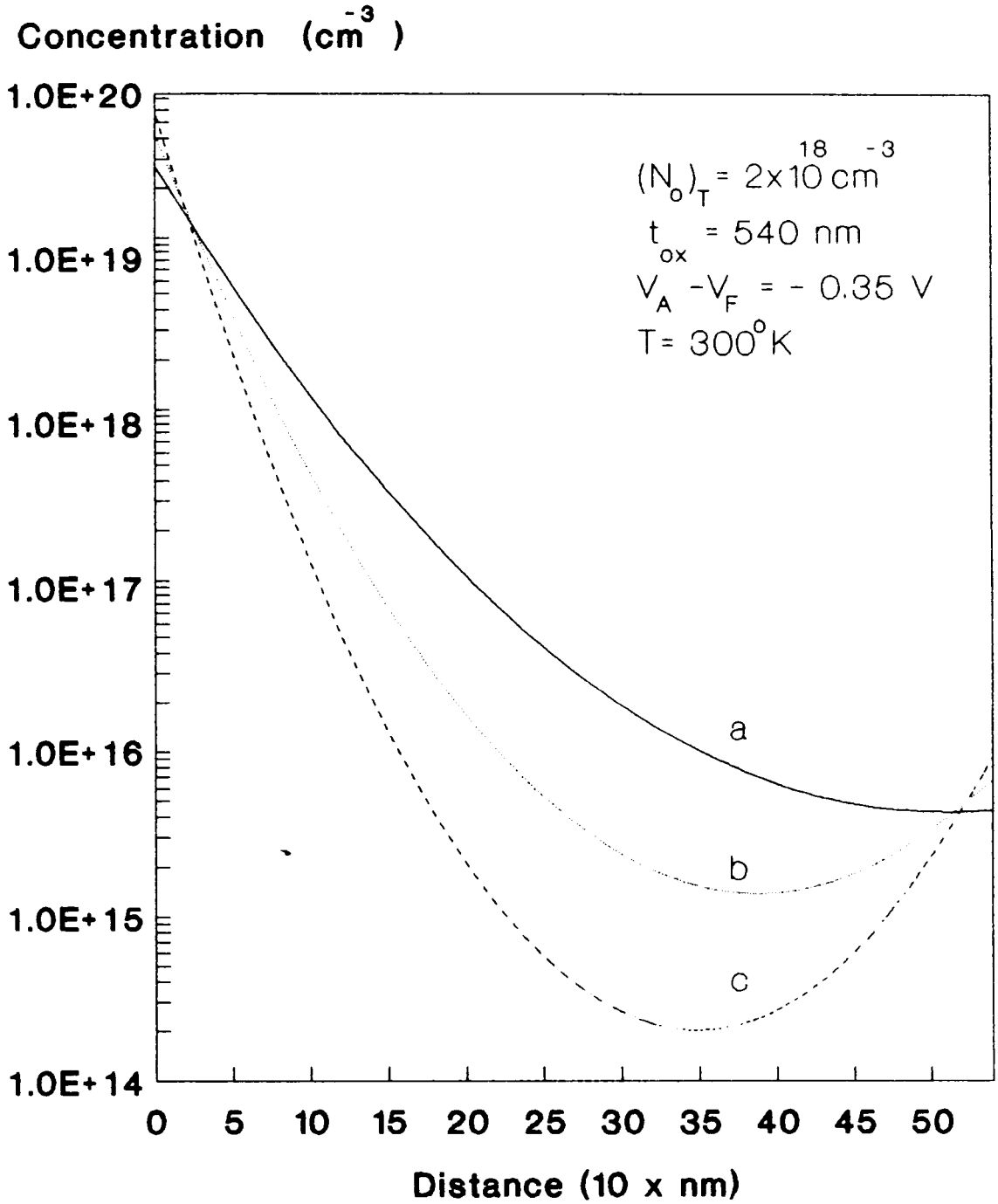

Fig. 6.3 Effect of the parameter Eo-Ed on the theoretical conentration profiles of the mobile ions. values of Eo-Ed used in the different curves are a) 0.1 eV b).2 eV c).3 eV.

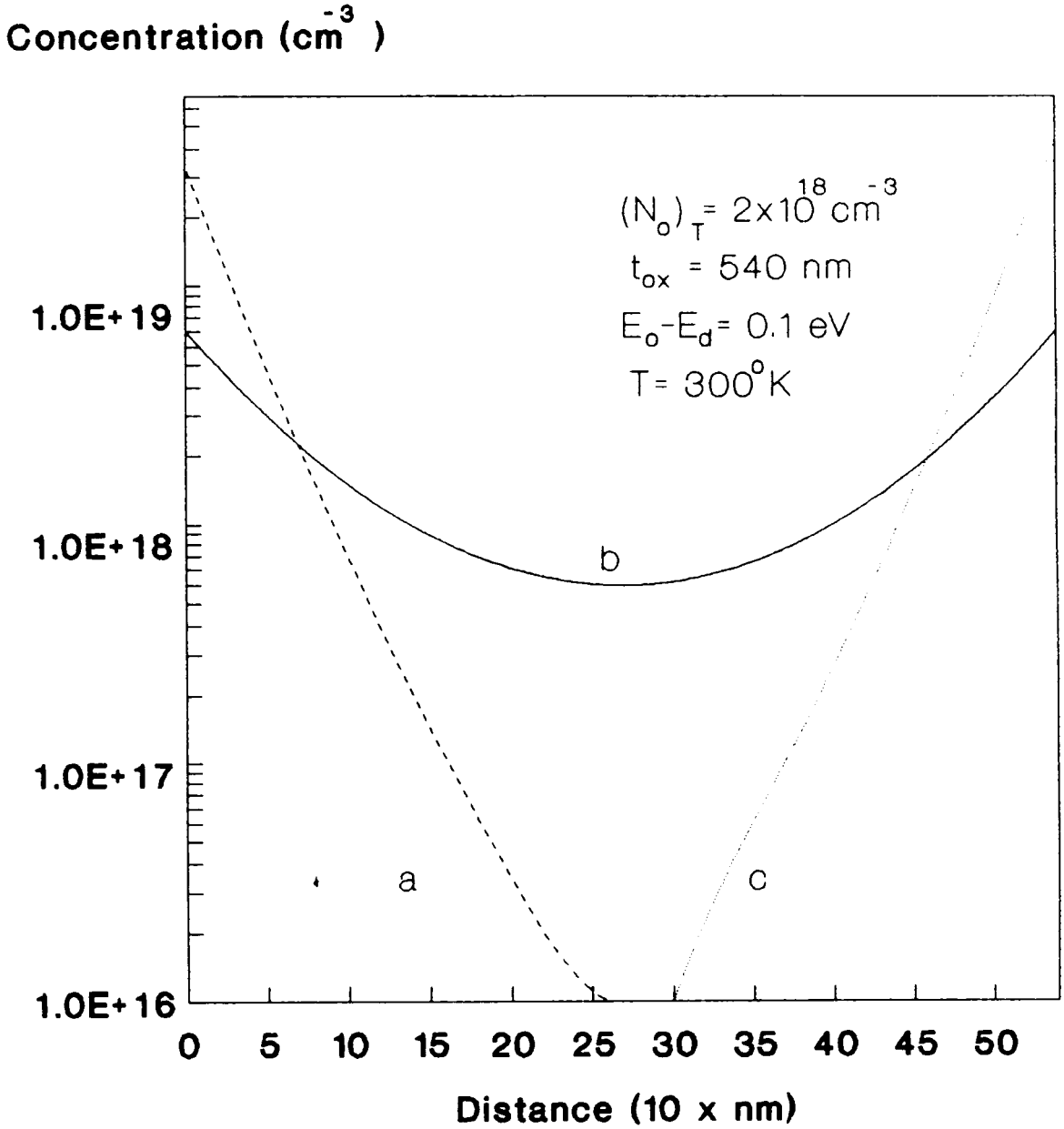

Fig. 6.4 Effect of the effective gate-voltage $V_A - V_F$ on the theoretical concentration profiles of the mobile ions.values of $V_A - V_F$ used in the different curves are a)-.5 b) o c).5 V.

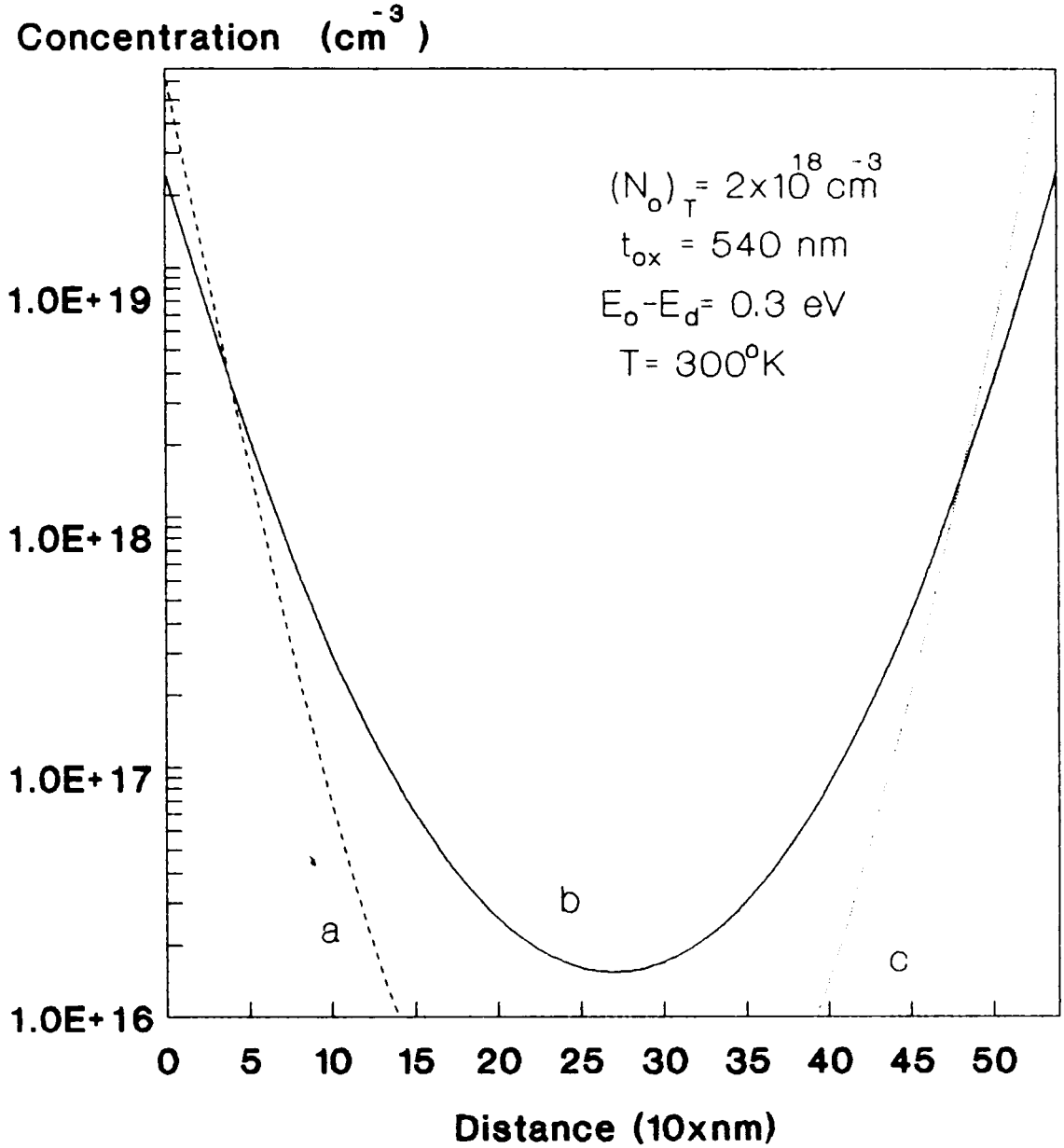

Fig. 6.5 Effect of the effective gate-voltage V_A-V_F on the theoretical concentration-profiles of the mobile ions. Vlues of V_A-V_F used in the different curves are (a) -0.5 V (b) 0 V (c) 0.5 V.

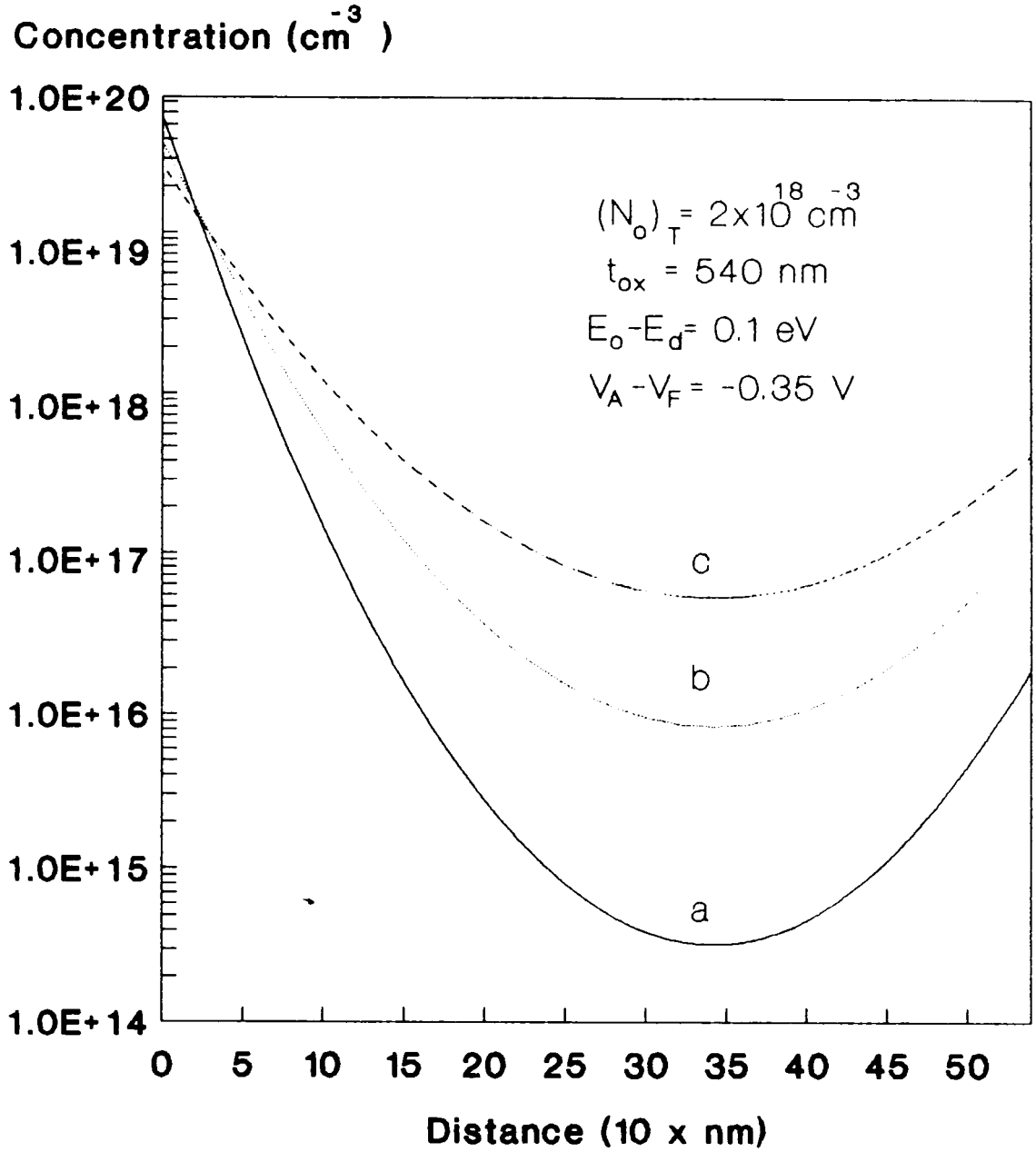

Fig.6.6 Effect of temperature T on the theoretical concentration of the mobile ions. Values of T used in the different curves are (a) 300 K (b) 423 K (c) 573 K.

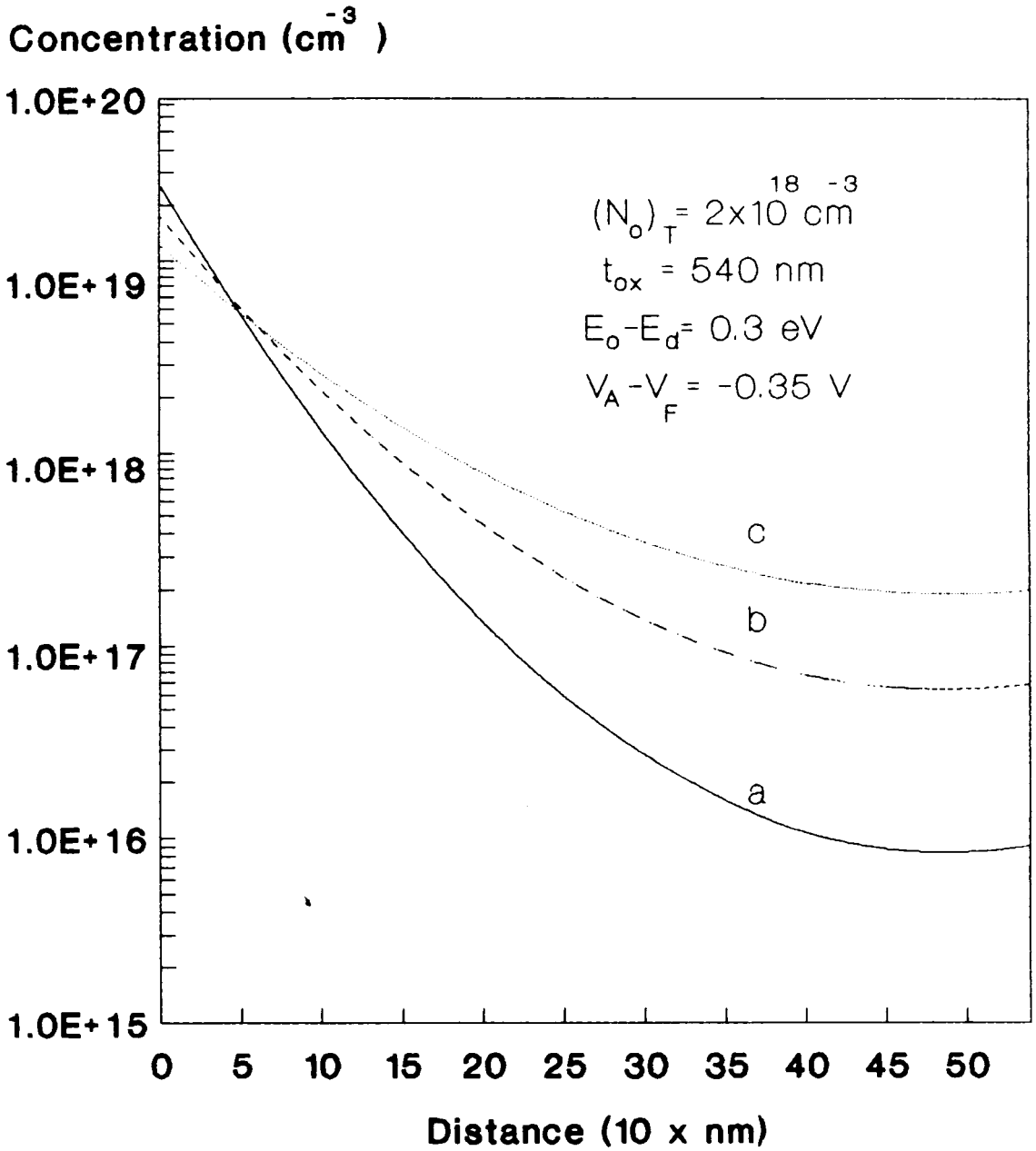

Fig.6.7 Effect of temperature T on the theoretical concentration profiles of the mobile ions. Values of T used in the different curves are (a) 300 K, (b) 423 K, (c) 573 K.

$(V_A - V_F)$ acquires enough positive value, the theoretical curves for the density-distribution of the mobile ions are nearly exponential in nature and the ion-density falls rapidly as the distance is moved from the metal-oxide interface. However, as the effective gate-voltage $(V_A - V_F)$ becomes more and more positive, the concentration of the ions starts building up at the SiO_2-Si interface and the distribution-curve takes a U-shape. Finally when $(V_A - V_F)$ attains enough positive value, the distribution-curve shows an exponential increase of the ions towards the Si-SiO_2 interface. These curves are in exact conformity with the previous results [64,60,72].

Direct experimental determination of the concentration-profile of the mobile ions in the oxide using step-etching has also been carried out [54]. These experiments mostly yield the total mobile charge per unit area and hence the total density $(N_x)_T$ of the mobile charge in the residual oxide as a function of etched oxide-thickness x. Such an experimental $(N_x)_T$-x curve is compared with that obtained from Eq.(6.32) of the present theoretical model for certain values of the effective gate-voltage $(V_A - V_F)$ using $(E_o - E_d)$=0.3 eV in Fig.6.8. It may be noted that the experimental curve agrees well with the theoretical curve corresponding to the effective gate-voltage $(V_A - V_F)$=-0.185 V.

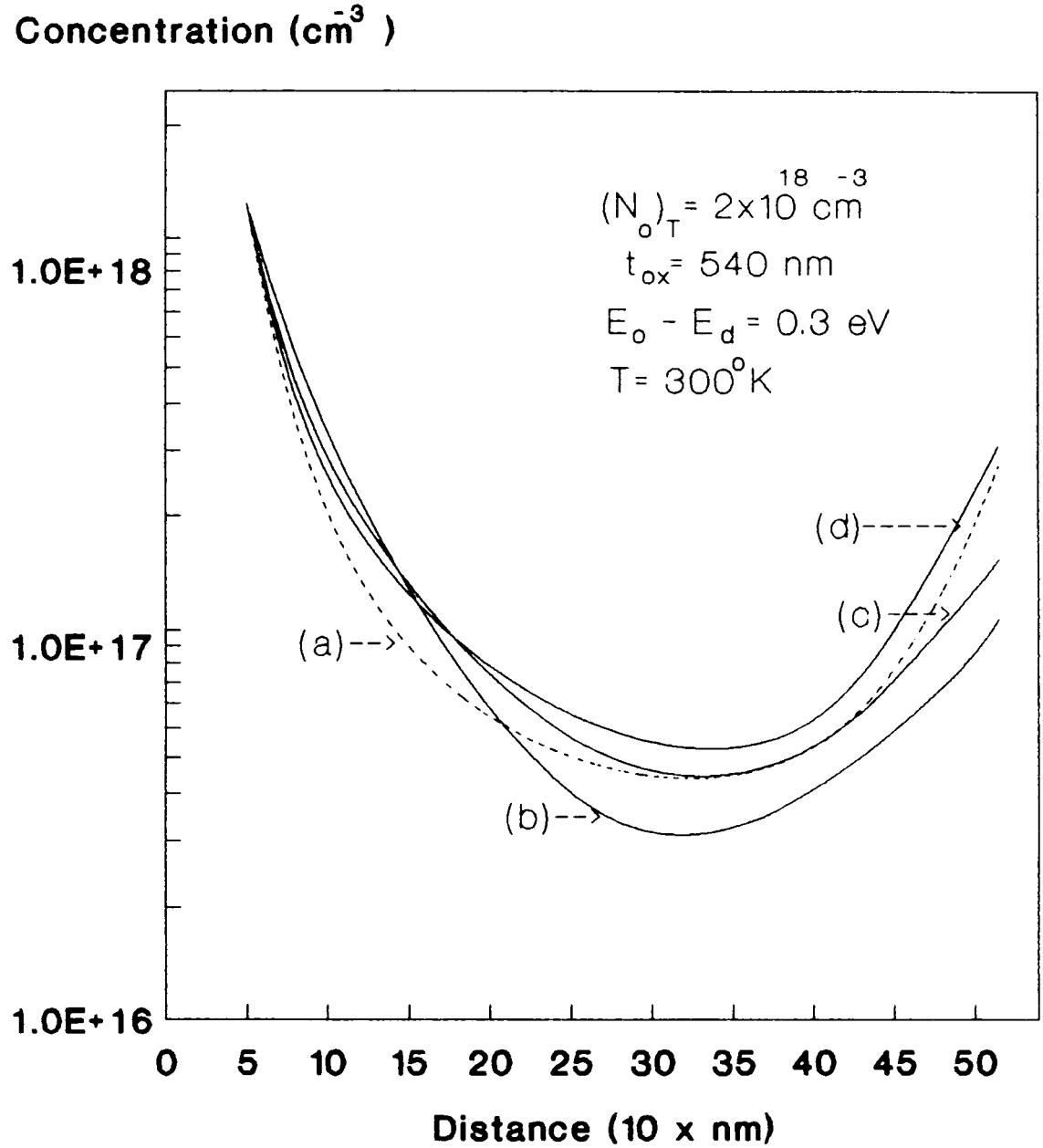

Fig. 6.8 Comparison of the theoretical and experimental total concentration profiles of the mobile ions in MOS capacitor. Experimental curve is shown by dotted line in (a)[54] Theoretical curves are shown by the full lines with values of V_A-V_F =-0.2 V in (b), -0.185 V in (c) and -0.17 V in (d).

To further test the validity of the present theoretical model, the flat-band-voltage shift δV_{FB} has been calculated with the help of Eq.(6.33) and compared with the experimentally obtained value. For example, δV_{FB} can be obtained from the experimentally determined C-V curves before and after intentional contamination of the device. Such C-V curves are reproduced from two earlier measurements [11,73] in Figs.6.9 and 6.10 respectively. The values of δV_{FB}, as obtained from each of these figures, are compared with the corresponding theoretical values in Table 1. The two sets of the value of δV_{FB} show quite a good agreement. The consistency, with which the theoretical results agree with the experiments, are indicative of the validity of the proposed theoretical model of the distribution of the mobile ions in the oxide of the MOS structures.

The computed parameter values such as the total density and the falt-band voltage shift have been carried out by using numerical methods. Programs in HP basic and their listings are illustrated in appendices B and C. The flow chart of these programs are shown in Figs. 6.11 and 6.12.

The role of temperature needs special discussion. It may be seen that the present study does not put any such constraint that equilibrium density-distribution can not be attained without rise of temperature. In fact equilibrium

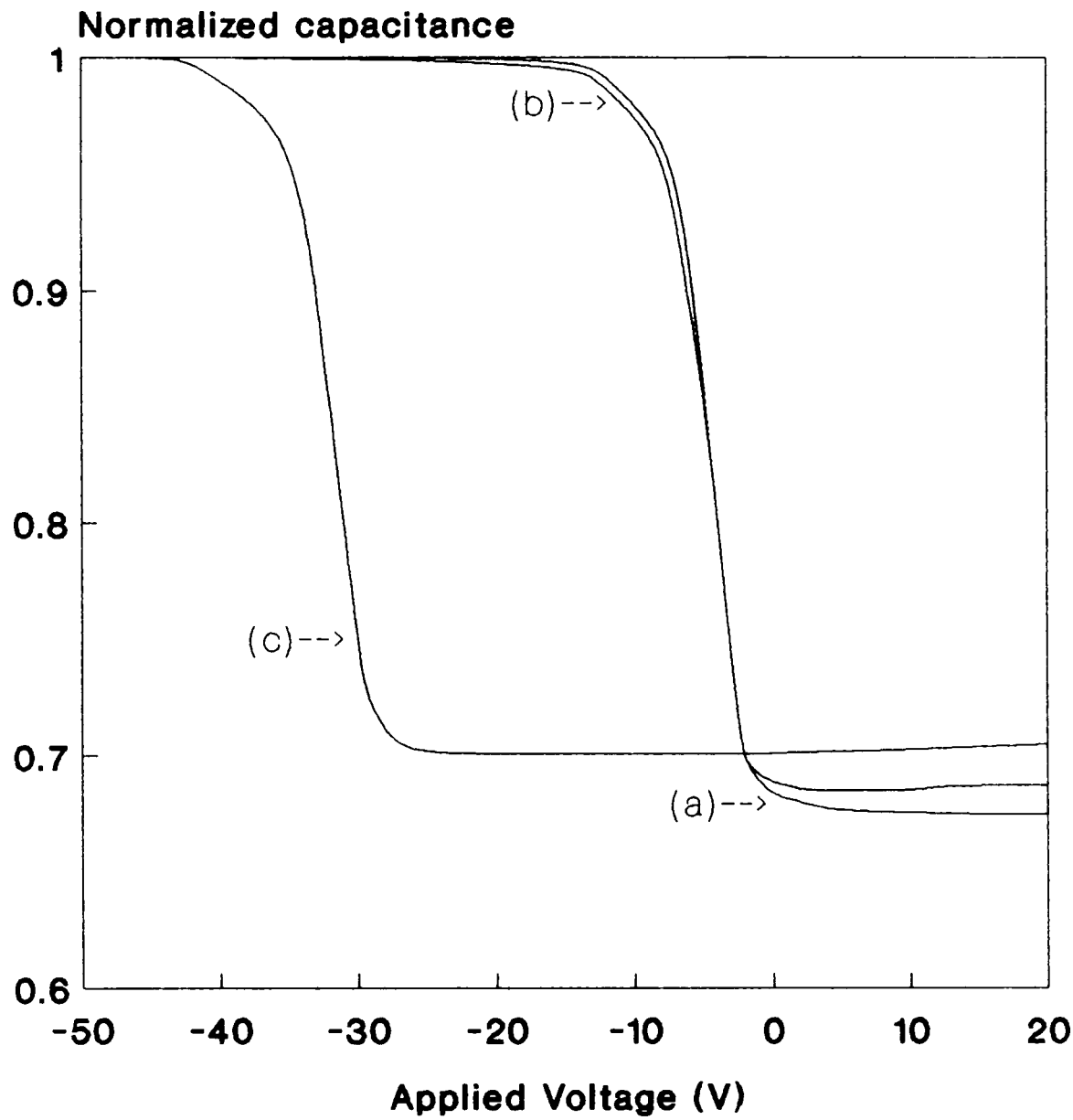

Fig. 6.9 Capacitance-voltage (C-V) curves of MOS structure. (a) before and, (b) after contamination (c) after 5 min of biasing [11].

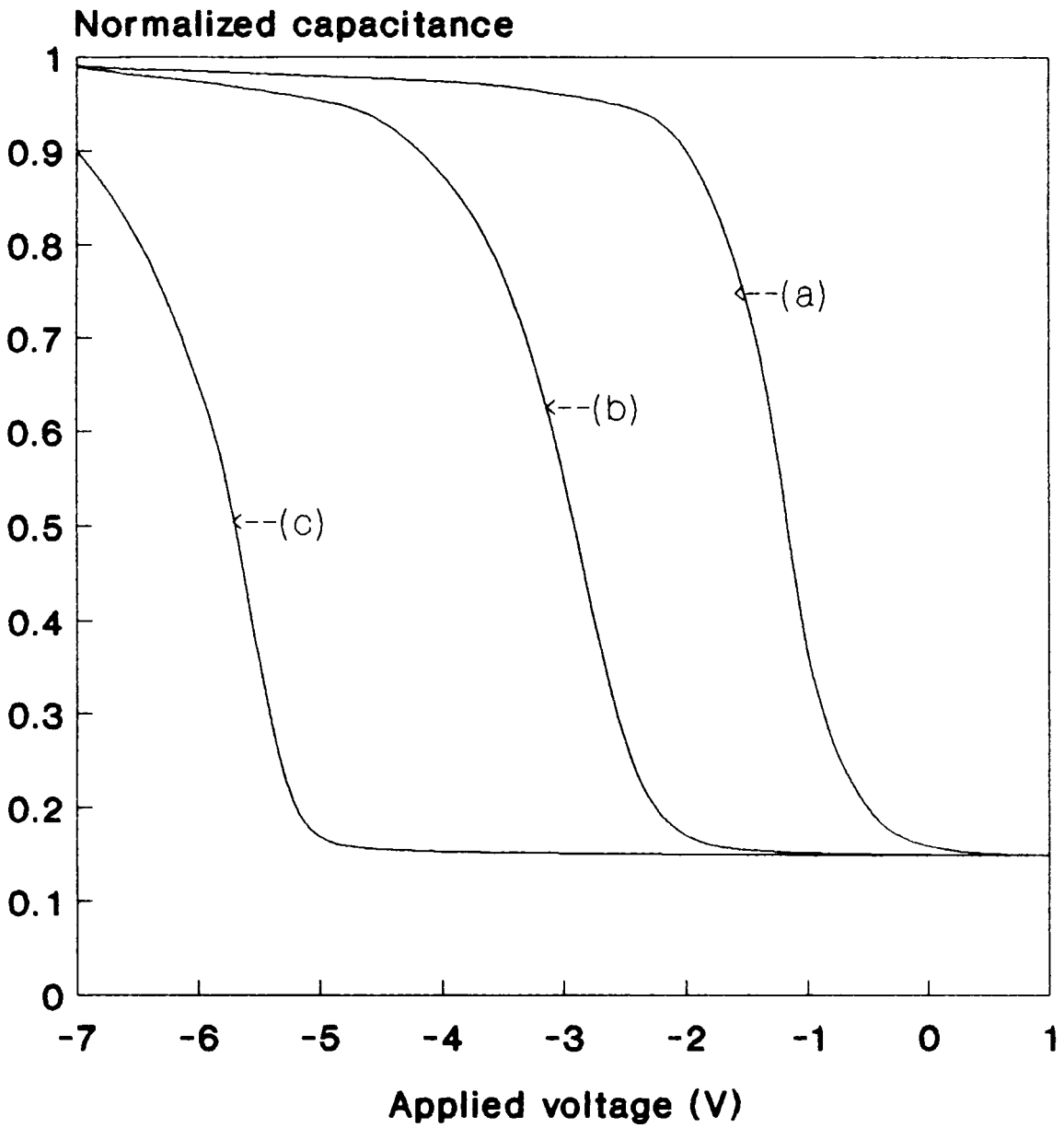

Fig. 6.10 Capacitance-voltage (C-V) curves of MOS capacitor (a) before activation, (b) after activation, (c) after 2700 sec of biasing [73].

ɔle II. Comparison of the experimental and theoretical values of the flat-band-voltage shift δV_{FB} resulting from sodium-ions contamination\activation in MOS diodes.

ɛf.	$(N_a)_T$ (cm^{-3})	t_{ox} (nm)	$(E_a - E_d)$ (eV)	$(V_A - V_F)$ (V)	Expt. δV_{FB} (V)	Cal. δV_{FB} (V)
a	1.5×10^{17}	200	0.1	-0.45	1.4	1.4
b	1.2×10^{18}	35	0.1	-0.09	1.6	1.5

ı see ref. 11

› see ref. 73

'able II. Comparison of the experimental and theoretical values of the flat-band-voltage shift δV_{FB} resulting from sodium-ions contamination\activation in MOS diodes.

Ref.	$(N_a)_T$ (cm^{-3})	t_{ox} (nm)	$(E_a - E_d)$ (eV)	$(V_A - V_F)$ (V)	Expt. δV_{FB} (V)	Cal. δV_{FB} (V)
a	1.5×10^{17}	200	0.1	-0.45	1.4	1.4
b	1.2×10^{18}	35	0.1	-0.09	1.6	1.5

a see ref. 11

b see ref. 73

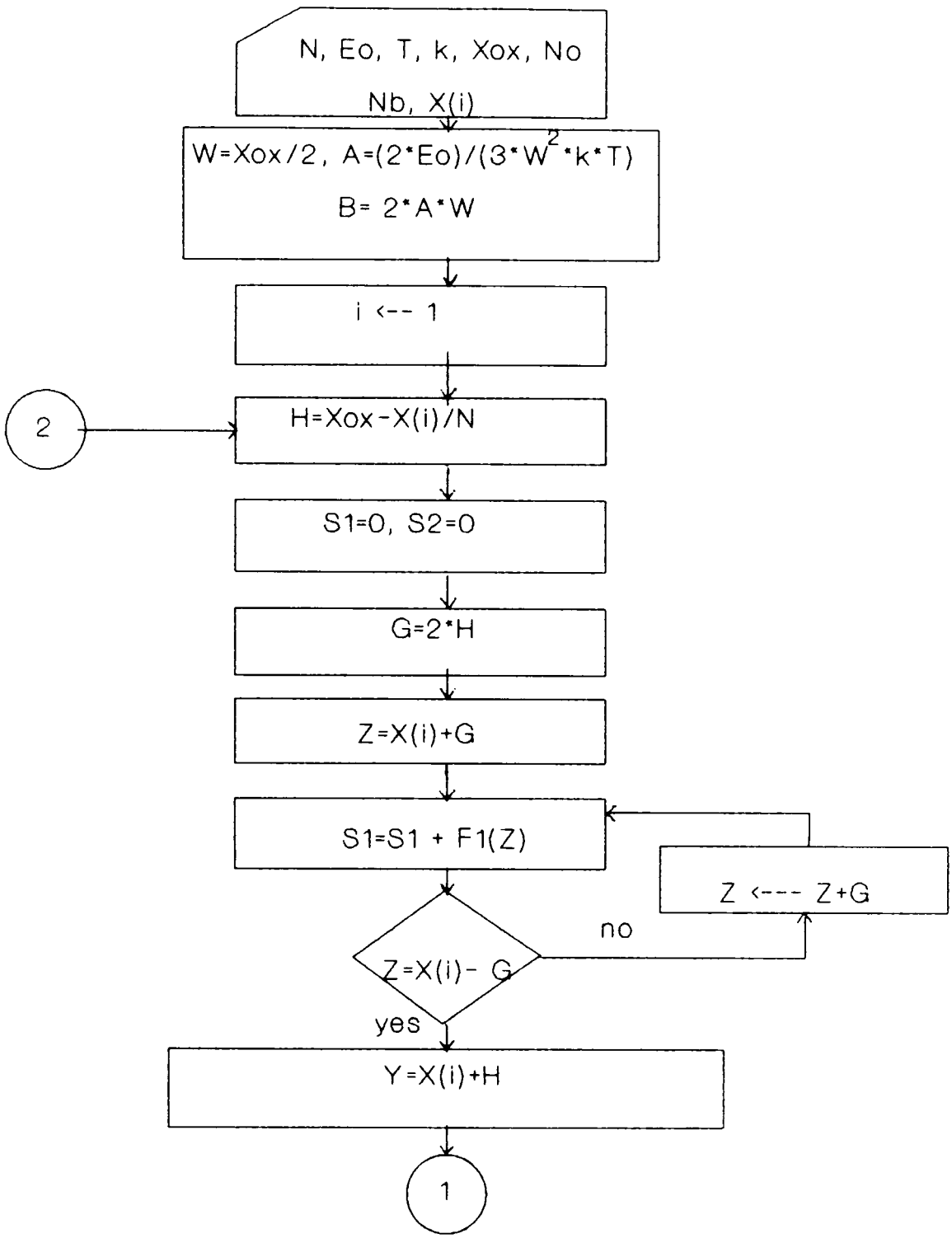

Fig. 6.11a flow chart for computing the total density of ions.

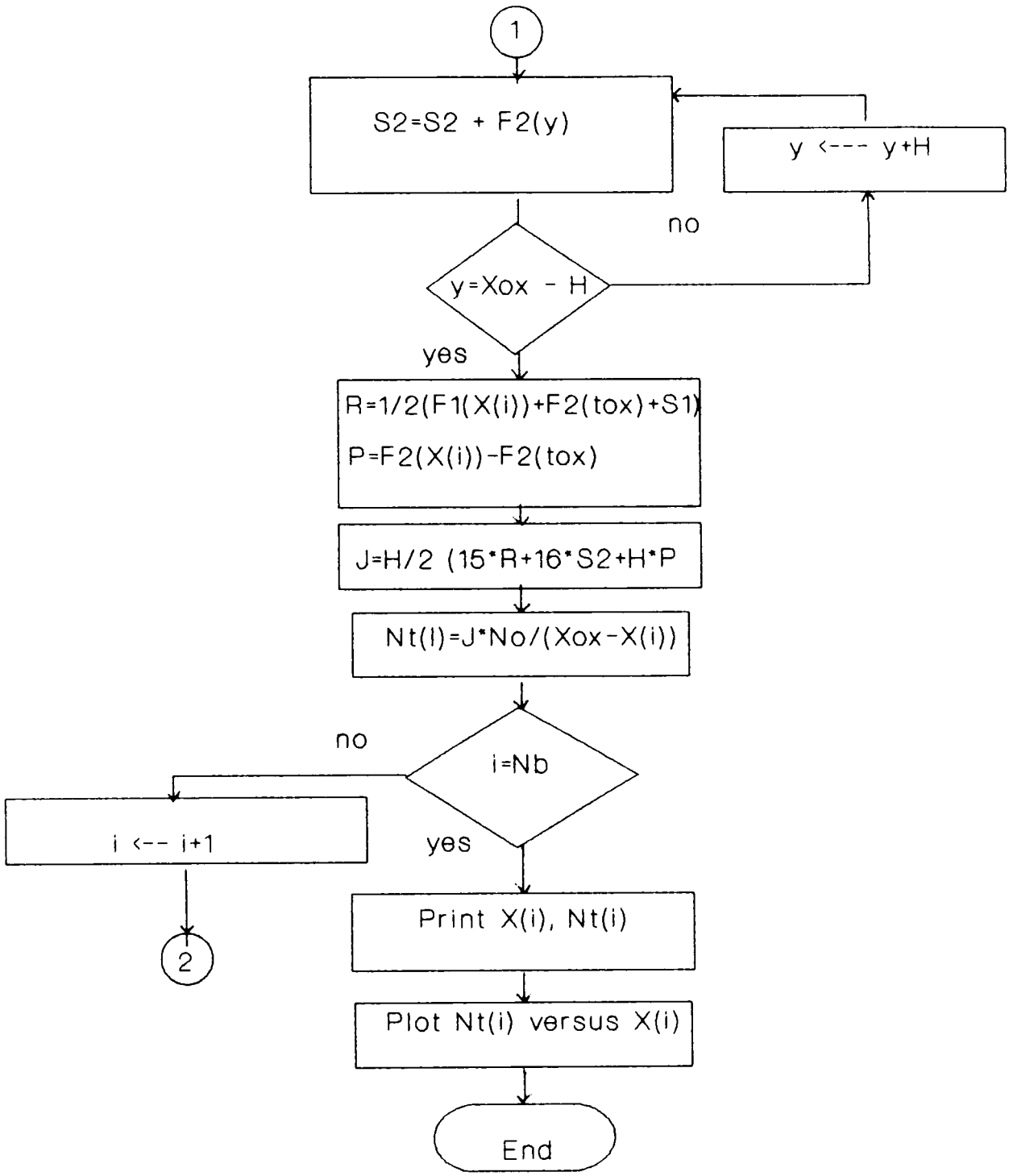

Fig. 6.11b flow chart for computing the total density of mobile ions for each etched off increment.

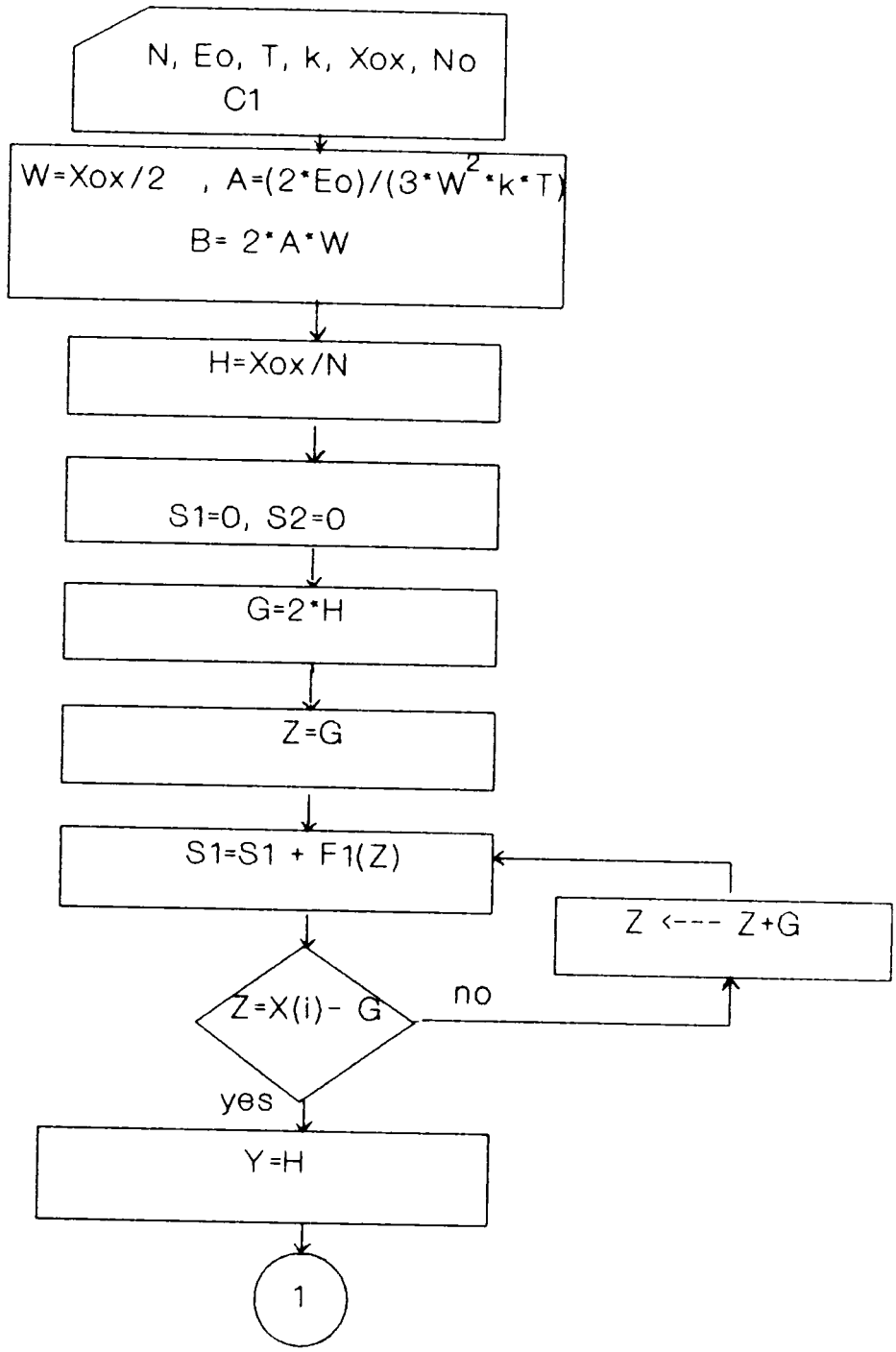

Fig. 6.12a flow chart for computing the flat-band voltage shift.

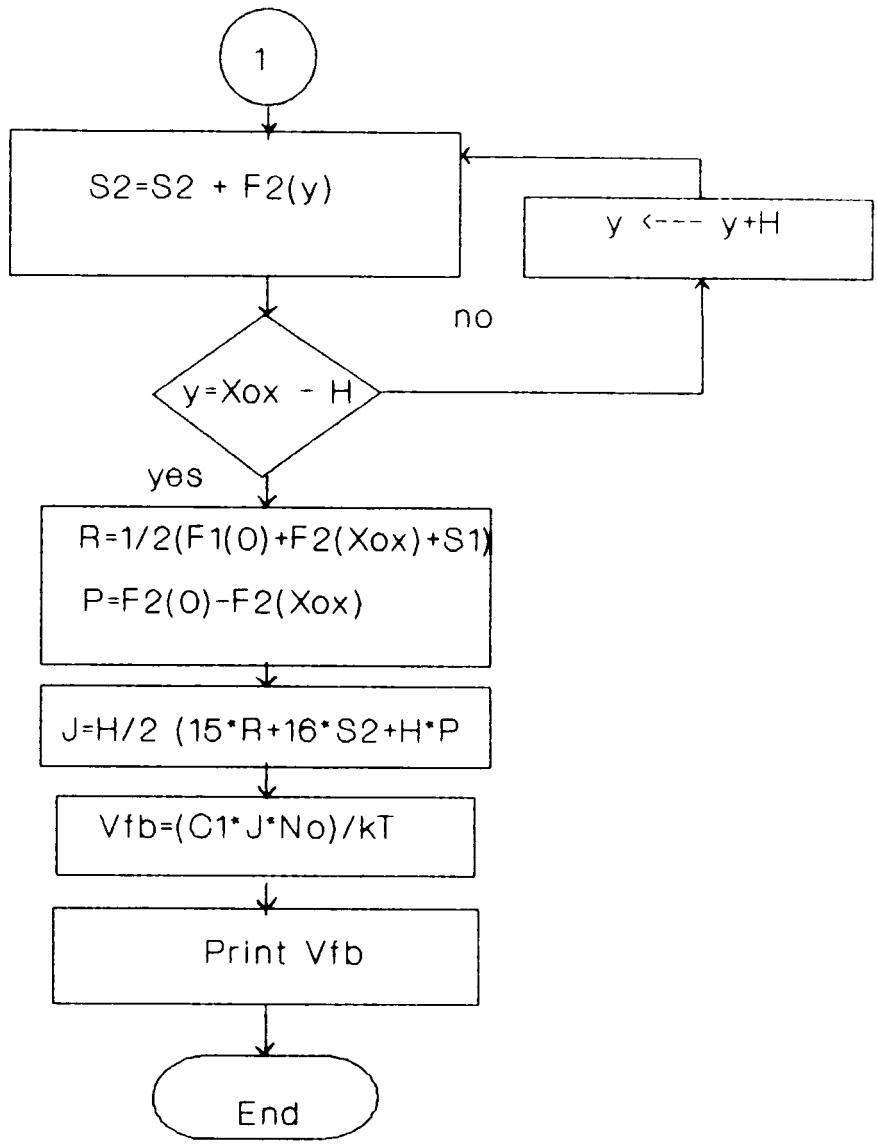

Fig. 6.12b flow chart for computing the flat-band voltage shift.

density-distribution can be attained even at room-temperature according to the present model although it may take place quite slowly. It is because the role of temperature is to provide thermal energy to the ions so that they are stimulated to overcome the trap-energy of the potential well which is nearly 0.66 eV. Assuming the energy of these ions to be governed by Boltzmann law, at least some fraction of the ions is always supposed to have energy above 0.66 eV and these ions will contribute to the ionic current. Obviously at the room-temperature, the fraction of such ions, which contribute to the ionic current, is very small and the attainment of the equilibrium density-distribution may take quite a long time. At high temperature this process is faster as may be seen from the exponential term in Eq.(6.31) which reveals that at any point x the concentration is more at higher temperature.

The present study also envisages that equilibrium density-distribution can be attained under the influence of internal electric field and thermal diffusion alone without the application of any external voltage. However, it may again take a long time to do so. The importance of thermal-electric stress in the experiments concerning ion-transport can be understood from the fact that in the absence of either heat or biasing the rate of drift and hence the

resulting ionic current may fall quite below the detection-limits.

It may be pointed out further that the role of heat is mainly to stimulate the ions to overcome the trap-energy of the potential well although it plays a role in the ion-drift also to some extent by way of thermal diffusion. Equation (6.24) can give more insight into the role of the trap-energy of the potential wells. In fact the drifting field is obtained by differentiating the activation energy of Eq.(6.24) in which the constant term E_d contributes nothing. However, this energy E_d does put a constraint on the number of ions which at any time are readily available for the drift by the drifting field. As the height of the potential barrier is greater at points closer to the metal-oxide interface, the effective depth of the potential well is increased at such points reducing thereby the number of ions readily available for the drift. Therefore the ions, trapped in the potential wells closer to the metal-oxide interface, contribute to less ionic current than those located away from it. Obviously the drift of such ions can be increased by increasing the temperature as per requirement of Eq.(6.31). It is this effect which has led to the earlier conclusion that the ionic current is emission-limited and that it needs at first detrapping of the ions by heating

before they can be drifted by the applied electric field [74].

Finally, this analytical model yields the distribution expression in a closed form identical to Eq.(5.4). The theoretical distribution curves as obtained by using this analytical model are also given in Figs.6.13 and 6.14 for comparison with the distribution-curves as obtained a result of computation of Eq.(5.4) in chapter 5. A closed agreement between the theoretical and computed distribution provides an experimental support to the present analytical model because the mobile ion-distribution in the oxide of the MOS structures as obtained in chapter 5 is based on the experimentally measured C-V curves.

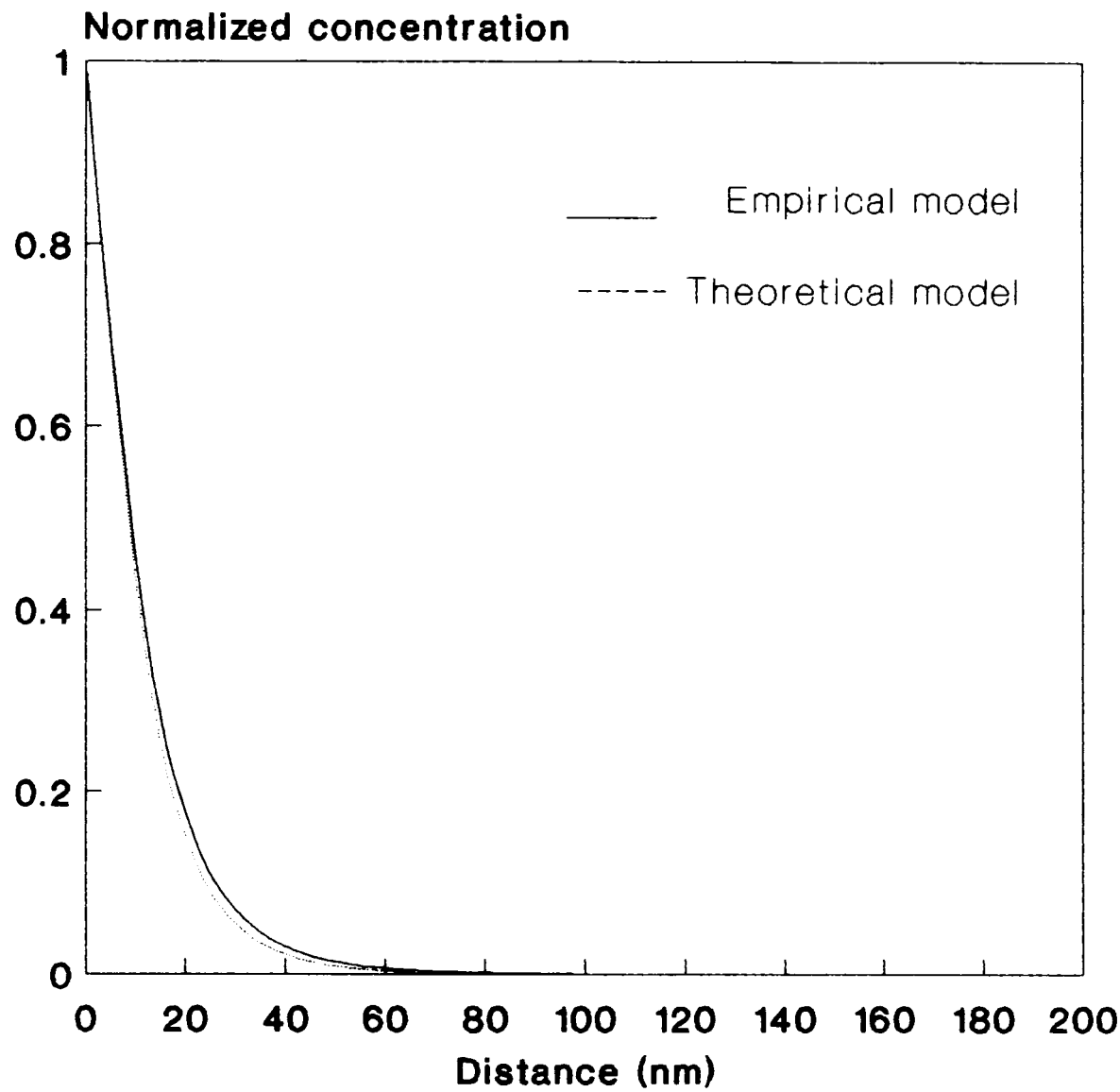

Fig. 6.13 Comparison of computed and theoretical mobile ion-concentration profile in a MOS structure with oxide-thickness 200 nm.

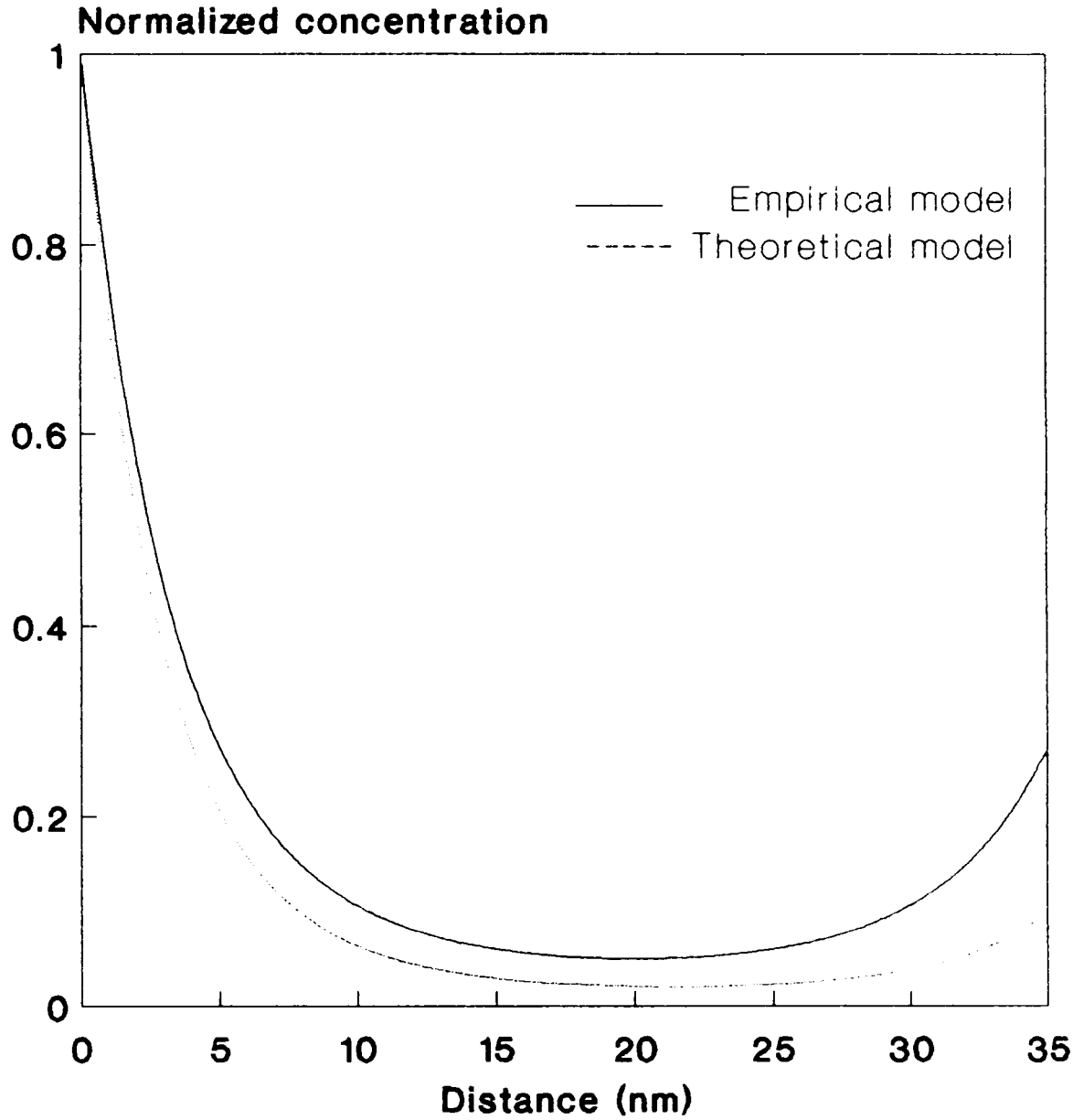

Fig. 6.14 Comparison of computed and theoretical mobile ion-concentration profile in a MOS structure with oxide-thickness 35 nm.

CONCLUDING REMARKS AND FUTURE SCOPE OF THE PRESENT STUDY

7.1.Conclusion

The study of the mobile ions in the oxide is of considerable importance as their presence can greatly affect the electrical characteristics of the MOS devices. Even the clean fabrication process and gettering do not ensure full safeguard against the problem of the mobile ions because it is not only the initial sodium ion contamination but the activation of already existing neutral sodium or additional contamination during subsequent device processing can also cause serious problems in the device performance. The use of intentionally contaminated devices for oxide characterization has further enlarged the importance of this subject.

These mobile ions are supposed to attain an equilibrium density distribution under the effect of various internal and external forces. The knowledge of the exact distribution of the mobile ions in the oxide would be of greater help to

account for their influence in the device performance. However none of the experimental or theoretical investigations, which have been made so far, could achieve this objective. Experimental approaches have mainly concentrated in obtaining the total ion concentration. Certain profiling experiments have also been carried out which employ the step etching technique but they do not yield the true concentration profile. It is because these experiments give the average concentration $(N(x))_T$ in the residual oxide after etching as a function of etched thickness x. Besides, this total ion concentration $(N(x))_T$ in the residual oxide is manipulated from the experimentally measured flat band voltage shift under an assumption that the sodium ions are concentrated in a thin layer at either interface of the oxide instead of considering their actual distribution. On the other hand, all the theoretical treatments involve computation of highly complicated differential equations which have been carried out under either certain assumed boundary conditions or assumed parameters. These theoretical treatments may throw some light on the possible trend of the distribution under certain assumed conditions but are not capable of giving the exact profile under any specific case.

All the above considerations formed the basis of undertaking the present work of the thesis. A two-fold programme was laid down. The first part aimed at the development of a method to determine the density distribution of mobile ions

from the experimentally measured flat band voltage shift. The second part aimed at the development of an analytical model which can give the density distribution of mobile ions in terms of certain known physical constants and device parameters.

In the first method, we have shown that it is possible to determine the distribution of the mobile ions along the oxide-thickness of the MOS device simply from the knowledge of the flat band voltage shift. It is based on the concept that the mobile ions attain in general an equilibrium density-distribution after their entry in the oxide-layer and that the flat-band voltage of the contaminated device has a strong dependence upon this equilibrium distribution. Indeed, this method is easy to carry out because it needs only the experimentally obtained values of the flat-band voltage of the given MOS device under three conditions first before contamination/activation, second after contamination-/activation and finally after drift of the ions under stressing. Besides, it is free from any assumption about the initial distribution of mobile ions before their drift under thermal-electric stress from one edge of oxide-layer to the other. The simple expressions, which have been used in this method, have been developed from the well known formulae of the flat-band voltage shift and the total concentration of

mobile ions. To use these expressions for computing the distribution parameters, the necessary program has been developed in HP basic.

The second attempt presented a one-dimentional analytical model of the distribution of the mobile ions along the oxide-thickness of the MOS structure. It is based on the concept that the equilibrium concentration of the mobile ions is attained in the oxide when all the internal and external mobilizing forces, arising from different origins, namely, thermal diffusion, internal and external electric fields, become just sufficient to overcome the total activation energy. Unlike the previous theoretical studies, all these forces acting on a single ion have been obtained here independent of each other from fundamental considerations and finally combined to get the density-distribution of the ions under the equilibrium conditions.

Both methods were used to determine the profile of the ions concentration in MOS structures and appeared to be in good agreement when the results were compared with previous experimental results for the same device parameters. In both cases, the distribution of mobile ions has been obtained closer to gaussian distribution.

The final expression, used for plotting the normalized density distribution of mobile ions versus depth curves in the present analytical model, involves the use of a few

device parameters such as oxide thickness t_{ox}, the difference of maximum and minimum values of activation energy (E_c-E_d), the applied effective gate voltage (V_A-V_F) and the temperature T besides a few physical constants such as electron charge q and Boltzmann constant k. Except for the quantity (V_A+V_F) all other quantities are explicitly known. The only quantity which is not known explicitly is the effective gate voltage V_F which arises due to the presence of fixed oxide charge Q_f and the interface trap charge Q_{it}. In fact V_F is the contribution of Q_{it} and Q_f to the flat band voltage of device. Under a condition when all the mobile ions are shifted to the metal-oxide interface, the oxide trap charges Q_t and the difference of metal and silicon work functions ϕ_{MS} are the additional factors contributing to the flat band voltage besides (Q_f+Q_{it}). After subtracting the contribution of Q_t and ϕ_{MS} from the total flat band voltage of the device, the value of V_F can be roughly estimated. However in the lack of this information, we have plotted the density distribution curves for certain assumed values of (V_A-V_F). A value of (V_A-V_F)=-0.2 V agrees well with the experimental curve [54].

In order to have a more exact verification of the model, the evaluation of the quantity V_F and hence that of Q_f and Q_{it} is needed for the device whose experimental $(N(x))_T$-x curve is compared with the theoretical curve. In the absence of precise value of V_F, we have also verified

the model indirectly by comparing the value of δV_{fb} as obtained by our model and that from the C-V curve of two experimental investigations [11,73] used here. Further, the density distribution curves, as obtained by the present model are compared with that obtained with the help of our other approach (as described in chapter 5) which is based on the experimentally measured values of the flat-band voltage shifts. The two N(x)-x curves show quite a good agreement and provide an indirect experimental support to our theoretical model.

7.2.Suggestion for Further Work

An important point which needs further discussion is the response time of the mobile ions in which their equilibrium distribution is attained after a given thermal-bias condition is applied to the device. As already discussed this response time has strong dependence on the temperature. At higher temperature, the attainment of equilibrium is quick but as the temperature is decreased, the time of the attainment of equilibrium is increased. At room temperature this time may become so high that practically any profile, which is produced under a given temperature-bias condition, may be supposed to be frozen after the temperature-bias is removed.

It would be quite interesting and useful to investigate

the role of time on the process of attainment of the equilibrium density distribution by studying the continuity equation within an element dx of the oxide thickness under varying voltage by applying gate voltage pulse of different periods. The resulting current transport so obtained may then be compared with the observed current transport at such gate voltage pulses. The limiting period at which the two results start deviating can give an idea of the response time of the mobile ions at a given temperature.

REFERENCES

1. L. M. Terman, " An investigation of Surface States at Silicon-Silicon Oxide Interface Employing Metal Oxide Silicon Diodes ", Solid-State Electronics **5**, pp. 285-299 (1962).

2. E. H. Nicollian and J. R. Brews, *MOS Physics and Technology*, Wiley, New York, (1982).

3. A. S. Grove, B. E. Deal, E. H. Snow, and C. T. Sah, " Investigation of Thermally Oxidized Silicon Surface Using MOS Structures ", Solid-St. Electr. **8**, pp. 145-163 (1965).

4. W. L. Brown, Phys. Rev. **91**, pp. 518-527 (1953).

5. C. G. B. Garrett and W. H. Brattain, Phys. Rev. **99**, 376 (1955).

6. J. R. Ligenza, J. Phys. Chem. Solids **65**, pp. 2011-2014 (1961).

7. J. A. Hoerni, IRE Electron Devices Meeting, Washington, D.C. (1960).

8. A. H. Agajanian, *Semiconductor Devices. A Bibliography of Fabrication Technology, Proprties, and Applications*, New York, Planum, pp. 547-619 (1976).

9. Y. C. Cheng, " Electronic States at the Silicon-Silicon Dioxide interface ", Prog. Surface Sci. **8**, p. 181 (1977).

10. B. E. Deal, " The Current Understanding of Charges in the Thermally Oxidized Silicon Structure ", J. Electrochem. Soc. **121**, pp. 198C-205C (1974).

11. E. H. Snow, A. S. Grove, B. E. Deal, and C. T. Sah, " Ion Transport Phenomena in Insulating Films ", J. Appl. Phys. **36**, pp. 1664-1673 (1965).

12. M. W. Hillen and J. F. Verwey, " Mobile ions in SiO_2 layers on Si ", in G. Barbottain and A. Vapaille ed., *Instabilities in Silicon Devices*, Vol. **I**, North-Holland, Amsterdam, pp. 404-439 (1986).

13. V. Mitra, H. Bentarzi, R. Bouderbala and A. Benfdila, "Determination of the Distribution of Mobile Charges in the Oxide of the MOS Structure ", ICEA 92, **Vol.1**, pp. 208-216, Tizi-Ouzou , ALGERIA, (1992).

14. V. Mitra, H. Bentarzi, R. Bouderbala and A. Benfdila, "A Theoretical Model for the Density-Distribution of

Mobile Ions in the Oxide of the Metal-Oxide-Semiconductor Structures", a paper communicated for publication J. Appl. Phys., (1992).

15. A. Goetzberger and S. M. Sze, " Metal-Insulator-Semiconductor (MIS) Physics ", in *Applied Solid State Science*,R. Wolfe ed., Academic Press, New York, pp. 154-237 (1969).

16. S. M. Sze, *Physics of Semiconductor Devices*, Wiley, New York, (1981).

17. A. S. Grove, *Physics and Technology of Semiconductor Devices*, John Wiley and Sons, New York, (1967).

18. P. Richman, *MOS Field-Effect Transistors and Integrated Circuits*, John Wiley and Sons, New York, (1973).

19. H. M. Prezewlocki, " Work Function Disfference in MOS Structures; Current Understanding and New Measurement Methods ", (1982).

20. B. Maykusiak and A. Jakubowski, " A New Method for the Simultaneous determination of the Surface-Carrier Mobility and the Metal-Semiconductor Work-Function Difference in MOS Transistors ", IEEE Tran. Elect. Dev. **ED-35**, pp. 439-443 (1988).

21. M. J. McNutt and C. T. Sah, " Determination of the MOS Oxide Capacitance ", J. Appl. Phys. **46**, pp. 3909-3913 (1975).

22. B. E. Deal, " Standardized Terminology for Oxide Charge Associated with Thermally Oxidized Silicon ", IEEE Trans. Elect. Dev. ED-27, pp. 606-608 (1980).

23. D. J. DiMaria, " Defects and Impurities in Thermal SiO_2 ", in *The Physics of SiO_2 and its Inteface*, S. T. Partelides, Ed., Pergamon, New York, pp. 160-178, (1978).

24. T. Sungano, " Recent Understanding of Morphology of Si-SiO_2 Interface and Traps States at the Interface ", S. C. Jain and S. Radhakrishna ed., in *Physics of Semiconductor Devices*, pp. 212-221 (1982).

25. M. C. Ash, P. Chattopadhyay, and A. N. Daw, " Effect of Trichlorvethylene on the Oxide Charge and Interface State Density of a Silicon MIS Tunnnel Structure ", J. Instn. Electronics and Telecom. Engrs. **31**, pp. 63-64 (1985).

26. E. Avniand J. Shapir, " Modeling of Charge Injection Effects in Metal-Oxide-Semiconductor Structures ", J. Appl. **64**, pp. 734-742, (1988).

27. V. G. Litovchenko, V. Y. Kiblick, S. S. Georgiev and K. I. Kirov, " Radiation Induced Charges in Low-Temperature Oxide MOS Structures (Al-SiO_2-Si) ", Radiation Effects, Vol. **62**, pp. 1-5 (1982).

28. E. H. Nicollian, A. Goetzberger, " The Si-SiO_2 Interface: Electrical Proporties as Determined by the MIS Conductance Technique ", The Bell System Technical Journal, Vol. **46**, pp. 1055-1133 (1967).

29. D. M. Brown and P. V. Gray, " Si-SiO_2 Fast Interface State Measurements ", J. Electrochem. Soc. **115**, pp. 760-766, (1968).

30. S. Gourrier and P. Friedel, " Caracterisation electronique des etats electroniques d´interface Isolant/Semiconductor ", ACTA Electronica, Vol.**25**, pp. 217-240, (1983).

31. C. N. Berglund, "Surface States of Steam-grown Silicon Dioxide Interfaces ", IEEE Trans. Electron Devices, **ED-13**, pp. 701-705 (1966).

32. M. Kuhn, "A Quasi-Static Technique for MOS C-V and Surface state Measurements ", Solid State Electron. **13**, pp. 873-885 (1970).

33. D. V. Lang, "Deep-Level Transient Spectroscopy : A Method to Characterize Traps in Semiconductor ", J. Appl. Phys. **45**, pp. 3023-3032 (1974).

34. K. L. Wang and A. O. Evwaraye, " Determination of Interface and Bulk Trap states of IGFET's Using Deep-Level Transient Spectroscopy ", J. Appl. Phys. **47**, pp. 4574-4577 (1976).

35. K. Yamasaki and T. Sugano, Appl. Phys. Lett. **35**, p. 930 (1979).

36. H. Hasegawa and T. Sawada, J. Phys. Soc. Jpn. Suppl. A, **49**, p. 1125 (1980).

37. J. S. Brugler and P. G. A. Jespers, " Charge Pumping in MOS Devices ", IEEE Trans. Elect. Dev. **ED-16**, pp. 297-301 (1969).

38. A. B. M. Elliot, " The Use of Charge Pumping Currents to Measure Surface State Densities in MOS Transistors ", Solid State Electron, **19**, pp. 241-247 (1976).

39. W. V. Backensto and C. R. Vishwanathan, "Measurement of Interface State Characteristics of MOS Transistor Utilizing Charge-pumping Techniques ", Proc. IEE, **128**, Pt. I, pp.44-52 (1981).

40. G. Groeseneken, H. E. Maes, N. Beltran and R. F. DeKeersmaeker, " A Reliable Approuach to Charge Pumping Measurements in MOS-Transistors ", IEEE Trans. Elect. Dev. **ED-31**, pp. 42-53 (1984).

41. W. L. Tseng, " A New Charge Pumping Method of Measuring Si-SiO_2 Interface States ", J. Appl. Phys. **62**, pp. 591-599 (1987).

42. P. Heremans, J. Witters, G. Groeseneken and H. E. Maes, " Analysis of the Charge Pumping Technique and Its Application for the Evaluation of MOSFET Degradation ", IEEE Trans. Elect. Dev. **ED-36**, pp. 1318-1335 (1989).

43. V. Q. Ho and T. Sugano, " An Temperature of the Interface Properties of Plasma Anodized SiO_2/Si System for the Fabrication of MOSFET's ", IEEE Trans. Elect. Dev. **ED-28**, pp.1060-1064 (1981).

44. A. J. Learn and D. W. Hess, " Effects of Ion Implantation on Charges in the Silicon-Silicon Dioxide System ", J. Appl. Phys. **48**, pp.308-312 (1977).

45. B. E. Deal, M. Sklar, A. S. Grove, and E. H. Snow, J. Electrochem. Soc. **114**, pp. 226-274, (1967).

46. S. M. Tang, W. B. Berry, R. Kwor, M. V. Zeller and L. G. Matus, " High Frequency Capacitance-Voltage Characteristics of Thermally Grown SiO_2 Films on β-Sic ", J. Electrochem. Soc. **137**, pp.221-225 (1990).

47. D. J. DiMaria, " The Properties of Electron and Holes Traps in Thermal Silicon Dioxide Layers Grown on Silicon ", S. T. Partelides Ed., in *The Physics of Si-SiO_2 and Its Interface*, Pergamon, New York, pp. 160-178 (1978).

48. E. H. Nicollian, C. N. Berglund, P. F. Schmit and J. M. Andrews, J. Appl. Phys. **42**, p. 5654, (1971).

49. C. N. Berglund and R. J. Powell, " Photoinjection into SiO_2: Electron Scattering in the Image Force Potential Well ", J. Appl. Phys. **42**, pp.573-579 (1971).

50. J. R. Brews, " Limitations upon Photoinjection Studies of Charge Distributions Close to Interfaces in MOS Capacitors ", J. Appl. Phys. **44**, pp.379-384 (1973).

51. H. M. Przewlocki, " Determination of Trapped Charge Distributions in the Dielectric of a Metal-Oxide-Semiconductor Structure ", J. Appl. Phys. **57**, pp.5359-5366 (1985).

52. J. R. Davis, *Instabilities in MOS Devices*, Vol. **1**, Gordon and Breach Science Publshers, London, (1977).

53. Kriegler, Y. C. Cheng and D. R. Colton, " The Effect of HCl and Cl2 on the thermal Oxidation of Silicon", J. Electrochem. Soc. **119**, pp. 388-392, (1972).

54. E. Yon, W. H. Ko and A. B. Kuper, "Sodium Distribution in Thermal Oxide on Silicon by Radiochemical and MOS Analysis ", IEEE Trans. Elect. Dev. **ED-13**, pp. 276-280, (1966).

55. M. Yamin, " Charge Storage Effects in Silicon Dioxide Films ", IEEE Trans. Elect. Dev. **ED-12**, pp. 88-96, (1965).

56. N. J. Chou, " Application of Triangular voltage Sweep Method to Mobile Charge Studies in MOS Structures ", J. Electrochem. Soc. **118**, pp. 601-609, (1971).

57. M. Kuhn and D. J. Silversmith, " Ionic Contamination and Transport of Mobile Ions in MOS Structures ", J. Electrochem. Soc. **118**, pp. 966-970, (1971).

58. M. Pepper and W. Eccleston, " Cation Transport in SiO_2 ", Phys. Stat. Sol. (a) **12**, pp. 199-207, (1972).

59. H. M. Przewlocki and W. Marciniak, " The Triangular Voltage Sweep Method as a Tool in Studies of Mobile Charge in MOS Structures ", Phys. Stat. Sol. (a) **29**, pp. 265-274, (1975).

60. A. G. Tangena, J. Middelhoek and N. F. DeRooij, " Influence of Positive Ions on the Current-Voltage Characteristics of MOS Structures ", J. Appl. Phys. **49**, pp. 2876-2879, (1978).

61. D. J. DiMaria, " Room-Temperature Conductivity and Location of Mobile Sodium Ions in the Thermal Silicon Dioxide Layer of a Metal-Silicon dioxide-Silicon Structure ", J. Appl. Phys. **48**, pp. 5149-5151, (1977).

62. T. W. Hickmott, " Thermally Stimulated Ionic Conductivity of Sodium in Thermal ", J. Appl. Phys. **46**, pp. 2583-2598, (1975).

63. P. K. Nauta and M. W. Hillen, " Investigation of Mobile Ions in MOS Structures Using the TSIC Method ", J. Appl. Phys. **49**, pp. 2862-2865, (1978).

64. M. W. Hillen, " Dynamic Behaviour of Mobile Ions in SiO_2 Layers ", in *The Physics of SiO_2 and Its Interface*, S. T. Partelides, Ed., Pergamon, New York, pp.179-183, (1978).

65. M. R. Boudry and J. P. Stagg, " The Kinetic Behaviour of Mobile Ions in the Al-SiO_2-Si System ", J. Appl. Phys. **50**, pp. 942-950, (1979).

66. T. W. Hickmott, " Dipole Layers at the Metal-SiO_2 Interface ", J. Appl. Phys. **51**, pp. 4269-4281, (1980).

67. R. J. Kriegler and T. F. Devenyi, " Direct Measurement of Na^+ Ion Mobility in SiO_2 Films ", Thin Solid Films **36**, pp. 435-439, (1976).

68. M. W. Hillen, G. Greeuw and J. F. Verweij, " On the Mobility of Potassium Ions in SiO_2 ", J. Appl. Phys. **50**, pp. 4834-4837, (1979).

69. G. F. Derbenwick, " Mobile Ions in SiO_2: Potassium ", J. Appl. Phys. **48**, pp. 1127-1130, (1977).

70. J. P. Stagg, " Drift Mobilities of Na^+ and K^+ Ions in SiO_2 Films ", Appl. Phys. Lett. **31**, pp. 532-533, (1977).

71. V. P. Romanov and Yu. A. Chaplygin, " Stationary Distribution of mobile Charge in the Dielectric of MOS Structures ", Phy. Stat. (a) **53**, pp. 493-498, (1979).

72. F. J. Feigl and S. R. Butler, Electrochem. Soc. Meeting, Atlanta Oct 9-14 (1977).

73. A. Raychaudhuri, A. Ashok and S. Kar, " Ion-Dosage Dependent Room-Temperature Hystersis in MOS Structures with thin Oxides ", IEEE Trans. Elect. Dev. **38**, pp. 316-322, (1991).

74. S. R. Hofstein, IEEE Trans. Elect. Dev. **ED-14**, p. 749, (1976).

75. E. H. Nicolian, A. Goetzberger and C. N. Berglund, Appl. Phys. Lett. **15**, p. 174, (1969).

76. J. Frenbel, Phys. Rev. **54**, p. 647, (1938).

77. J. J. O'Dwyer, *The Theory of Electrical Conduction and Breakdown in Solid Dielectrics*, Clarendon, Oxford, (1973).

78. M. Av-Rom, M. Shatzkes, T. H. Distefano and I. B. Cadoff, " The Nature of Electron Tunneling in SiO_2 ", in S. T. Pantelider Ed., *The Physics of SiO_2 and its Interface*, Pergamon, New York, (1978).

```
'*****************************************
'***PROGRAME TO CALCULATE THEORETICAL VALUES OF =0 AND =DLATGE*
'*****************************************
K=100
INPUT "Xox=",Xox
INPUT "Nt=",Nt
INPUT "Vfb1=",Vfb1
INPUT "Vfb2=",Vfb2
'*****************************************
'***=UBPROGRAME FOR CALCULATING Vfb AT MEDIUM ...  N ====***
'*****************************************
FOR N=1 TO 3 STEP 1
S1=0
S2=0
H=Xox/K
FOR C=1.E-9 TO Xox STEP 1.E-9
  FOR X=H TO Xox-H STEP H
    S1=S1+X*EXP((-X^N)/(2*C^N))
    S2=S2+EXP((-X^N)/(2*C^N))
  NEXT X
  U=EXP(-Xox^N/(2*C^N))
  R1=(Xox*U+2*S1)*H/2
  R2=(U+1+2*S2)*H/2
  G1=-1+U-(N*U*Xox^N)/(2*C^N)
  IF N=1 THEN 242
  G2=-(N*U*Xox^(N-1))/(2*C^N)
  GOTO 250
  G2=-U/(2*C)+1/(2*C)
  I1=R1-(G1*H^2)/12
  I2=R2-(G2*H^2)/12
  Vmo=(4.536*Nt*I1*1.E-9)/I2
  PRINT Vmo
  D1=ABS(Vmo-Vfb1)
'*****************************************
'*******SUBPROGRAME FOR CALCULATING Vfb AT ...  ...N  ...-...CE
'*****************************************
  S3=0
  S4=0
  H=Xox/K
  FOR X=H TO Xox-H STEP H
    S3=S3+X*EXP((-1)^(N+1)*((X-Xox)^N)/(2*C^N))
    S4=S4+EXP((-1)^(N+1)*((X-Xox)^N)/(2*C^N))
  NEXT X
  R3=(Xox+2*S3)*H/2
  R4=(1+EXP(((-1)^(N+1)*(-Xox)^N)/(2*C^N))+2*...*...2
  U=EXP(((-1)^(N+1)*(-Xox)^N)/(2*C^N))
  IF N=1 THEN 542
  G3=-U+1
  G4=(-U*N*(-1)^(N+1)*(-Xox)^(N-1))/(2*C^N)
  GOTO 550
  G3=1+Xox/(2*C)-U
  G4=1/(2*C)-U/(2*C)
  I3=R3-(G3*H^2)/12
  I4=R4-(G4*H^2)/12
  Vos=4.636E-9*Nt*I3/I4
  PRINT Vos
  D2=(Vos-Vfb2)
  IF D1<1.E-1 AND D2<1.E-1 THEN 611
 NEXT C
NEXT N
C=2*C
PRINT N,C
END
```

```
      DIM File$(1200)[40]
      DIM A$[40],U(100),Nt(100),X(100)
      FOR I=0 TO 100
      X(I)=0
      Nt(I)=0
      NEXT I
      !*****************************************************
      !***PROGRAM FOR CALCULATING THE TOTAL DENSITY ***
      !******** OF IONS FOR EACH INCREAMENT**********
      N=150
      Eo=1.6*1.E-20
      T=300
      K=1.38E-23
      INPUT "Xox=",Xox
      INPUT "No=",No
      INPUT "VA-VF=",V
      W=Xox/2
      A=(2*Eo)/(3*(W^2)*K*T)
      B=(2*A*W)
      C=(2*V*1.6E-19)/(3*Xox*K*T)
      PRINT "   X   "," I ","  Nt  "
      PRINT "-------------------------------------------------------------"
      FOR I=1 TO 5 STEP 1
      READ X(I)
      DATA 0,1.0E-7,2.6E-7,4.4E-7,4.9E-7
      H=(Xox-X(I))/N
      S1=0
      S2=0
      G=2*H
      FOR Z=X(I)+G TO Xox-G STEP G
      S1=S1+EXP(-B*Z+A*Z^2+C*Z)
      NEXT Z
      FOR Y=X(I)+H TO Xox-H STEP G
      S2=S2+EXP(-B*Y+A*Y^2+C*Y)
      NEXT Y
      F=EXP(-B*Xox+A*Xox^2+C*Xox)
      R=(1/2)*(EXP(-B*X(I)+A*(X(I))^2+X(I)*C)+F)+S1
      P=(-2*A*X(I)-B+C)*EXP(-B*X(I)+A*(X(I))^2+C*X(I))-(-2*A*Xox-B+C)*F
      J=(H/15)*(14*R+16*S2+H*P)
      Nt(I)=J*No/(Xox-X(I))
      PRINT X(I),"  I  ",Nt(I)
      NEXT I
      PRINT "ENTER 1 TO PLOT LOG SCALE OR 2 TO PLOT LINEAR SCALE
      PRINT "OR 3 TO END THE PROGRAM"
      INPUT K
      IF K=1 THEN 102
      IF K=2 THEN 233
      IF K=3 THEN 606
      !***************** SUBROUTINE*********************
      INIT
      PLOTTER IS 3,"INTERNAL"
      GRAPHICS ON
      X_gdu_max=100*MAX(1,RATIO)
      Y_gdu_max=100*MAX(1,1/RATIO)
      CORG 6
      FOR I=-.3 TO .3 STEP .1
      MOVE X_gdu_max/2+I, 9*Y_gdu_max
      LABEL " THE TOTAL DENSITY"
      NEXT I
      DEG
```

```
1     LABEL "Nt (m^-3)"
2     LORG 4
3     LDIR 0
4     MOVE X_gdu_max/2,.09*Y_gdu_max
5     LABEL "DISTANCE X (*1.E-8 m)"
6     VIEWPORT .2*X_gdu_max,.88*X_gdu_max,.20*Y_gdu_max,.8*Y_gdu_max
7     RETURN
8     !************************ LOGARITHMIC SCALE ***********************
9     GOSUB 72
10    WINDOW 0,54,0,4
11    AXES 1,1,0,0,10,10,3
12    CLIP OFF
13    CSIZE 2.5,.5
14    LORG 6
15    FOR I=0 TO 54 STEP 10
16       MOVE I,-.01
17       LABEL USING "#,K";I
18    NEXT I
19    LORG 8
20    FOR I=0 TO 4 STEP 1
21      S=10^(I+21)
22      MOVE -1,I
23      LABEL USING "#,K";S
24    NEXT I
25    FOR I=0 TO 4
26      FOR J=1 TO 9
27      K=I+LGT(J)
28      MOVE +.47,K
29      !LABEL "-"
30      NEXT J
31    NEXT I
32    X(6)=Xox
33    FOR I=1 TO 5 STEP 1
34    X(I)=(X(I)+(X(I+1)-X(I))/2)*1.E+8
35    Nt(I)=LGT(Nt(I))-21
36    MOVE X(I),Nt(I)
37    CSIZE 3,.4
38    LABEL "X"
39    NEXT I
40    GOTO 63
41    !*********LINEAR SCALE*****************
42    GOSUB 72
43    WINDOW 0,54,0,1
44    AXES 1,.1,0,0,10,1,3
45    CLIP OFF
46    CSIZE 2.5,.5
47    LORG 6
48    FOR I=0 TO 54 STEP 10
49       MOVE I,-.01
50       LABEL USING "#,K";I
51    NEXT I
52    LORG 8
53    FOR I=0 TO 1 STEP .1
54      MOVE -.4,I
55      LABEL USING "#,K";I
56    NEXT I
57    X(0)=X(0)*1.E+8
58    Nt(0)=Nt(0)
59    MOVE X(0),Nt(0)
60    FOR I=1 TO 35 STEP 1
61    X(I)=X(I)*1.E+8
62    Nt(I)=Nt(I)/Nt(0)
63    DRAW X(I),Nt(I)
```

```
263     NEXT I
264     GOTO 63
606     END
```

APPENDIX C

```
10      ********************************************************
20      ***PROGRAM FOR CALCULATING THE FLAT BAND VOLTAGE***
30      ********************************************************
11      N=150
12      Eo=1.6*1.E-20
16      T=300
17      K=1.38E-23
18      INPUT "Xox=",Xox
20      INPUT "No=",No
26      INPUT "VA-VF=",V
28      W=Xox/2
29      A=(2*Eo)/(3*(W^2)*K*T)
30      B=(2*A*W)
31      C=(2*V*1.6E-19)/(3*Xox*K*T)
40      H=Xox/N
50      S1=0
60      S2=0
70      P=2*H
80      FOR Z=0 TO Xox-G STEP G
90      S1=S1+Z*EXP(-B*Z+A*Z^2+C*Z)
100     NEXT Z
110     FOR Y=H TO Xox-H STEP G
120     S2=S2+Y*EXP(-B*Y+A*Y^2+C*Y)
130     NEXT Y
135     F=EXP(A*Xox^2-B*Xox+C*Xox)+S1
140     F=(1/2)*Xox*F+S1
150     F=1-F-(Xox*(+2*A*Xox-B+C)*F)
160     R=(H/15)*(14*R+16*S2+H*P)
170     Vfb=(1.6E-19*J*No)/(3.9*8.85E-12)
180     PRINT "Vfb=";Vfb
190     END
```

A N N E X E

Liste et composition du jury en vue de la soutenance du Memoire de Magister en.....Electronique..Appliquée.....

de/)/)r..BENTARZI...Hamid.....

PRESIDENT /: Dr.M.BENZOHRA,Professeur, U.S.T.O.

RAPPORTEUR/: Dr.VED.MITRA, Professeur, I.N.E.L.E.C.

MEMBRES /: Dr.M.BOUMAOUR, Chargé de Recherche, UDTS (SERS).

Dr.H.BOURDOUCEN, Chargé de Recherche, INELEC

Dr.L.REFOUFI, Maitre Assistant, PhD, INELEC.